THIS REPORT HAS BEEN DELIMITED
AND CLEARED FOR PUBLIC RELEASE
UNDER DOD DIRECTIVE 5200.20 AND
NO RESTRICTIONS ARE IMPOSED UPON
ITS USE AND DISCLOSURE.

DISTRIBUTION STATEMENT A

APPROVED FOR PUBLIC RELEASE;
DISTRIBUTION UNLIMITED.

NOLR-1217
copy 4

CONFIDENTIAL

NAVAL ORDNANCE LABORATORY
LIBRARY

MAR 18 1958

WT-1009 (NOLR-1217)
Copy No. 248 A

AD-361918L

Operation WIGWAM

May 1955

Project 1.5

PHOTOGRAPHIC MEASUREMENTS OF SURFACE PHENOMENA



This material contains information affecting the national defense of the United States within the meaning of the espionage laws Title 18, U. S. C., Secs. 793 and 794, the transmission or revelation of which in any manner to an unauthorized person is prohibited by law.

COMMANDER TASK GROUP 7.3

CONFIDENTIAL

D-787/1

If this report is no longer needed, return it to
AEC Technical Information Service Extension
P. O. Box 401
Oak Ridge, Tennessee

AEC Technical Information Service Extension
Oak Ridge, Tennessee

WT-1009 (NOLR-1217)
(Supersedes ITR-1059)

This document consists of 106 pages
No. 248 of 250 copies, Series A

Report to the Scientific Director

PHOTOGRAPHIC MEASUREMENTS OF SURFACE PHENOMENA

By

G. A. Young
J. F. Goertner
R. L. Willey

Approved by: C. J. ARONSON
Project Officer

LT COL G. F. WATKINS, USAF
Director, Program I

Approved by: A. B. FOCKE
Scientific Director
Operation Wigwam

Explosives Research Department
Naval Ordnance Laboratory
White Oak, Silver Spring, Maryland
October 1956

This material contains information affecting the national defense of the United States within the meaning of the espionage laws Title 18, U. S. C., Secs. 793 and 794, the transmission or revelation of which in any manner to an unauthorized person is prohibited by law.

ABSTRACT

The visible surface phenomena of a nominal 30-kt nuclear weapon exploded underwater at a depth of 2000 ft were measured photographically. The direct underwater shock wave produced a slick with a 14,000-ft radius and a spray dome with a 7000-ft radius and a central height of 170 ft. The initial velocity of rise of the central portion of the spray dome was 115 ft/sec, which was 33 per cent higher than expected on the basis of high-explosive results. The first bubble pulse produced a spiky second dome that reached a height of 900 ft. Peak air-shock pressures, calculated from shock velocities, indicated an overpressure at Surface Zero (SZ) of 4.43 psi. Large possible errors in measurement, however, make this value questionable. The negative phase of the air shock wave produced a cone-shaped condensation cloud with its base at 700 ft and top at 2800 ft. The bottom-reflected shock wave formed a distinct slick, which grew to a radius of at least 34,000 ft.

Plumes appeared at 10 sec, reached a height of 1450 ft and a diameter of 3100 ft, and then spread laterally to form a large base surge. The surge expanded to a radius of 4600 ft at 90 sec and possibly more than 7000 ft at 15 min after Surface Zero Time. The maximum observed height was 1900 ft at 4 min, after which time the surge cloud was not visible on surface camera records.

The maximum wave height was 37 ft from trough to crest at a distance of 5520 ft from SZ and decreased linearly with the reciprocal of distance.

The foam ring, which probably showed the extent of contaminated surface water, was measured until 13 min, when it had reached a diameter of 10,400 ft.

Although a considerable amount of useful data was obtained, the results indicated that current knowledge of the surface phenomena of deep underwater explosions, which is based mainly on high-explosive tests, is inadequate for the prediction of most nuclear-weapon surface effects and that additional experimentation is needed for the development of better scaling laws.

PREFACE

This weapon test report summarizes the surface-phenomena measurements made by Project 1.5. Discussion of theory is held to a minimum. Some of the information presented here is incomplete, and it is felt that more information and perhaps a better understanding of the phenomena can be obtained with additional study of the Operation Wigwam photographic records.

The data presented here will be useful for the development of naval tactics, but it is clear that many of the effects do not scale to high-explosive test results in a simple manner. Since the scaling laws are not fully understood, some of the Wigwam data cannot be extrapolated to other yields and depths with confidence at the present time. It is planned to continue to study the surface phenomena of deep underwater explosions at the Naval Ordnance Laboratory to establish scaling laws for a range of operational conditions.

CONFIDENTIAL

ACKNOWLEDGMENTS

The authors wish to acknowledge the cooperation of the personnel of the Lookout Mountain Laboratory (Program VI) both before and after the test. Particular thanks are due Harold R. Albert, Jr., Charles P. Bradley, Leslie G. Elliott, and M/Sgt James T. Painter, whose efforts were essential to the success of the project. Lt Col George F. Watkins, Director of Program I, provided valuable assistance in various forms during all phases of the operation.

Naval Ordnance Laboratory personnel who assisted in the data analysis and report preparation were Sherman L. Woolley, Mary L. Milligan, Thomas Heathcote, Charles Mangold, E. Roland Kirkland, Joseph G. Connor, Jr., Shirley G. Miller, and Ethel L. Rankin. Their contributions are greatly appreciated.

CONTENTS

	Page
ABSTRACT	3
PREFACE	5
ACKNOWLEDGMENTS	7
CHAPTER 1 INTRODUCTION	13
1.1 Objectives	13
1.2 Military Significance	13
1.3 Experimental Background	14
1.4 Description of Phenomena and Theory of Scaling	14
1.4.1 Shock Effects	15
1.4.2 Mass-motion Effects	18
CHAPTER 2 EXPERIMENTAL PROCEDURE	23
2.1 Photographic Plan	23
2.2 Photogrammetry	24
2.3 Aircraft Positions	29
2.4 Recommendations	37
CHAPTER 3 RESULTS	39
3.1 Spread of Underwater Shock Waves	39
3.1.1 Direct Underwater Shock Wave	39
3.1.2 Comparison of Rates of Spread: First Visible Surface Effects and Underwater Shock Wave	42
3.1.3 Shock-wave Reflections and Bubble Pulses	47
3.2 Air Shock Wave	50
3.3 Condensation Clouds	56
3.4 Weapon Position	61
3.5 Motion of YC-473	63
3.6 Spray Domes	65
3.6.1 Description	65
3.6.2 Calculations of Underwater-shock-wave Peak Pressures	72
3.7 Plumes	74
3.7.1 Description	74
3.7.2 Discussion of Plume Formation	78
3.8 Base Surge	81
3.9 Surface Waves	85
3.10 Foam Ring	93

CONFIDENTIAL

CONTENTS (Continued)

Page

CHAPTER 4 EVALUATION OF RESULTS 98

4.1 Summary 98
4.2 Comparison with Crossroads Baker 99
4.3 Conclusions 100
4.4 Recommendations 101

ILLUSTRATIONS

CHAPTER 1 INTRODUCTION

1.1 Slick and Crack Formed by a 10-lb Pentolite Explosion 16
1.2 Surface Phenomena of a 300-lb TNT Explosion at a Depth of 85 Ft 20

CHAPTER 2 EXPERIMENTAL PROCEDURE

2.1 Positions of C-54 Photographic Aircraft 33

CHAPTER 3 RESULTS

3.1 Initial Surface Effects 40
3.2 Spread of Direct-shock-wave Effects 41
3.3 Radius of Spray Dome (Viewed from Surface Stations) Vs Time 43
3.4 Spread of First Visible Surface Effects Viewed from Aircraft 46
3.5 Observed Slicks and First Spray Dome, Sequence of Events 48
3.6 Spread of Bottom-reflected Shock Wave 49
3.7 Air Shock Wave 51
3.8 Times of Origin of Air Shock Wave 53
3.9 Air-shock-wave Velocity and Peak Overpressure 54
3.10 First Condensation Cloud 57
3.11 Pressure Drops Required for Condensation 59
3.12 Times of Formation and Dissipation of Condensation Cloud 60
3.13 Contours of ΔP_c and ΔP_s 62
3.14 Position of Weapon in Relation to Well of YC-473 64
3.15 Vertical Motion of YC-473 66
3.16 First Spray Dome 67
3.17 Tracing of Dome Profiles 68
3.18 Height of Spray Domes Vs Time 70
3.19 Second Spray Dome 71
3.20 Calculated Peak Overpressure at the Surface Vs Distance 73
3.21 Plume Formation 75
3.22 Plume Collapse 76
3.23 Plume Height Vs Time 77
3.24 Diameter of Plumes Vs Time 79
3.25 Base Surge at Early Times 80
3.26 Early Base-surge Radial Growth 82
3.27 Base-surge Contours 83
3.28 Base-surge Extent 84
3.29 Base-surge Height Vs Time 86
3.30 Base Surge at Late Times 87
3.31 Surface Waves 88
3.32 Vertical Motion of Barges with Passage of Surface Waves 90

ILLUSTRATIONS (Continued)

Page

3.33 Maximum Wave Height Vs Radial Distance 92
3.34 Surface-wave Radii Vs Time 34
3.35 Foam Ring 94
3.36 Foam-ring Diameter Vs Time 95

TABLES

CHAPTER 2 EXPERIMENTAL PROCEDURE

2.1 Cameras on YFNB's 25
2.2 Cameras on Support Vessels 26
2.3 Cameras on Aircraft 27
2.4 Relative Positions of Elements in the Wigwam Array 28
2.5 Photographic Data for YFNB Cameras 30
2.6 Photographic Data for Cameras on Support Vessels 31
2.7 Photographic Data for Aircraft Cameras 32
2.8 Radar Data for Aircraft Positions 35
2.9 Initial Horizontal Range of Photographic Aircraft from SZ 37

CHAPTER 3 RESULTS

3.1 Shock Arrival Times 44
3.2 Air-shock Data from Scaled TNT Tests 61
3.3 Apparent Horizontal Excursion of Weapon as Viewed from Different Camera Stations 63
3.4 Initial Velocity of Spray in Vicinity of SZ 69
3.5 Maximum Wave Heights 91
3.6 Wave Radii Vs Time Data 93

CHAPTER 1

INTRODUCTION

1.1 OBJECTIVES

In Operation Wigwam a nuclear weapon with a nominal yield of 30 metric kt was fired at a depth of 2000 ft in about 15,000 ft of water. The bomb was suspended from a modified barge, the YC-473, which was at the end of a 30,000-ft towline. Various other vessels were attached to the tow or maintained positions in an array surrounding the bomb support barge. The detonation occurred at 1300 PDT on 14 May 1955 at a position about 600 nautical miles west-southwest of San Diego, Calif.

Project 1.5 was established to determine the characteristics of the visible surface phenomena of the burst. The major objective of this project was the study of the slicks, spray domes, plumes, base surge, and residual cloud by means of timed technical photography. Plans were also made to measure any other important visible effects that appeared.

In addition to constituting a hazard to surface vessels and aircraft, the surface phenomena of an underwater explosion can provide information concerning the shock-wave and bubble behavior. With ideal experimental conditions the surface effects indicate the depth of the explosion, the position of the weapon, the peak pressures at the water surface from Surface Zero (SZ) to a considerable radial distance, the periods of bubble oscillation, and the phase of the bubble at the time it breaks the surface. The values calculated from photographic measurements provide a useful check on the data obtained from other types of instrumentation. In a nuclear test the measurements of the plumes and base surge are essential for the interpretation of nuclear-radiation and residual-contamination effects.

A secondary objective was to compare the Wigwam results with high-explosive data in order to check explosion theories and to determine whether simple scaling relations could be established which would be useful for the prediction of the surface effects of relatively deep nuclear detonations over a range of yields and depths.

1.2 MILITARY SIGNIFICANCE

The surface phenomena of conventional underwater explosions are not considered to be of great military importance, although some use has been made of the damaging power of the vertical jets formed by shallow explosions for the demolition of bridges.[1] Jets and plumes also constitute a hazard to low-flying aircraft. However, surface phenomena have been used primarily as a means of learning about underwater-shock-wave and bubble phenomena and for ranging the depth of explosions.[2]

On a nuclear scale the plumes are large enough to do severe physical damage. In addition, the plumes and base surge must be avoided because of the hazard due to radioactive contami-

nants. The radiological hazard may be particularly serious if the surge cloud moves into areas where ships are immobilized by blast.

1.3 EXPERIMENTAL BACKGROUND

The discussion presented in the remainder of this report will be limited to the surface effects of underwater explosions, such as Operation Wigwam, which occur deep enough so that the explosion bubble undergoes one or more complete oscillations before venting.

The surface phenomena of these relatively deep explosions were studied during and following World War I,[3,4] but the most intensive study of these effects took place during World War II. A considerable amount of work was done at the Underwater Explosives Research Laboratory, Woods Hole, Mass.,[2] and at the Marine Aircraft Experimental Establishment, Helensburgh, Scotland,[5,6] for the purpose of determining the depth of explosion of depth charges by examining the slick, spray-dome, and plume phenomena. The techniques included the measurement of the radial spread of the underwater-shock-wave disturbance at the water surface,[7] the initial velocity of rise of the spray dome,[8,9] the distribution of velocity in the dome,[5] the shape of the dome,[6,8,9] and the time of appearance of the plumes.[11] Initial dome velocities were also used as a check on peak-pressure measurements.[12,13] Extensive studies of small-charge dome and plume effects have been made,[14–16] and similar data from large charges are also available (references 1, 3, and 17–19).

In preparation for Operation Wigwam, Project 1.5 personnel at the Naval Ordnance Laboratory (NOL) conducted two series of underwater-explosion tests. The first was a group of small TNT charges fired for the study of problems involved in the photography of the spray domes and slicks. Close-up pictures were obtained showing the detailed structure of the phenomena and the effects of surface roughness. The second series consisted of twelve 300-lb TNT depth charges fired in deep water in the Chesapeake Bay at depths bracketing the scaled Wigwam condition. The results of the latter program will be reported separately by NOL.

1.4 DESCRIPTION OF PHENOMENA AND THEORY OF SCALING

The surface phenomena of relatively deep underwater explosions can be divided into two groups, those produced by the shock waves emitted at the time of the explosion and at bubble minimums and those produced by the mass motion of the water caused by bubble pulsation and venting.

The scaling of shock waves is relatively simple and is based on the principle that a change in the linear size of the charge by a factor of k means that pressures will be unchanged if distances and times are multiplied[2] by the same factor. Since the charge weight is proportional to the volume, the cube root of the charge weight can be used as a linear scale factor.

Shock-wave phenomena can therefore be scaled in the following manner:

$$\lambda_c = \frac{D}{W^{1/3}} \tag{1.1}$$

where λ_c = reduced charge depth, ft/lb$^{1/3}$
D = charge depth, ft
W = charge weight, lb

Charges of different weight exploded at the same reduced depth, λ_c, should produce similar shock-wave effects at the water surface.

This principle of similarity cannot be applied to bubble phenomena because of the effect of gravity on the motion of the bubble.[2,20] In practice the gravitational motion of a bubble is scaled in terms of the Froude number, which should be the same in both prototype and model. For this purpose the Froude number can be defined as

$$F = \frac{L}{T^2 g} \tag{1.2}$$

where F = the Froude number (dimensionless)
L = a characteristic length
T = a characteristic time
g = acceleration due to gravity

The maximum bubble radius may be used as the characteristic length, and the period of the bubble pulsation, as the characteristic time. In addition, approximate geometric similarity must be preserved between prototype and model. Experiments employing Froude scaling are performed in small test tanks since such experiments generally require reduction of the air pressure above the water surface in order to scale the total hydrostatic pressure at the depth of the explosion.[21,22]

Present techniques for the scaling of bubble behavior for a deep burst are usually adequate for only the first bubble pulsation but not for the subsequent migration of the bubble. The efforts to correlate bubble motion and venting with the size and nature of the resulting plumes have given qualitative results, but quantitative predictions of plume heights and diameters from a knowledge of bubble behavior are not possible at present.

1.4.1 Shock Effects

The shock wave produced by an underwater explosion propagates outward radially at an extremely high velocity, which decreases rapidly, approaching the speed of sound. When the shock wave reaches the surface of the water, it is reflected as a tension wave.[2,23] As the tension wave travels downward, it is superimposed on the tail of the positive phase of the shock wave, which is moving upward. The result is a net tension in the water beneath the surface, which produces cavitation. The nature of the region of cavitated water is not fully understood, but its thickness is dependent, in part, on the tensile strength of water. The reported values of the tensile strength of water vary within wide limits, depending on experimental conditions, but there is evidence that it reaches low values and is not uniform in turbulent sea water that contains dissolved gases.[14]

Published descriptions of the first visible effects that appear at the water surface after a moderately deep underwater explosion are not consistent. This disagreement may be due, in part, to real differences in physical effects, the nature of which is not fully understood. In some cases, however, differences in the angle of view and light conditions may be responsible for the discrepancies in the literature. In addition, the high-speed photography required for proper resolution has not always been available.

The following is an attempt to present a consistent, though somewhat simplified, description of the surface phenomena resulting from the shock wave. A detailed study in the future may reveal complexities not considered here.

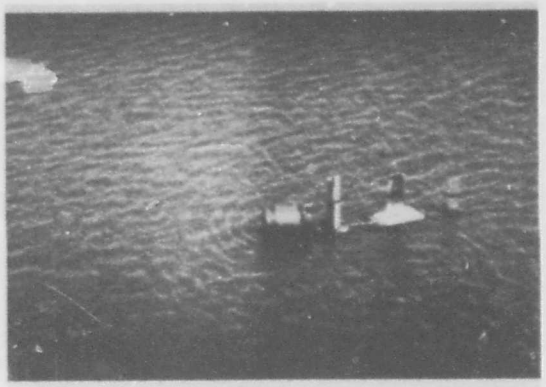
The first visible effect on the surface after an underwater explosion is a circular patch of darkened water, sometimes called the "slick,"[2] which spreads across the water at an extremely rapid rate, representing the intersection of an expanding sphere (the shock wave) with a plane (the water surface). Following just behind this darkened region is a white circular patch, which has been called the "crack" by British authors.[14] Evidence exists that the surface of the water is initially undisturbed and, therefore, that the whiteness occurs underwater, probably as a result of the cavitation produced by the tension wave.

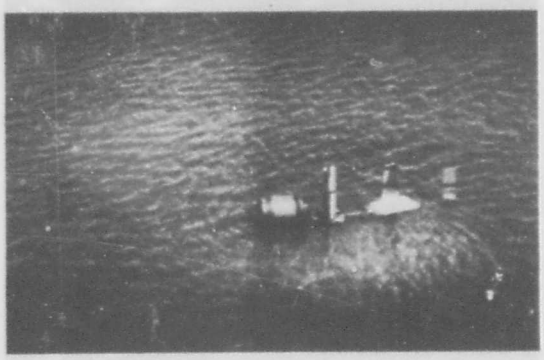
The appearance of the slick and the crack, as recorded on a small-scale test conducted in preparation for Operation Wigwam, is illustrated in Fig. 1.1. The charge was a 10-lb pentolite cone, and the camera was an Eastman High Speed, aimed at an angle of 23 deg from the horizontal. The figure gives experimental details.

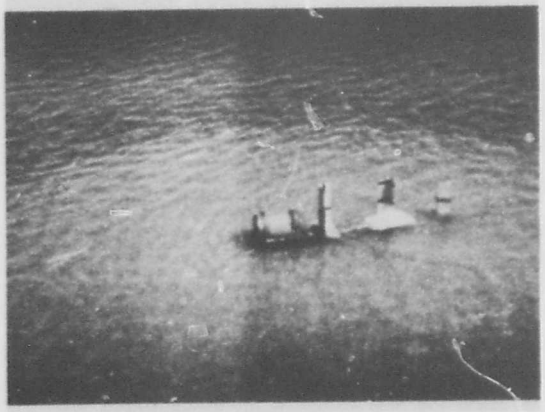
The record is not typical since the majority of tests showed only the whitened patch and not the slick. This result indicates the importance of photographic variables such as lighting and viewing angles for obtaining a complete history of the surface phenomena.

For practical purposes the leading edge of the slick closely represents the front of the expanding underwater shock at its intersection with the surface of the water. Geometrical considerations indicate that the velocity of spread is a function of charge depth, and measurements

CONFIDENTIAL







CHARGE:
10-LB PENTOLITE TAPERED CONE
LENGTH:
48 INCHES
DIAMETER:
LARGE END = 3 INCHES
SMALL END = 3/4 INCH
SUSPENDED VERTICALLY WITH SMALL END UP.
SMALL END 5 FEET BENEATH THE SURFACE.

WATER DEPTH:
19 FEET

SCALE:
HEIGHT OF VERTICAL SCALE MARKER NEXT TO 5 GALLON CHARGE SUPPORT CAN = 16 INCHES

CAMERA:
EASTMAN HIGH SPEED
HEIGHT ABOVE WATER:
16.4 FEET
HORIZONTAL DISTANCE:
38.1 FEET
ANGLE WITH HORIZONTAL:
23 DEGREES
CAMERA SPEED:
ABOUT 1000 FRAMES/SEC

Fig. 1.1—Slick and crack formed by a 10-lb pentolite explosion.

CONFIDENTIAL

of the rate of growth of the surface disturbance have been used to determine the depth of explosions.[7]

Shortly after the crack appears, the central region of cavitated water above the explosion rises vertically to form a white mound of spray. This is due to the particle velocity imparted to the water surface by the reflection of the shock wave and the subsequent breakup of the surface layer into drops of spray.

The particle velocity at a shock front is given by the expression

$$u = \frac{P}{\rho U} \tag{1.3}$$

where u = particle velocity, ft/sec
P = peak overpressure in the shock wave, lb/ft^2
ρ = ambient density of the water, slugs/ft^3
U = shock-front propagation velocity, ft/sec

Directly above the charge the initial vertical velocity of the spray is equal to the sum of the particle velocities imparted by the incident and reflected shock waves. These are assumed to be equal in magnitude and are directed upward. Therefore

$$V_0 = \frac{2P}{\rho U} \tag{1.4}$$

where V_0 = initial vertical velocity of spray, ft/sec.

For a clearly defined spray dome to form, cavitation must take place in the water, which means that the tension wave must be strong enough to rupture the water. The vertical spray velocity is therefore reduced as a result of the work done in cavitating the water. For greater accuracy Eq. 1.4 should be modified to

$$V_0 = \frac{2P - T}{\rho U} \tag{1.5}$$

where T = effective tensile strength of water, lb/ft^2.

At positions away from SZ the velocity of a particle at the surface is the resultant of the vertical components of the particle velocities in the incident shock wave and reflected tension wave. The initial spray velocity is therefore given completely by

$$V_0 = \frac{(2P \cos \theta) - T}{\rho U} \tag{1.6}$$

where θ = the angle with the vertical of the line from the explosion to the point on the surface.

A small error is introduced in the foregoing equations by the assumption that perfect reflection occurs at the water surface. However, the correction due to this factor is usually negligible.

The correct value of T to be employed in Eqs. 1.5 and 1.6 has not been established. When determined indirectly, T was seen to decrease as the size of the charge was increased,[13] indicating a dependence on the duration of the shock wave. Since the significance of the tensile strength of water in the formation of the crack, dome, and black ring is not clearly understood, indirect methods of determining this may possibly give misleading results.

Theory, first developed by Taylor,[24] shows that an accelerated liquid surface is unstable if the acceleration vector is directed into the liquid.[14,25] It is this instability which accounts for the breakup of the water surface into drops of spray.

The initial velocity of rise of spray has been measured for the purpose of determining the depth of explosion of a charge of known weight[8,9] and as a check on the peak pressure of the

CONFIDENTIAL

underwater shock wave.[12,13] These methods have been successful; however, it has been noted in some high-explosive tests that the initial spray velocity is significantly higher than expected on the basis of Eq. 1.4. After a brief interval, e.g., 0.1 sec for 300 lb of TNT at a depth of 40 ft, the velocity levels off at a value approximately equal to that shown by Eq. 1.4. The high initial velocities have not been fully explained.

Spray-dome heights decrease with increasing charge depth but show a tendency to increase with increasing charge weight when charges are fired at the same reduced depth, although the peak pressure at the surface remains constant in the latter case.

This might be explained on the basis of the thickness of the surface layer of water which is separated by the shock-wave reflection. Since the thickness increases with charge weight, it appears likely that larger droplets are formed by the breakup of the thicker layers. The larger droplets are retarded less by atmospheric drag and reach a greater height than those of smaller size.

Spray-dome diameters increase with increasing charge depth, and, since the heights decrease, the dome profiles become flatter. Consequently measurements of the shape of the spray dome have been used as a technique for determining the depth of explosions.[6,8,10]

It has been noted that dome diameters are greater in rough water than in calm water and that the structure of the dome is striated as if it were conforming to the wave pattern originally present in the water.[14]

If a charge is exploded at a great depth, scattered patches of spray may form instead of a continuous dome.[26]

The dome is surrounded by a region called the "black ring" or "dark ring,"[14] where small isolated jets or spikes of water can be seen. The dark appearance is an optical effect due to reduced regular reflection of light and depends on the position of the observer. Cameras at high elevations usually do not record a clearly defined dark ring, and under some lighting conditions the ring even appears lighter than the surrounding water.[14] The dark ring is more sharply defined in calm water than in rough water. Close-up photographs have shown that the jets of water seem to form mostly on wave crests or inhomogeneities in the water.

The exact nature of the dark ring is not understood. Its outer edge corresponds to a vertical component of peak pressure about one-half that at the edge of the spray dome. Several theories have been proposed to account for the black ring, along with the other surface phenomena caused by the shock wave.[14] However, none of these appears to explain all the observed effects.

After the primary shock wave is emitted by an underwater explosion, the gaseous bubble of explosion products oscillates and emits a secondary pressure wave each time it reaches a minimum size. These pressure waves may be visible as secondary slicks[26] and may cause the formation of secondary spray domes.[2,17] In many cases the second dome remains hidden within the primary dome.

1.4.2 Mass-motion Effects

If the depth of explosion is not too great and the bubble reaches the surface while it is still oscillating, spectacular plume formation may occur. The phenomena are complex, with some plumes being formed by bubble motion before venting occurs and others by the actual breakthrough of the gases. (Venting may occur with the internal gas pressure either higher or lower than atmospheric pressure. In the former case, explosion products are ejected rapidly; in the latter, the initial gas flow is inward.[16]) Plumes may also be formed by the collapse of the bubble cavity at the water surface. Usually two or more stages of plume development are discernible.

Bubble migration is most rapid when the bubble is at a minimum size. Consequently a bubble that vents near its minimum size forms a narrow vertical jet that rises at a high speed. A bubble venting near its maximum size forms a low, broad vertical plume accompanied by extensive radial or lateral plumes.[17]

The vertical plumes are thought to be due to the upward mass motion of water which accompanies the migrating bubble (references 1, 17, 27, and 28). The initial velocities and maximum heights of these plumes vary with the depth of detonation for a particular charge

CONFIDENTIAL

size, the vertical plumes being highest when a bubble minimum occurs near the water surface.[17]

The time of emergence of the vertical plume does not increase continuously with charge depth; the discontinuous increments correspond roughly to the successive periods of bubble pulsation.[1,27]

The radial plumes are considered to be primarily due to the expansion of the explosion gases on venting. Radial plumes may also be projected as the cavity in the water collapses; two successive projections of radial plumes have sometimes been observed. The radial plumes appear either simultaneously with, or later than, the vertical plume.[17]

The plumes formed by a bubble that approaches the surface while it is expanding have characteristics different from the plumes formed by a bubble that approaches the surface while contracting.[27] The time interval between successive plume phases also depends on the state of the bubble motion when it approaches the surface.[11] Factors such as these, if placed on a satisfactory quantitative basis, may have value for the determination of bubble behavior when timed photographs of plume phenomena are the only explosion data available.

Since the time of appearance of the first plumes is not a continuous function of charge depth, the measurement of these times is not a good method for determining the depth of an explosion.[27] In addition, the value on this method is limited because plume times are highly variable for charges fired at a constant depth.[8]

If bubble oscillation has been damped appreciably by the time the bubble reaches the surface, the first visible effect following the spray dome is an upheaval of the water surface. This may be followed by the emergence of small radial plumes. At still greater depths of burst, the bubble probably breaks up into small bubbles that rise to the surface at a constant speed.[15,29]

When the plumes formed by an underwater explosion collapse, the larger droplets and masses of water fall back to the underlying surface, but the smaller droplets remain suspended in the air. This aerosol spreads outward radially from the base of the falling plumes and forms a torus-shaped cloud, known as the base surge.

After the plumes have subsided and the base surge has dissipated or drifted away, a relatively smooth patch of darkened water remains above the position of the burst. The smooth area is enclosed by a ring of foam and debris which expands slowly. The patch is sometimes referred to as a "carbon slick" because it contains carbon or other materials brought to the surface by the rising bubble. The carbon slick may be observed when the detonation is so deep that few or no other surface effects occur.

An underwater explosion also generates surface waves, which radiate from the area of bubble breakthrough. Waves from deep explosions are generated principally by the oscillation of the water cavity resulting from the venting of the bubble.[30]

It is not possible to scale both the spray-dome and plume phenomena of a large burst with small charges fired at one depth. For example, on the basis of a 30-metric-kt effective yield, the Wigwam slick and dome phenomena can be scaled by firing a 300-lb TNT charge at a depth of 33 ft. The explosion bubble will vent after it has completed one oscillation and is in the expanding phase of the second oscillation.[17]

To simulate the Wigwam plumes with 300-lb TNT charges, it was necessary to fire at greater depths since it had been predicted that the Wigwam bubble would vent shortly after completing three oscillations. Depths ranging from 65 to 100 ft were investigated.

An explosion at a depth of 85 ft formed a bubble that vented shortly after its third oscillation was completed. The surface phenomena are shown in Fig. 1.2. The dome rose with an initial velocity at the center of about 31 ft/sec and reached a height of 15 ft and a diameter of 240 ft. Previous work had indicated that the three bubble periods[17] for a burst at this depth would be about 0.56, 0.48, and 0.47 sec, making a total of 1.51 sec. (These should not be considered to indicate scaled values for the Wigwam bubble periods. Scaling of the Wigwam bubble motion was not attempted in these experiments.) The water surface started to rise about this time, and the bubble broke through to form a group of radial plumes, which reached a maximum height of 65 ft. The plumes settled and formed a well-defined base surge.

This test and data from other sources were used as a guide for predicting the nature and size of the Wigwam plumes and base surge.

CONFIDENTIAL

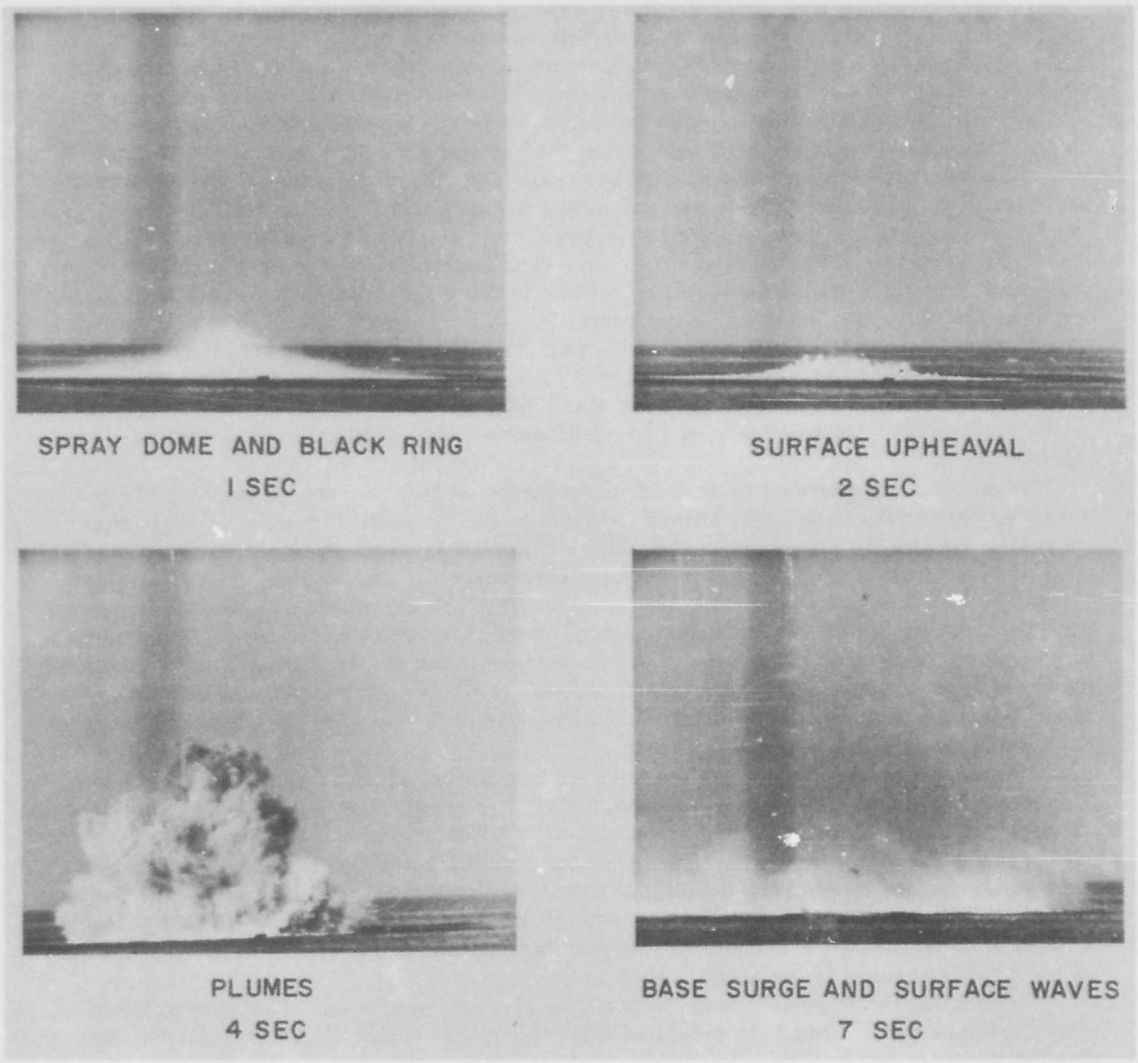


Fig. 1.2—Surface phenomena of a 300-lb TNT explosion at a depth of 85 ft.

REFERENCES

[References 3–6, 13, 23, 27, 29, and 30 have been reproduced in Underwater Explosion Research, a compendium of British and American reports, Office of Naval Research, 1950.]

1. W. Wunderlich, Introduction to the Theory of Underwater Explosions, Chemical-Physical Research Institute of the German Navy, David W. Taylor Model Basin Translation 208, July 1948. (Confidential)
2. R. H. Cole, "Underwater Explosions," Princeton University Press, Princeton, N. J., 1948. (Unclassified)
3. H. W. Hilliar, Experiments on the Pressure Wave Thrown Out by Submarine Explosions, Admiralty Experimental Station, 1919. (Unclassified)
4. G. W. Walker, Analysis of the Spray Dome, Mine Design Department. Admiralty, 1919. (Unclassified)
5. R. A. Shaw, A Method of Determining the Depth of Underwater Explosions, Marine Aircraft Experimental Establishment, Scotland, December 1941. (Unclassified)
6. R. A. Shaw, A Further Investigation into the Dome Analysis Method of Determining the Depth of Underwater Explosions, Marine Aircraft Experimental Establishment, Scotland, April 1942. (Unclassified)
7. R. R. Halverson, Methods of Ranging the Depth of Explosion of Aerial Depth Bombs. III. The Shock-wave Spread Method, Div. 2 Interim Report on Underwater Explosives and Explosions, UE-26, Report OSRD-4259, October 1944. (Confidential)
8. C. L. Pekeris, Determination of Depth of Explosion of Statically Fired Depth Bombs from Photographs of the Dome of Spray, Columbia University, OSRD Div. 6, Sec. 6.1, June 1944. (Confidential)
9. R. R. Halverson, Methods of Ranging the Depth of Explosion of Aerial Depth Bombs. II. The Dome Velocity Method, Div. 2 Interim Report on Underwater Explosives and Explosions, UE-25, Report OSRD-4149, September 1944. (Confidential)
10. R. R. Halverson, The Dome-ratio Method of Determining the Depth of an Underwater Explosion, Div. 2 Interim Report on Underwater Explosives and Explosions, UE-33, Report OSRD-5160, May 1945. (Confidential)
11. Determination of Depth by Time Interval Method, Div. 2 Interim Report on Underwater Explosives and Explosions, UE-28, Report OSRD-4407, December 1944. (Confidential)
12. A. B. Arons and A. M. Shanes, Measurement of Shock Wave Peak Pressure by the Dome Velocity Method, Div. 2 Interim Report on Underwater Explosives and Explosions, UE-27, Report OSRD-4406, November 1944. (Confidential)
13. D. A. Wilson, B. A. Cotter, and R. S. Price, The Determination of Peak Pressure of an Underwater Explosion from a Study of the Initial Dome Velocity, Report NAVORD-13-47, May 1947. (Unclassified)
14. H. Kolsky, J. P. Lewis, M. T. Sampson, and C. I. Snow, Splashes from Underwater Explosions. Part II. Domes from Deep Charges, Imperial Chemical Industries Limited, Report UNDEX-163, October 1945. (Confidential)
15. H. Kolsky, J. P. Lewis, M. T. Sampson, and C. I. Snow, Splashes from Underwater Explosions. Part III. The Bubble, Imperial Chemical Industries Limited, Report UNDEX-170, October 1945. (Confidential)
16. C. O. J. G. Palmer, Phenomena Associated with Small Underwater Explosions, Naval Construction Research Establishment, Report UNDEX-263, November 1950. (Confidential)
17. C. P. Slichter, W. G. Schneider, and R. H. Cole, Measurement of Bubble-pulse Phenomena, Report OSRD-6242, March 1946. (Confidential)
18. Note on the Time Intervals from the Appearance of the Slick to the Appearance of Plumes Following an Underwater Explosion, Div. 2 Interim Report on Underwater Explosives and Explosions, UE-33, Report OSRD-5160, May 1945. (Confidential)
19. H. M. Schauer, The Plumes Caused by Underwater Explosions, Underwater Explosions Research Unit, Norfolk Naval Shipyard, Report UERD-5-48, 1948. (Unclassified)

20. H. G. Snay, Possibilities of Studying Bubble Migration on a Small Scale, Fourth Conference on Research on Ship Protection Against Underwater Explosions, Report NAVSHIPS-250-423-14, December 1951. (Confidential)
21. J. F. Goertner, Vacuum Tank Studies of Underwater Explosion Bubbles Scaled to the Nuclear Range, Report NAVORD-3714, April 1954. (Secret)
22. J. F. Goertner, Vacuum Tank Studies of Gravity Migration of Underwater Explosion Bubbles, Report NAVORD-3902, March 1956. (Confidential)
23. E. N. Fox, "A Review of Underwater Explosion Phenomena," Cambridge University Press, New York, 1947. (Unclassified)
24. G. I. Taylor, The Instability of Liquid Surfaces When Accelerated in a Direction Perpendicular to Their Planes, Part I, Proc. Roy. Soc. (London), 201A: 192 (1950). (Unclassified)
25. J. B. Keller and I. Kolodner, Instability of Liquid Surfaces and the Formation of Drops, J. Appl. Phys., 25: 918-921 (July 1954). (Unclassified)
26. J. E. Eldridge, Surface Phenomena Following Underwater Explosions, Div. 2 Interim Report on Underwater Explosives and Explosions, UE-20, April 1944. (Confidential)
27. G. K. Hartmann, The Relation Between the Appearance of the Plumes and the Gas Globe Behavior in Underwater Explosions, Naval Ordnance Laboratory, 1947. (Unclassified)
28. A. B. Ward, On the Time Interval Between an Underwater Explosion and the Appearance of the Plume, Mine Design Department, Report UNDEX-41, July 1943. (Confidential)
29. H. N. V. Temperley and Ll. G. Chambers, The Rate of Rise of Large Volumes of Gas in Water, Admiralty Undex Works, Rosyth, Scotland, January 1945. (Unclassified)
30. W. G. Penney, Gravity Waves Produced by Surface and Underwater Explosions, Report UNDEX-119, March 1945. (Unclassified)

CHAPTER 2

EXPERIMENTAL PROCEDURE

2.1 PHOTOGRAPHIC PLAN

In preparation for the technical photography, predictions were made of the times of appearance, rates of growth, and maximum sizes of the expected surface phenomena. Initially it was assumed that the shock wave would resemble that formed by the explosion of 30 metric kt of TNT at a depth of 2000 ft. Thus the slick and spray-dome phenomena could be estimated by using data obtained from TNT charges exploded at the same reduced depth, $\lambda_c = 4.95$ ft/lb$^{1/3}$. When more refined shock-wave predictions became available, these introduced changes in the estimated effects, but they were not of sufficient magnitude to necessitate changes in the photographic plan.

The predictions of bubble phenomena made by Project 1.1 were used as a basis for estimating the magnitude of the plumes and base surge. It had been predicted that the Wigwam bubble would oscillate three times and vent at a minimum size. Therefore the plume phenomena of high-explosive charges fired at depths that would permit three bubble oscillations before venting occurred were extrapolated to the Wigwam scale.

The predictions were used as a basis for the selection of cameras and lenses. However, since the scaling techniques were uncertain, the photographic plan was formulated so that adequate records would be obtained even if the results were radically different from those predicted. In addition, extra cameras were included as backups in case of equipment or power failure, particularly on the unmanned stations.

Camera stations were established by the Lookout Mountain Laboratory (LML) on the three YFNB's towed in the array, on the USS Mt. McKinley, the USS Fort Marion, and the USS Curtiss, and on three C-54 aircraft. On each YFNB the cameras were housed in an 8-ft, cubical, steel-reinforced plywood house. Shock mounting was accomplished by resting each house on aircraft tires partially filled with sand. Upward motion was restrained by securing each house to the deck with cables, each linked to a small tire under tension. Lateral motion was prevented by vertical pipes, which were welded to the deck at each corner of the house. Power was supplied to the YFNB cameras from 24-volt batteries located in a box secured to the deck.

The cameras on the Mt. McKinley, Curtiss, and Fort Marion were on tripods or special mounts secured to the decks and were powered by the ships' generators, except for the Fairchild F-56 cameras, which were battery operated.

The aircraft cameras were mounted in specially designed racks, which permitted one operator to aim from three to six cameras simultaneously. The planes' generators were used to supply the cameras with power, which was converted and stepped up as required.

The starting of all cameras was automatic, with provision for manual starting if the equipment failed. A Multiflex sequence timer, started by the −15-sec radio time signal, operated relays to start and stop all except the Fastax high-speed cameras, which were started by the

CONFIDENTIAL

– 5-sec pulse, the length of running time being controlled by a Microflex interval timer. The Multiflex and Microflex timers were manufactured by the Eagle Signal Corp., Moline, Ill.

All but a few of the motion-picture films obtained for Project 1.5 were timed with marks placed on the edges by neon lamps flashing at 0.02- and 0.5-sec intervals. The 0.02-sec marks were controlled by an electrically driven tuning fork at each camera station and ran for the entire length of each film record. The 0.5-sec marks were controlled by the Edgerton, Germeshausen & Grier, Inc. (EG&G), radio-transmitted fiducial signal, which started shortly before detonation. [The zero radio-transmitted fiducial signal was reported by Program V (EG&G) to have occurred 29 ± 1 msec before the detonation.[1] However, Project 1.2.1 found that the interval of 29 msec was inconsistent with the measured shock-wave arrival times at the pressure gauges suspended from the YC; these data indicated that radio fiducial zero time occurred about 12.5 msec before detonation.[2] At the time of writing this discrepancy is unresolved.] The F-56 aerial camera records were timed by a small clock photographed in the corner of each frame.

The cameras operated on the test for Project 1.5 and the pertinent photographic data are listed in Tables 2.1 to 2.3; the Program VI documentary coverage of the test is also listed (cameras not having NOL numbers). In the Tables, times are measured from the first appearance of visible surface effects. For the purposes of this report, this is defined as surface zero time (SZT).

The degree of success of the technical photography is difficult to evaluate numerically. A total of 43 cameras were used, 35 of which yielded records that were at least partially useful.

The YFNB cameras were not pointing directly at the explosion, and many did not show the desired phenomena. No records were obtained from timed cameras on the YFNB-12. In addition, several records were incomplete as a result of temporary power failures on the Fort Marion and the Mt. McKinley. These losses necessitated additional combining of data from various sources in order to obtain a complete description of the surface phenomena.

The records obtained on the photographic aircraft were the most complete, but detailed analysis of these was limited by inaccurate knowledge of the plane positions at all times (Sec. 2.3).

In general, the starting and timing systems operated satisfactorily, although there were a few malfunctions in both systems. The 0.5-sec marks were somewhat erratic, but at only one station, the YFNB-29, were they completely absent from the camera records. Also, no 0.5-sec time signals were transmitted during the period from 8.5 sec to about 50 sec after radio fiducial zero time owing to power failure on the Mt. McKinley.[1] Power was resumed at about 30 sec after SZT, but the time signals did not start immediately. Comparison of the 0.02- and 0.5-sec timing marks, where possible, indicated agreement to within 1 part in 1000, provided that the time interval compared to minimize the error introduced by any one mark was long enough. In some cases this error was as large as 2 or 3 msec and occurred notably on the records from the G aircraft station.

On records F-1 and F-2 a spurious 2-cycle timing mark appeared 0.17 sec before radio fiducial zero time. In addition, the zero fiducial time signal was missing. (The other F station record with 2-cycle timing, F-4, was not examined.)

2.2 PHOTOGRAMMETRY

Length scales were established on the photographic records by using the distances between cameras and subject and the focal lengths of the lenses. The positions of the surface camera stations relative to SZ, taken as the position of the YC-473 at H-hour (see Sec. 3.4), and to some of the other elements in the array were determined by Project 1.2 (reference 3) and Project 1.5 personnel from deductions based on shock-wave arrival times (detonation was taken as occurring 13 msec after the zero fiducial radio-transmitted time signal), aerial photographs, surface photographs, and ship-borne radar. These data are presented in Table 2.4, along with the headings of some of the vessels at H-hour. The distances given in Table 2.4 for elements of the tow (M-boats, YFNB's, and Squaws) are considered accurate to about ±50 ft; distances for ships, to about ±1 per cent; and angular measurements, to about ±2 deg.

Table 2.1 — CAMERAS ON YFNB's

Camera position*	NOL camera No.	LML film No.	Camera model	Nominal frame rate, frames/sec	Nominal focal length, mm	End of record (approx. time after SZT)	Remarks
YFNB-12	A-1		35-mm Mitchell	100	152		Relay malfunction
5440 ft, 352°T	A-2		35-mm Eyemo	24	75		Relay malfunction
	A-3		16-mm Fastax	1000	50.8		Relay malfunction†
	A-4		16-mm Bell & Howell	64	150		Relay malfunction†
	A-5		35-mm Bell & Howell	24	24		Relay malfunction
	A-6	RKF 644	16-mm Maurer	64	25	4 min	Relay malfunction‡
	A-7		35-mm Mitchell	100	305		Relay malfunction
YFNB-13	B-1	MZF 51	35-mm Mitchell	100	152	1 min	
7870 ft, 360°T	B-2	MAG 2	35-mm Bell & Howell	24	25	10 min	
	B-3	RKF 642	16-mm Bell & Howell	24	17	10 min	
	B-4	RZF 5	16-mm Fastax	1000	50.9	10 sec	†
	B-5	RKC 196	16-mm Bell & Howell	64	150	1 min	†
	B-6	MAF 29	35-mm Eyemo	24	100	4 min	
		RKF 646	16-mm Maurer	64	63	1.5 sec	Camera malfunction
			K-24	½	305		
YFNB-29	C-3	7LCI 11	F-56 Fairchild	½	209.2	8 min	
10,860 ft, 002°T	C-3A	7LCI 1	F-56 Fairchild	½	212.9	6.5 min	
	C-5	RKC 187	16-mm Bell & Howell	64	152	1 min	†
	C-6	MAG 3	35-mm Bell & Howell	24	75	10 min	
		RKF 658	16-mm Maurer	30	63		
		DPY 5	K-24		305		

*Radial distance and bearing from YC.

†Camera aimed at water surface directly behind YFNB.

‡Camera started approximately 1 sec late with arrival of initial shock wave.

CONFIDENTIAL

Table 2.2—CAMERAS ON SUPPORT VESSELS

Camera position*	NOL camera No.	LML film No.	Camera model	Nominal frame rate, frames/sec	Nominal focal length, mm	End of record (approx. time after SZT)	Remarks
USS Fort Marion	D-2	MAF 30	35-mm Eyemo	24	100	6 sec	Partial record†
33,600 ft,	D-3	7LCI 23	F-56 Fairchild	½ and 1/10	508	10 min	Partial record†
350°T	D-3	7LCI 18	F-56 Fairchild	½	508	19 min	Second load‡
	D-3A	7LCI 22	F-56 Fairchild	½ and 1/10	508	7 min	Partial record†
	D-4	RKF 661	16-mm Bell & Howell	24	75		Camera malfunction
USS Curtiss	E-1	MAF 32	35-mm Eyemo	48	300	15 sec	Camera malfunction
34,350 ft,	E-2	7LCI 2	F-56 Fairchild	1/3 and 1/10	210.7	25 min	
303°T	E-3	7LCI 19	F-56 Fairchild	½	1016	6 min	
	E-3	7LCI 3	F-56 Fairchild	1/10	1016	29.5 min	Second load
	E-3A	7LCI 4	F-56 Fairchild	½ and 1/10	1016	6.5 min	
	E-5	MZF 52	35-mm Mitchell	100	1219	1 min	
		DPY 11	K-24	~1	508		
USS Mt. McKinley	F-1	MAF 39	35-mm Eyemo	24	450	2 min	Partial record†
30,600 ft,	F-2	MAG 4	35-mm Bell & Howell	24	152	10 min	Partial record†
060°T	F-3	7LCI 15	F-56 Fairchild	1/10	212	26.5 min	
	F-4	RKF 643	16-mm Bell & Howell	24	17	10 min	Partial record†
		DPY 8	K-24	~1	508		Partial record†

*Radial distance and bearing from YC.

†Cameras stopped running when arrival of bottom-reflected shock wave caused failure of ship's power.

‡Four minutes between loads.

CONFIDENTIAL

Table 2.3—CAMERAS ON AIRCRAFT

Camera position	NOL camera No.	LML film No.	Camera model	Nominal frame rate, frames/sec	Nominal focal length, mm	End of record (approx. time after SZT)	Remarks
Plane 5561	G-1	MZG 10A	35-mm Fastax	1000	50	3 sec	Every other frame blurred
Initially* at							
17,600 ft,	G-2	MZF 65	35-mm Mitchell	100	305	1 min	
218°T	G-3	MZF 66	35-mm Mitchell	100	50	1 min	
	G-4	MZF 67	35-mm Mitchell	100	18.5	1 min	
	G-5	7LCI 30	F-56 Fairchild	½	210.2		Film light struck
		DPY 17	K-24	Max.	177.8		Blank record
		DPY 22	K-24	~½	304.8		
		RKC 18	16-mm Bell & Howell	48	18		Blank record
		RKC 19	16-mm Bell & Howell	64	25		
Plane 5482	H-1	MZF 70	35-mm Mitchell	100	152	1 min	
Initially* at	H-2	MZF 71	35-mm Mitchell	100	50	1 min	
21,400 ft,	H-3	7LCI 33	F-56 Fairchild	½	212.7	12.5 min	
087°T	H-4	RKF 631	16-mm Mitchell	24	25	5 min	
		DPY 23	K-24	~½	177.8		
		DPY 24	K-24	Max.	304.8		
		RKC 20	16-mm Bell & Howell	24	17		
		RKC 21 & 25	16-mm Bell & Howell	64	76.2		
Plane 5615	J-1	MZF 72	35-mm Mitchell	100	18.5	1 min	
Initially* at	J-2	MZF 73	35-mm Eyemo	48	25	1½ min	
22,000 ft,	J-3	7LCI 35	F-56 Fairchild	1/10	211	14 min	
279°T	J-4	RKF 632	16-mm Mitchell	64	15	4 min	
		DPY 26	K-24	Max.	305		
		DPY 27	K-24	Max.	508	~1 min	
		RKC 22	16-mm Bell & Howell	64	25		
		RKC 23	16-mm Bell & Howell	32	63		
RB-50 No. 162 5000-ft altitude (above clouds)		MAF 24	35-mm Eclair	36	50		

*Radial distance and bearing from YC at time of appearance of first surface effects.

CONFIDENTIAL

Table 2.4 — RELATIVE POSITIONS OF ELEMENTS IN THE WIGWAM ARRAY

Vessel	Distance from YC, ft	True bearing from YC, deg	True heading of vessel, deg
Position of Elements Relative to the YC at H-hour			
O-1 M-boat	2,150	008	
A-2 M-boat	3,400	360	
O-2 M-boat	3,650	359	
YFNB-12: Camera station A	5,440		
Center of YFNB	5,520	352	333
NOL[3] EPT string	5,600		
Mast	5,610		
YFNB-13: Camera station B	7,870		
Center of YFNB	7,950	360	349
NOL[3] EPT string	8,030		
Mast	8,040		
Squaw-29	10,200	002	
YFNB-29: Camera station C	10,860		
Center of YFNB	10,950	002	007
NOL[3] EPT string	11,030		
Mast	11,040		
USS Fort Marion: Camera station D	33,600	350	017
USS Curtiss: Camera station E	34,350	303	000
USS Mt. McKinley: Camera station F	30,600	060	000
USS McKean	32,000	274	
USS Small	31,000	091	
Distances of Objects from the YFNB-29 Camera Station at H-hour			
O-2 M-boat: A frame	7,220		
Bow ramp	7,170		
YFNB-12: Loudspeaker	5,550		
Center of YFNB	5,470		
Mast	5,400		
YFNB-13: Loudspeaker	3,000		
Center of YFNB	2,900		
Mast	2,820		

The cameras on the YFNB's were aimed dead astern from a position located about 42 ft forward of the stern and about 10 ft to starboard of the centerline, at an average elevation of about 27 ft above the surface of the ocean. On the support vessels the approximate camera elevations above the water surface were: Fort Marion, 34 ft; Curtiss, 59 ft (E-1 and E-2) and 52 ft (E-3, E-3A, and E-5); and Mt. McKinley, 57 ft.

The distance between each camera station and the visible horizon was computed by use of Eq. 2.1, which takes into account the refraction of light due to atmospheric conditions.[4] The formula is based on the meteorological data obtained on the Curtiss at 1348 PDT (Sec. 3.3).

$$S = 1.16\sqrt{z} \qquad (2.1)$$

where S = distance from camera to horizon, nautical miles, and z = height of camera, ft. In all cases the measured phenomena were between the cameras and the horizon.

Most of the lenses used for the technical photography were calibrated to obtain the equivalent focal length and/or a calibrated focal length.[5,6] All but one of the motion-picture cameras were calibrated at EG&G by photographing a collimated light source, the parallel beam being split by a prism to form two beams separated by a known angle. For these tests the camera

CONFIDENTIAL

speed was the same order of magnitude and the lens aperture about the same as those used for photographing the Wigwam shot. The remaining motion-picture camera, E-5, was calibrated at the Naval Ordnance Test Station. The 8¼-in. focal length F-56 aerial cameras were calibrated at the National Bureau of Standards by photographing a bank of collimators spaced at known angles. The longer focal length F-56 cameras were calibrated visually by placing an illuminated scale in the focal plane and measuring with a telescope the angular deviations of the pencils of light emerging from the camera objective.[6,7]

All the times given in this report are measured from the time of the first appearance of visible surface phenomena (SZT), except for the arrival times of the shock wave at the water surface and at various elements of the array. These latter times are measured relative to the radio-transmitted zero fiducial time signal.

The available photographic and timing data for the NOL cameras that functioned on the test are given in Tables 2.5 to 2.7. In these tables the zero frame is defined as the first frame in each record to show any surface effects. The times of the zero frames are given relative to SZT, which was determined by extrapolating the development of the surface phenomena backward.

In the record analysis certain sources of photogrammetric error were neglected. Among these were film shrinkage and movement of the surface craft. Film shrinkage[5] can amount to about 0.5 per cent. Since all measurements were made from positive film or paper prints, such errors were introduced twice. Movement of the surface craft, both relative and absolute, during the period of measurement was certainly slight, judging from radar measurements by Project 2.8 of the movement of the tow relative to an anchored skiff.[8] In most cases these sources of error were considerably less serious than those introduced by uncertainties in the initial camera distances and/or poorly or irregularly defined phenomena.

Measurements were made from continuous-strip contact prints of the F-56 camera records and from tracings of the projected images of the 35-mm records. A Recordak microfilm reader, which projected the image from behind on a translucent screen, was modified by replacing the screen with clear plastic and adding a frame counter. Measurements were also made directly on the translucent screen of a 35-mm Moviola film viewer.

2.3 AIRCRAFT POSITIONS

The three C-54 photographic aircraft (camera stations G, H, and J) were to have been at radial distances of 10,000, 15,000, and 20,000 ft, respectively, from SZ at H-hour, with H to starboard and G and J to port of the tow; all aircraft were then to circle SZ in a counterclockwise direction for the duration of the surface phenomena. The planes were positioned by instructions from a controller using ship-borne air-search radar from the Mt. McKinley. Air-search radar was also used on the Mt. McKinley, the McKean, and the Small to track the plane positions as functions of time. These radarscopes, along with a frame counter and a clock, were photographed once each sweep by cameras synchronized with the antennas.[9]

In addition, the McKean and the Small were to have followed the C-54 photographic aircraft with locked-in fire-control radar systems that present the range and bearing of particular planes numerically on a data panel. However, none of these data were obtained since there was equipment failure on the Small upon shock-wave arrival and the McKean tracked other aircraft.

Figure 2.1 shows aircraft positions vs time, as measured from photographs of the air-search radarscopes on the McKean, the Mt. McKinley, and the Small; these data are given in Table 2.8. Ranges and bearings were measured to the center of the near side of the scope image of each aircraft in order to minimize the errors caused by beam-width and pulse-length distortion.[10] Since equipment or power failure due to the arrival of the shock wave caused at least partial loss of all radar records from the Mt. McKinley and the Small, practically all the data shown in Fig. 2.1 and Table 2.8 were obtained from the McKean air-search radar, the other radar being used for checking purposes and filling in gaps in the McKean

(Text continues on page 37.)

CONFIDENTIAL

Table 2.5 — PHOTOGRAPHIC DATA FOR YFNB CAMERAS

NOL camera No.	Calibrated lens focal length, mm	Measured frame rate: Frames/sec	Measured frame rate: Time* of measurement	Time* of zero frame, sec	Timing, cycles/sec	Film type	Aperture (f-stop)	Shutter setting	Filter type
A-6		69.6†	+138 sec		None	Com. Kdcr.	4	180 deg	83
B-1		90.2	Frame 0	0.047	50 and 2	Tri-X	8	40 deg	None
B-2	25.87	24.3	Frame 0	0.010	50 and 2	Plus-X	16	40 deg	None
B-3		23.0			50 and 2	Com. Kdcr.	7	203 deg	83
B-4					50	Tri-X	3.5	‡	None
B-5					50 and 2	Com. Kdcr.	3	203 deg	83
B-6		21.1	+0.6 sec		2	Plus-X	16	80 deg	None
C-3	209.38§			2.0	Clock	Aero Super-XX	8	$\frac{1}{225}$ sec	K-2
C-3A	212.82§			1.0	Clock	Aero Super-XX	10	$\frac{1}{150}$ sec	K-2
C-5					50	Com. Kdcr.	4	203 deg	83
C-6	75.39	23.5	Frame +20		50	Plus-X	16	40 deg	None

* Measured from first appearance of surface effects.

† Average speed from +113 to +163 sec.

‡ Effective exposure is about $\frac{1}{6}$ of the interval between frames.

§ Equivalent focal length.[6]

CONFIDENTIAL

Table 2.6 — PHOTOGRAPHIC DATA FOR CAMERAS ON SUPPORT VESSELS

NOL camera No.	Calibrated lens focal length, mm	Measured frame rate		Time* of zero frame, sec	Timing, cycles/sec	Film type	Aperture (f-stop)	Shutter setting	Filter type
		Frames/sec	Time* of measurement						
D-2	99.36	38.3	Frame 0		50 and 2	Plus-X	16	165 deg	K-2
D-3 (first load)	510.86†			1.7	Clock	Aero Super-XX	8 or 11	$1/225$ sec	K-2
D-3 (second load)	511.48†			876	Clock	Aero Super-XX	8 or 11	$1/225$ sec	K-2
D-3A	513.93†			0.7	Clock	Aero Super-XX	8 or 11	$1/225$ sec	K-2
E-1	318.3				None	Plus-X	8 or 11	165 deg	K-2
E-2	210.77‡			2.6	Clock	Aero Super-XX	8 or 11	$1/225$ sec	K-2
E-3 (first load)	1024.59†			2.0	Clock	Aero Super-XX	11 or 16	$1/150$ sec	K-2
E-3 (second load)	1024.19†			384.5	Clock	Aero Super-XX	11 or 16	$1/150$ sec	K-2
E-3A	1018.86†			1.0	Clock	Aero Super-XX	11 or 16	$1/150$ sec	K-2
E-5	1219	101.8	Frame 0	0.0083	50 and 2	Tri-X	8	30 deg	K-2
F-1	459.98	22.9	Frame 0		50 and 2	Plus-X	11	165 deg	K-2
F-2	152.3	20.5	Frame 0		50 and 2	Plus-X	9	40 deg	K-2
F-3	212.02‡			3.6	Clock	Super-XX	11	$1/225$ sec	12
F-4		24.3§	Frame +118		50 and 2	Com. Kdcr.	8	203 deg	83

* Measured from first appearance of surface effects.

† Calculated so that the sum of the measured radial distortions equaled zero when referred to the calibrated focal length (reference 5, p. 174).

‡ Equivalent focal length.[6]

§ Average speed from frame +39 to frame +197.

CONFIDENTIAL

Table 2.7—PHOTOGRAPHIC DATA FOR AIRCRAFT CAMERAS

NOL camera No.	Calibrated lens focal length, mm	Measured frame rate		Time* of zero frame, sec	Timing, cycles/sec	Film type	Aperture (f-stop)	Shutter setting	Filter type
		Frames/sec	Time* of measurement						
G-1	51.50	1284	Frame +5	0 ± 0.0005	50 and 2	Tri-X	5.6	†	None
G-2	322.15	96.8	Frame 0	0.0024	50 and 2	Tri-X	11	70 deg	K-2
G-3	50.15	91.7	Frame 0	0.011	50 and 2	Tri-X	5.6	20 deg	None
G-4	18.90	109.0‡	Frame +300		50 and 2	Tri-X	11	70 deg	K-2
H-1	153.98	103.6	Frame 0	0.0095	50 and 2	Tri-X		75 deg	K-2
H-2	50.90	105	Frame +20		50 and 2	Tri-X		30 deg	None
H-3	212.74§			1.0	Clock	Aero Super-XX			
H-4					None	Com. Kdcr.		175 deg	83
J-1		112.5	Frame 0	0.0086	50 and 2	Tri-X	8	170 deg	K-2
J-2	25.58	40.7	Frame +10	0.009	50 and 2	Tri-X	11	80 deg	K-2
J-3	211.06§			7.0	Clock	Aero Super-XX	5.6	$1/225$ sec	Yellow
J-4					None	Com. Kdcr.	4.5	170 deg	83

* Measured from first appearance of surface effects.

† Effective exposure is about $1/6$ of the interval between frames.

‡ Speed constant from frame +200 to frame +400.

§ Equivalent focal length.[6]

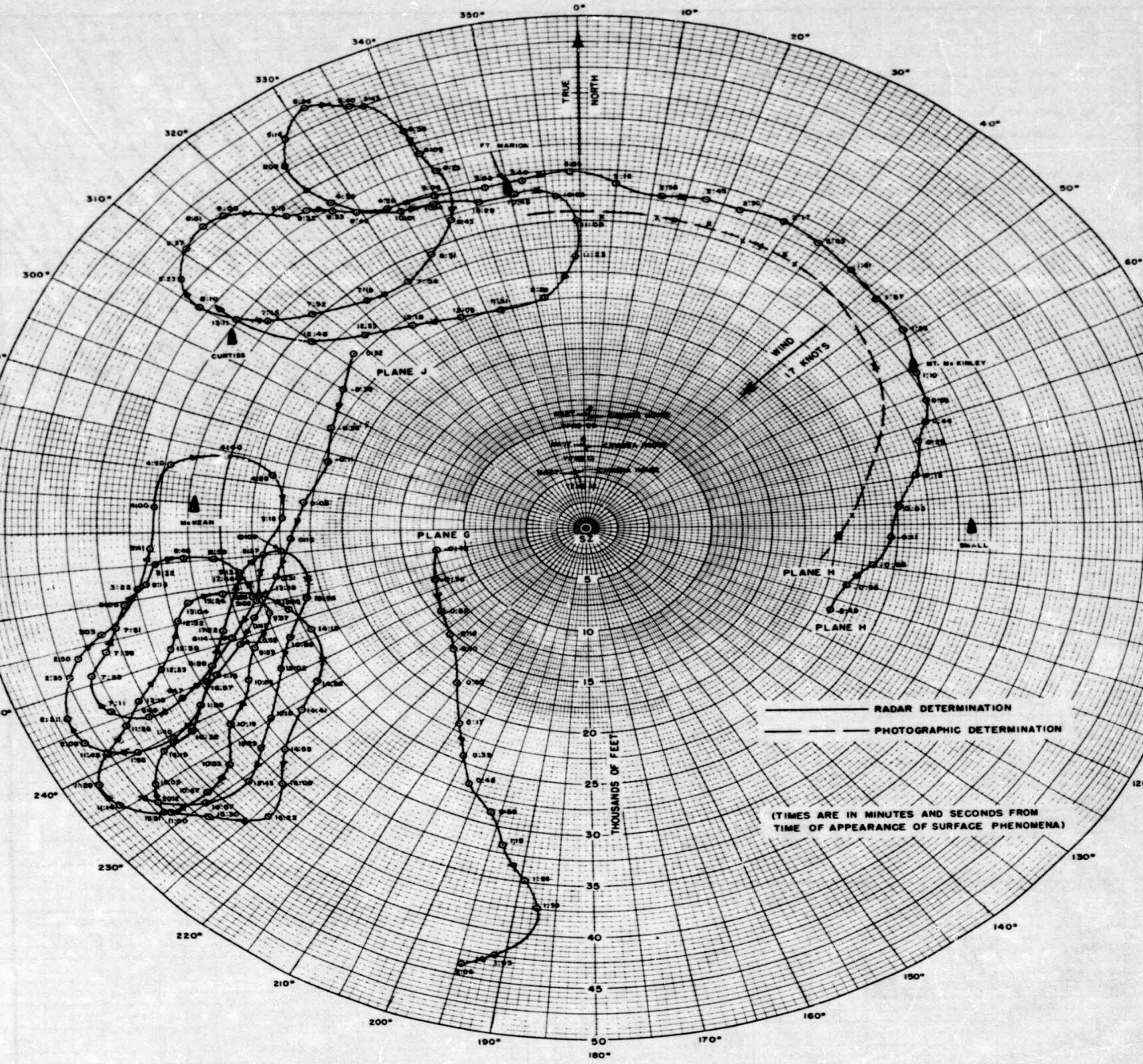
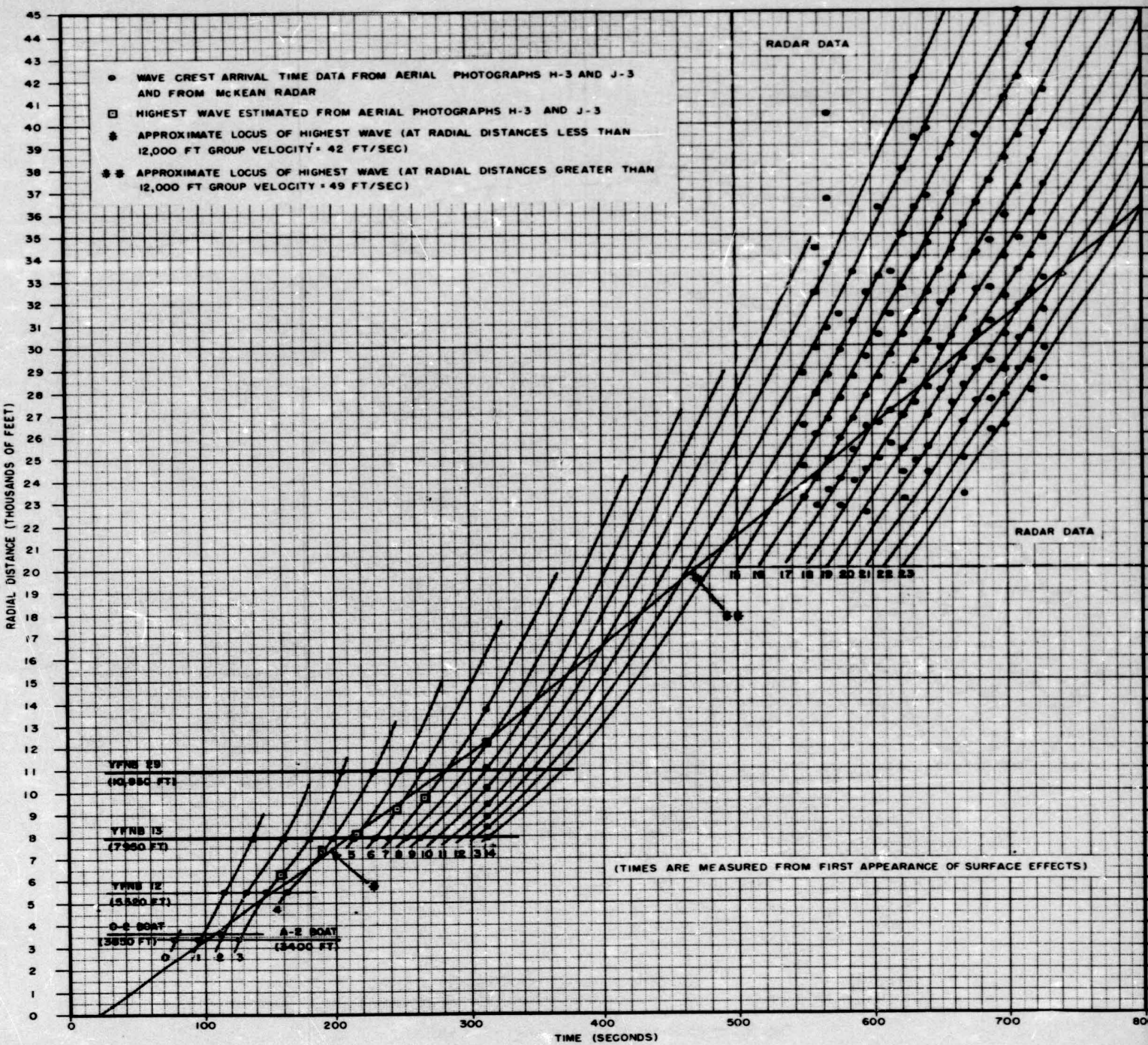


Fig. 2.1—Positions of C-54 photographic aircraft.



(See page 91)

Fig. 3.34—Surface-wave radii vs time.

CONFIDENTIAL

Table 2.8—RADAR DATA FOR AIRCRAFT POSITIONS

Time, min:sec	Horizontal range, thousands of feet	Bearing, deg	Time, min:sec	Horizontal range, thousands of feet	Bearing, deg
		Plane G			
−0:49	12.3	260.5	0:46	26.8	202.0
−0:36	13.2	248.5	0:58	28.8	196.5
−0:23	14.4	236.0	1:12	31.7	193.5
−0:16	15.2	228.0	1:25	34.8	189.5
−0:10	16.2	223.5	1:39	37.4	187.5
0:05	18.4	216.0	1:53	42.4	191.0
0:17	21.7	209.5	2:06	43.8	194.5
0:32	24.4	205.0			
		Plane H*			
−0:49	21.0	113.0	6:09	39.0	340.5
−0:36	21.5	105.5	6:23	36.9	341.5
−0:23	23.3(19.1)	99.5	6:43	32.0	340.5
−0:11	24.5(20.3)	92.5	6:51	29.5	335.5
0:03	25.2(21.7)	86.0	7:06	27.9	330.0
0:15	26.9(22.8)	79.5	7:18	28.5	322.0
0:29	27.8(24.1)	73.0	7:32	30.4	314.0
0:44	29.1(25.4)	70.0	7:45	33.1	308.5
0:56	30.0(26.4)	66.0	8:10	38.2	305.0
1:10	30.4(27.6)	61.0	8:23	41.0	307.0
1:23	31.9(28.5)	53.5	8:37	42.5	310.5
1:37	32.3(29.5)	47.0	8:51	42.8	314.0
1:51	33.0(30.3)	41.0	9:05	42.4	316.5
2:03	33.6(30.8)	34.5	9:19	39.0	322.0
2:17	34.0(30.9)	29.0	9:32	38.5	324.5
2:30	33.5(30.9)	22.5	9:33	37.2	327.0
2:45	33.5(30.9)	17.5	9:48	36.1	329.5
2:58	33.0(30.9)	11.5	10:01	34.3	335.0
3:12	33.7(30.9)	5.0	10:14	34.0	339.5
3:26	34.8(30.9)	358.5	10:29	32.9	345.5
3:40	34.4(30.9)	352.0	10:43	33.2	350.5
3:53	34.2	347.0	10:56	33.0	356.5
4:06	34.7	340.0	11:09	30.0	359.5
4:20	35.0	333.5	11:23	26.6	359.0
4:34	37.9	327.5	11:38	22.7	352.0
5:00	43.0	326.0	11:51	22.4	343.0
5:14	45.2	328.0	12:05	23.0	334.5
5:26	47.1	331.5	12:18	24.2	325.5
5:40	45.5	335.5	12:33	26.1	317.0
5:43	45.0	337.0	12:46	28.7	310.0
5:56	41.5	340.0	13:11	35.2	306.0

CONFIDENTIAL

Table 2.8 — (Continued)

Time, min:sec	Horizontal range, thousands of feet	Bearing, deg	Time, min:sec	Horizontal range, thousands of feet	Bearing, deg
		Plane J			
−0:52	25.5	312.5	9:37	27.3	253.0
−0:38	24.0	305.0	9:53	29.8	247.5
−0:25	23.0	296.0	10:06	31.5	242.5
−0:11	21.9	288.0	10:19	35.0	237.5
0:03	23.2	277.0	10:33	37.4	232.5
0:16	24.0	268.5	10:47	40.5	230.5
0:31†	25.7	260.0	11:00	44.0	231.5
0:47	28.6	253.0	11:14	47.0	235.5
0:59	30.6	249.0	11:28	47.2	238.5
1:13	33.7	245.5	11:43	44.8	241.5
1:26	36.0	242.0	11:56	42.5	243.5
1:40	39.6	239.5	12:10	40.5	246.0
1:55	43.0	240.0	12:23	37.5	249.0
2:08	46.2	243.5	12:38	36.0	251.5
2:22	46.4	247.0	12:52	34.6	255.5
2:35	44.7	251.5	13:04	33.3	258.0
2:50	43.5	253.5	13:24†	30.4	258.5
3:03	41.0	256.0	13:38†	27.6	257.0
3:22†	37.3	261.5	13:55†	25.5	252.5
3:41†	35.8	267.5	14:12	24.5	247.0
4:00†	35.5	274.0	14:26	26.6	236.5
4:20†	34.5	281.0	14:41	29.3	233.5
4:40†	30.4	284.0	14:55	32.8	229.5
4:59†	26.2	282.0	15:08	35.3	225.5
5:18†	24.8	273.0	15:22	38.6	223.5
5:37†	26.6	265.0	15:30	42.0	228.5
5:56†	28.0	256.0	15:51	44.4	232.0
6:14	31.0	250.5	16:05	43.4	235.5
6:28	33.5	247.0	16:19	40.9	238.5
6:47	36.9	244.0	16:32†	37.9	239.0
6:56	40.5	243.5	16:57†	34.4	245.0
7:11	43.0	246.0	17:22†	31.5	252.0
7:23	43.1	251.0	17:46†	28.9	261.0
7:36	41.2	253.5	18:09†	25.0	265.5
7:51	39.8	256.5	18:34	23.8	254.0
8:05	38.6	259.5	18:48	26.4	247.0
8:18†	36.5	262.0	19:02	28.4	242.0
8:32†	35.4	265.0	19:15	31.8	235.0
8:46†	33.0	265.5	19:29	34.3	232.0
8:59†	30.6	265.0	19:43	37.4	229.0
9:13†	28.8	262.0	19:57	41.3	230.0
9:26†	28.2	257.0	20:12	44.4	233.5

* Photographic determinations of distances are in parentheses.
† Interpolated.

CONFIDENTIAL

radar data for times when J plane came too close to the McKean to be within radar range. A correction of +7 deg was added to the bearings of all objects as determined from the McKean air-search radar in order to obtain agreement with other visual and radar position data. Apparently the azimuth scale surrounding the scope face was incorrectly set. The times given in Fig. 2.1 and Table 2.8 were determined from the clock reading and the azimuth position of the aircraft on the radarscope. The radar time scale was adjusted to SZT by means of the known time of passage of two planes, the RB-50 and the H plane (visible on both the radar and the H-3 camera record), since SZT could not be determined accurately from the radarscope photographs alone.

As a check on the radar determination of the aircraft positions shown in Fig. 2.1, the distances of the aircraft from SZ at the time of detonation were determined by photographic means. Length scales were established by measuring the major axis of the apparently elliptical first slick when it reached surface craft at known radial distances. The aircraft distances were then calculated by using these length scales and the calibrated focal lengths of the camera lenses. These photographically measured ranges were considered to be more reliable than the radar data.

The values of the initial distances of the aircraft obtained by both methods are presented in Table 2.9.

Table 2.9 — INITIAL HORIZONTAL RANGE OF PHOTOGRAPHIC AIRCRAFT FROM SZ

Aircraft	Photographic data, ft	Radar data, ft
G	17,600	17,700
H	21,400	25,300
J	22,000	22,600

At SZT the G and J radar determinations were within 0.6 per cent and 2.7 per cent, respectively, of the photographic determinations. This agreement was considered excellent; however, an 18 per cent discrepancy existed between the H aircraft radar distance and the photographic measurement. When the range of the H aircraft was checked in a similar manner for later times (using the surface wave rings as scale markers) differences ranging from 3000 to 4000 ft were indicated up to about 3.5 min after SZT.

A smooth curve for the photographically determined ranges is included in Fig. 2.1 and tabulated in Table 2.8. Since the discrepancy was not resolved, an average curve lying between the two curves shown in Fig. 2.1 for the H plane was used in the analysis for times from about 30 sec to about 4 min after SZT. At later times the radar data were used.

2.4 RECOMMENDATIONS

Although the task of tracking the C-54 photographic aircraft by radar was accomplished with a fair degree of success, it is felt that improvements are possible and, for some purposes, will be essential in future operations.

For example, the precision with which the aircraft positions were obtained was not adequate for measurements of the slick and dome phenomena. In this case the phenomena themselves, correlated with the known positions of the YFNB's and M-boats, were used to calculate aircraft distances with greater accuracy. The radar positioning was just adequate for measuring the late base-surge and foam-ring growth.

Although all radarscope images exhibit a certain degree of distortion and inaccuracy, the use of radar equipment with a higher degree of resolution than that used in Operation Wigwam would probably provide distance data of sufficient accuracy for most surface-phenomena measurements. In addition, the tracking of several aircraft on a PPI scope could be made easier by the use of a different IFF signal for each aircraft.

However, it is believed that the tracking of aircraft by locked-in fire-control radar systems is superior to the use of air-search radar because such systems are more precise. Each plane should be followed by two, or preferably three, separate radars located on different ships.

In Operation Wigwam various groups of military and civilian personnel were given the assignments of tracking the air and surface craft with radar and photographing the radarscopes and data panels. At the completion of the experimental phase of the operation, each scientific group needing position data was given a copy of the films and radar data sheets from which to extract the necessary data.

It is recommended that, on future operations, such as Operation Hardtack, a separate project be established to obtain position vs time data for surface and air craft by means of radar as requested by the scientific projects. This project should be responsible for coordinating all phases of the work, and the task should include the analysis of data and comparison of radar results with information from other sources in order to obtain a consistent position vs time history for the various craft. The complete system, including the analysis of data, should be tested in advance of the full-scale experiment.

The positions of the surface camera stations were established with adequate precision, but a needless loss of valuable photographic records resulted from the failure of ship's power on the Fort Marion and the Mt. McKinley. In future tests it is recommended that battery power be used for cameras mounted on ships, even though the probability of generator failure may seem remote.

In Operation Wigwam the use of a large number of cameras, including many backups, proved worth while. It is believed that this approach is justified on all nuclear test operations because previous experience has shown that 100 per cent performance of photographic equipment cannot be expected, even when tests are conducted in less difficult conditions than those on Wigwam. Since photography is one of the least costly experimental techniques, this method of obtaining data should be fully utilized.

REFERENCES

1. A. B. Focke, Interim Summary Report of the Scientific Director of Operation Wigwam, Report ITR-1053, May 1955. (Secret – RD)
2. C. B. Cunningham, Free-field Pressures, Station Zero, Operation Wigwam Project 1.2.1 Report, WT-1006, December 1955. (Secret – RD)
3. C. J. Aronson et al., Underwater Free-field Pressures to Just Beyond Target Locations, Operation Wigwam Project 1.2 Report, WT-1005, May 1956. (Secret – RD)
4. J. C. Johnson, "Physical Meteorology," Massachusetts Institute of Technology and John Wiley & Sons, Inc., New York, 1954. (Unclassified)
5. B. J. Brettler, "Photogrammetry," Edgerton, Germeshausen and Grier, Inc., Report No. 1140, 1954. (Unclassified)
6. F. E. Washer and F. A. Case, Calibration of Precision Airplane Mapping Cameras, National Bureau of Standards Research Paper No. 2108, 1950. (Unclassified)
7. Manual of Photogrammetry, 2d ed., American Society of Photogrammetry, Washington, D. C., 1952. (Unclassified)
8. P. L. Horrer, Subsurface Configuration of the Array, Operation Wigwam Project 2.8 Report (Part I), WT-1018, June 1956. (Secret)
9. E. H. Boldrick and V. G. Heger, Photographic Recording of Ship-borne Radar Information, Operation Wigwam Project 0.31 Report, WT-1038, May 1955. (Secret – RD)
10. Elementary Radar Scope Interpretation Manual, U. S. Naval Photographic Interpretation Center, Report NAVAER-10-35-615, March 1955. (Confidential)

CHAPTER 3

RESULTS

3.1 SPREAD OF UNDERWATER SHOCK WAVES

3.1.1 Direct Underwater Shock Wave

Viewed from the air, the first visible evidence of the Wigwam detonation was an expanding disk on the water surface which indicated the arrival of the shock wave (Fig. 3.1). The expanding disk appeared as a white patch with a dark fringe; initially, the leading edge of the white area lagged behind the dark fringe by about 2 msec. This time lag increased with radial distance from SZ, becoming about 5 msec at a radius of 1000 ft and about 9 msec at 2000 ft (Fig. 3.2). At a radius of about 7000 ft, the white area ceased to grow; the dark fringe continued to grow and was visible out to a radius of about 14,000 ft. The dark fringe appeared to be similar to the slicks observed in high-explosive tests and will be referred to here as the direct-shock-wave slick.

From surface stations the first visible effect was the appearance of the air shock waves, followed by the spray dome. Portions of the curves for the radial spread along the water surface of the first air shock and the spray dome observed from the surface are shown in Fig. 3.2, together with the data obtained from the air for the slick and white area.

A comparison of the two sets of data shows that the distance between the spray dome and the air shock wave at the water surface was about the same as the distance between the leading edge of the slick and the leading edge of the white area seen from the air (about 50 ft at a radius of 1500 ft). If it is assumed that the first appearances of the air shock and the slick coincide, then this agreement in spacing strongly indicates that the spray area seen from the surface stations and the white area seen from the air were the same phenomenon—the first spray dome. It is not considered significant that the growth curves in Fig. 3.2 do not actually coincide, because of the uncertainties in the determinations of zero time, SZ, and the linear scale factors, particularly for camera B-1, which was not pointing toward SZ.

The crack (the expanding white area that results from cavitation occurring beneath the water surface) was not generally visible on the Wigwam shot. Only camera B-5, which was pointing downward over the stern of the YFNB-13 at an angle of about 22 deg, showed the water turning milky on arrival of the shock wave. The proximity of the barge to the patch of water seen by the camera may have influenced this result, but this is considered unlikely. This phenomenon was not observed from the air, probably owing to the small elevations of these cameras, approximately 5 deg for the cameras in planes G, H, and J. In high-explosive tests, the crack follows closely behind the slick and occurs before the formation of spray.

The time of initial appearance of the spray dome at SZ, determined from camera record G-1, was 385.6 ± 2.0 msec after radio fiducial zero time. The initial appearance of the slick (not visible on record G-1) occurred perhaps 2 msec earlier. This measurement is in agreement with the time reported by Project 1.2.1 for the shock-wave arrival at SZ.[1] The Project

CONFIDENTIAL

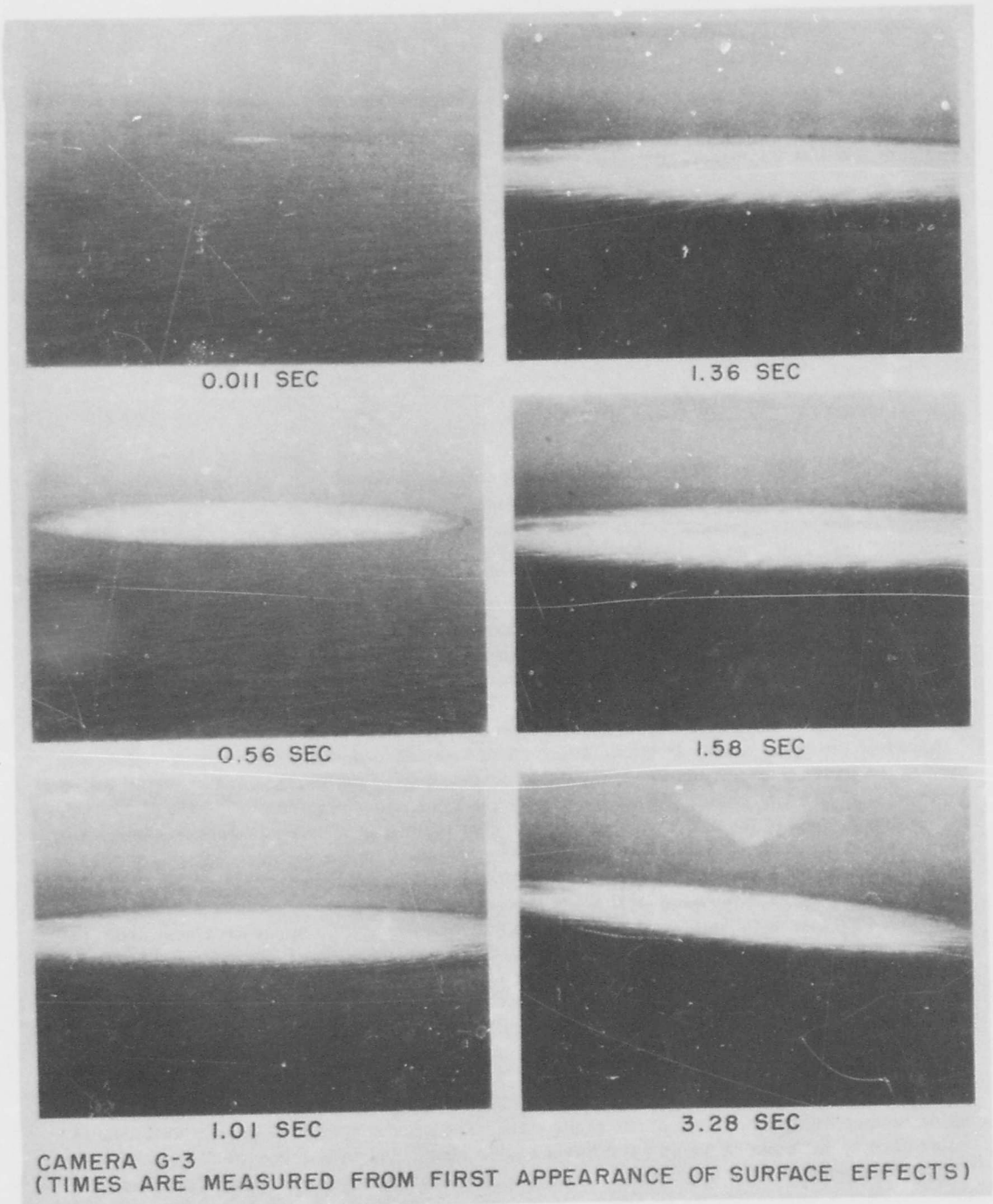


Fig. 3.1—Initial surface effects.

CONFIDENTIAL

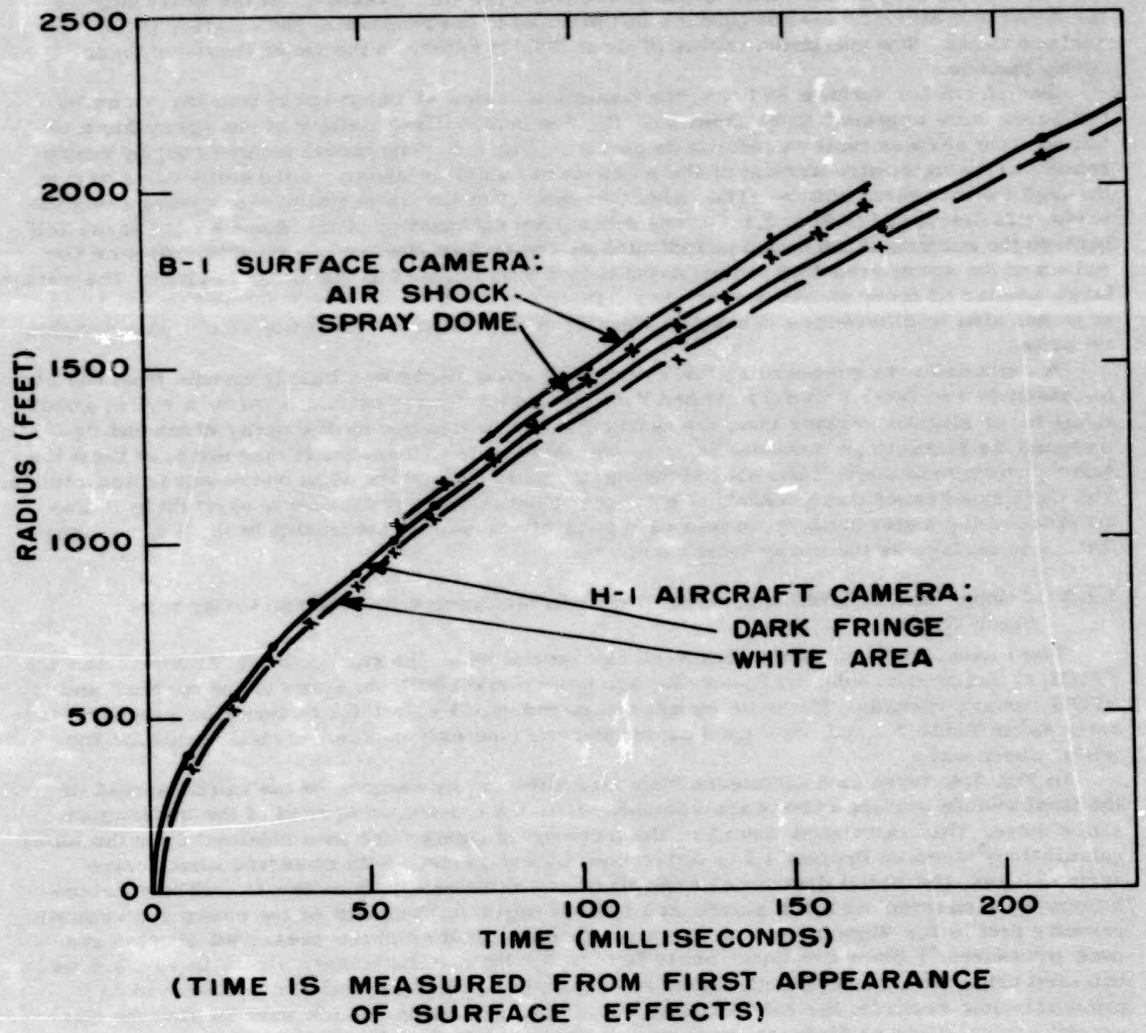


Fig. 3.2—Spread of direct-shock-wave effects.

CONFIDENTIAL

1.2.1 value of 385.5 msec after radio fiducial zero time was extrapolated from the shock arrival time at a gauge 25 ft beneath the YC-473.

Seen from the air, the first spray dome reached a maximum radius of about 7000 ft by about 1 sec after SZT, after which it contracted slowly as the spray fell back to the surface. The edge of the dome was by no means sharp or well defined, and the density of the spray diminished steadily as the radial distance from the center increased. At the outer edge of the dome, the spray formed in patches that seemed to correspond to the existing pattern of surface waves. The maximum radius of about 7000 ft refers to the outer limits of these spray patches.

Seen from the surface stations, the maximum radius at which spray was thrown up by the shock wave appeared to be about 5700 ft. The radius-time history of the spray dome obtained from surface camera records is shown in Fig. 3.3. The radial growth roughly corresponds to the calculated arrival of the shock wave, which is shown as the solid curve drawn through the measured points. (The calculated spread of the underwater shock wave along the surface is discussed in Sec. 3.1.2.) The subsequent contraction of the dome as the spray fell back to the surface of the ocean is indicated by the broken line, which roughly indicates the radius of the spray area that had apparent height with respect to the ocean surface. The rather large scatter of these measurements is attributed to the lack of a well-defined spray-dome edge and also to differences in camera elevations and distance resolution of the photographic records.

A darkened area surrounding the contracting spray dome was barely visible from the air for about 20 sec (aerial camera record H-3). The dark region extended out to a radius about equal to, or slightly greater than, the maximum radius attained by the spray dome and resembled the black rings observed in high-explosive tests. However, it may not have been the same phenomenon since it did not extend significantly beyond the area where spray was visible. The dark appearance was probably due to decreased regular reflection of skylight by a disturbance of the water surface, in this case possibly caused by the falling back of spray onto the ocean surface as the spray dome contracted.

3.1.2 Comparison of Rates of Spread: First Visible Surface Effects and Underwater Shock Wave

The times of arrival of the direct-shock-wave slick at the sterns of the YFNB-12 and the YFNB-13 and at the center of Squaw-29 have been measured from some of the aircraft and YFNB camera records. These times are compared with Project 1.2 underwater pressure-time records[2] in Table 3.1 and show good agreement with the extrapolated arrival times for the initial shock wave.

In Fig. 3.4, three measurements from aircraft camera records of the radial spread of the first visible surface effects are compared with the calculated spread of the underwater shock wave. This calculated spread of the underwater shock wave was obtained from the same calculations[2] used by Project 1.2 to determine, by comparison with observed shock-wave arrival times, the radial distances of the elements of the array from the YC. (These calculations were carried out for a source at a 2000-ft depth on the basis of the measured acoustic velocity profile for Wigwam and excess velocity calculated from the measured shock-wave peak pressures.[2]) Since the linear scale factors for the measurements shown in Fig. 3.4 were obtained using the distances determined from the shock-wave arrival times observed on pressure-time records, the calculated spread of the underwater shock wave is also the observed arrival-time vs distance curve when referred to the scale of these measurements.

The photographic data on the spray dome (cameras G-3 and J-2) generally indicate distances about 5 per cent below those on the calculated curve for the arrival of the underwater shock wave at the surface. About one-half of this 5 per cent can be attributed to the lag in the appearance of the spray dome as shown in Fig. 3.2. The remaining 2 or 3 per cent can easily be attributed to errors in measurement. However, the rather large discrepancy of about 8 per cent in the H-1 slick data must be attributed entirely to unknown errors in measurement since it is unlikely that there is any significant time lag between the arrival of the underwater shock wave and the appearance of the slick.

CONFIDENTIAL

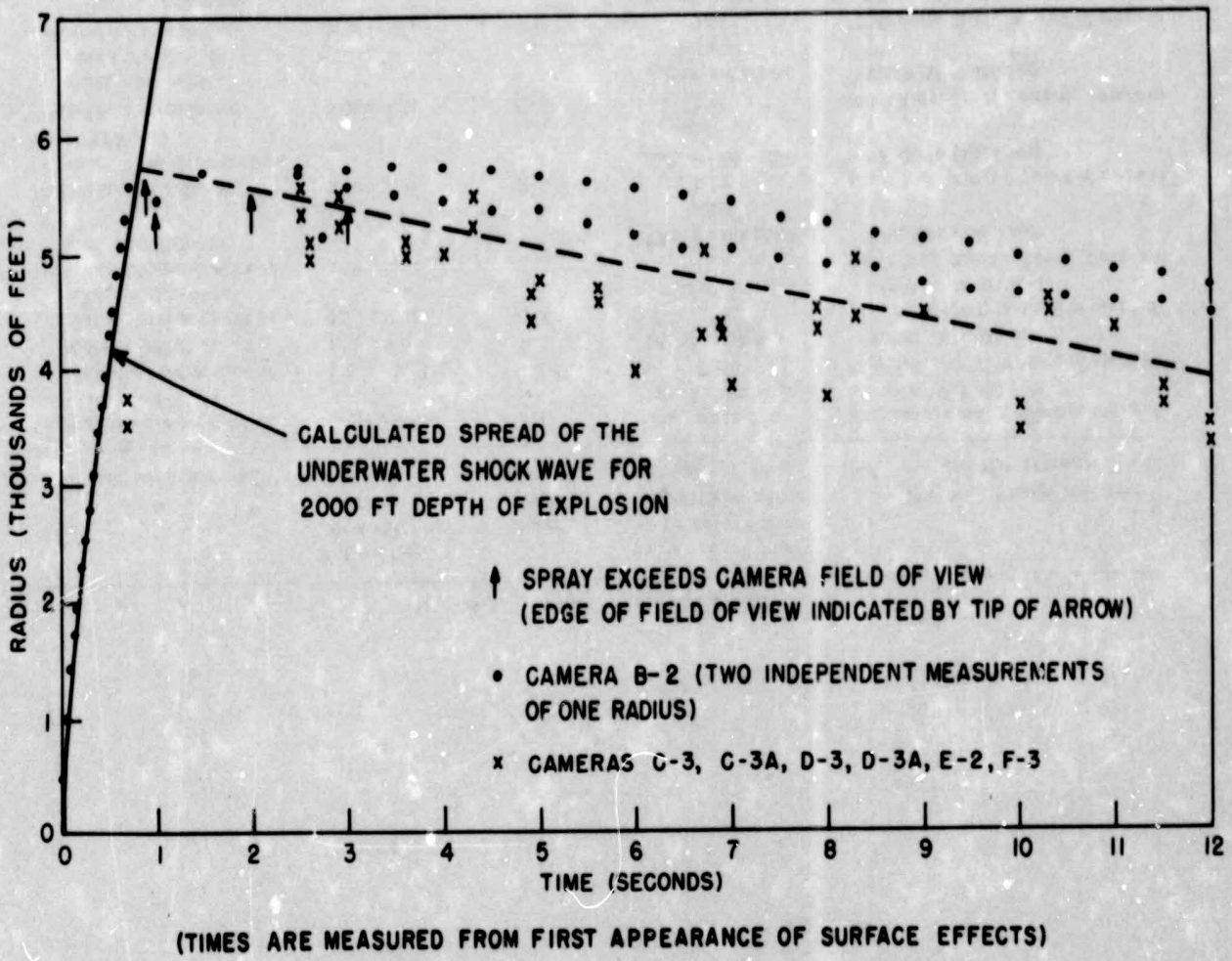


Fig. 3.3—Radius of spray dome (viewed from surface stations) vs time.

Table 3.1 — SHOCK ARRIVAL TIMES

Phenomena observed	Time from first surface disturbance, sec	Source of data (camera No.)	Shock arrival times* (extrapolated from nearest Project 1.2 gauge), sec	Project 1.2 gauge position and arrival time†
Initial shock-wave slick at stern of YFNB-12	0.756 ± 0.010	J-2	0.759 Initial shock wave	25 ft deep, 210 ft forward of stern of YFNB-12 (1.181 sec)
Initial shock-wave slick at stern of YFNB-13	1.230 ± 0.010 1.22 ± 0.04	J-2 B-3	1.228 Initial shock wave	25 ft deep, 210 ft forward of stern of YFNB-13 (1.653 sec)
Initial shock-wave slick at center of Squaw-29	1.70 ± 0.02	C-6	1.70 Initial shock wave	25 ft deep, 210 ft forward of stern of YFNB-29 (2.254 sec)
First bubble-pulse slick at stern of YFNB-13	4.10 ± 0.13	B-3	4.05 First bubble pulse (peak)	100 ft deep, 210 ft forward of stern of YFNB-13 (4.473 sec)
First bottom-reflected shock-wave slick at stern of YFNB-13	5.76 ± 0.04	B-3	5.74 Bottom reflection (bottom)	100 ft deep, 210 ft forward of stern of YFNB-13 (6.114 sec)
First bottom-reflected shock-wave slick at center of Squaw-29	6.00 ± 0.04	C-6	6.01 Bottom reflection (bottom)	100 ft deep, 210 ft forward of stern of YFNB-29 (6.436 sec)
Second distinct bottom-reflected shock-wave slick at stern of YFNB-13	5.89 ± 0.04	B-3	5.91 Bottom reflection (sub-bottom)	100 ft deep, 210 ft forward of stern of YFNB-13 (6.292 sec)

Third distinct bottom-reflected shock-wave slick at stern of YFNB-13	7.55 ± 0.04	B-3	7.55 Bottom reflection (deep sub-bottom)	500 ft deep, 210 ft forward of stern of YFNB-13 (7.835 sec)
Bottom-reflected shock-wave slick at Fort Marion	8.71 ± 0.02	D-2	8.65 Bottom reflection	Estimated arrival time assuming: water depth = 15,500 ft; average shock velocity at radii greater than 2000 ft = 4900 ft/sec‡
Bottom-reflected shock-wave slick at Mt. McKinley	8.12 ± 0.05 8.15 + 0.02 − 0.06	F-2 F-4	8.20 Bottom reflection	Estimated arrival time assuming: water depth = 15,500 ft; average shock velocity at radii greater than 2000 ft = 4900 ft/sec‡
First jarring of camera on Curtiss	8.82 ± 0.02	E-5	8.77 Bottom reflection	Estimated arrival time assuming: water depth = 15,500 ft; average shock velocity at radii greater than 2000 ft = 4900 ft/sec‡
First jarring of camera on YFNB-29	1.83 ± 0.04	C-6	1.82 Initial shock wave	25 ft deep, 210 ft forward of stern of YFNB-29 (2.254 sec)
Second jarring of camera on YFNB-29	6.22 + 0.04 − 0.09	C-6	6.14 Bottom reflection (sub-bottom)	100 ft deep, 210 ft forward of stern of YFNB-29 (6.519 sec)

* Time from first surface disturbance.

† Time from radio fiducial zero time.

‡ The time of arrival of the shock wave at a radius of 2000 ft was taken as 0.385 sec after radio fiducial zero time.[1]

CONFIDENTIAL

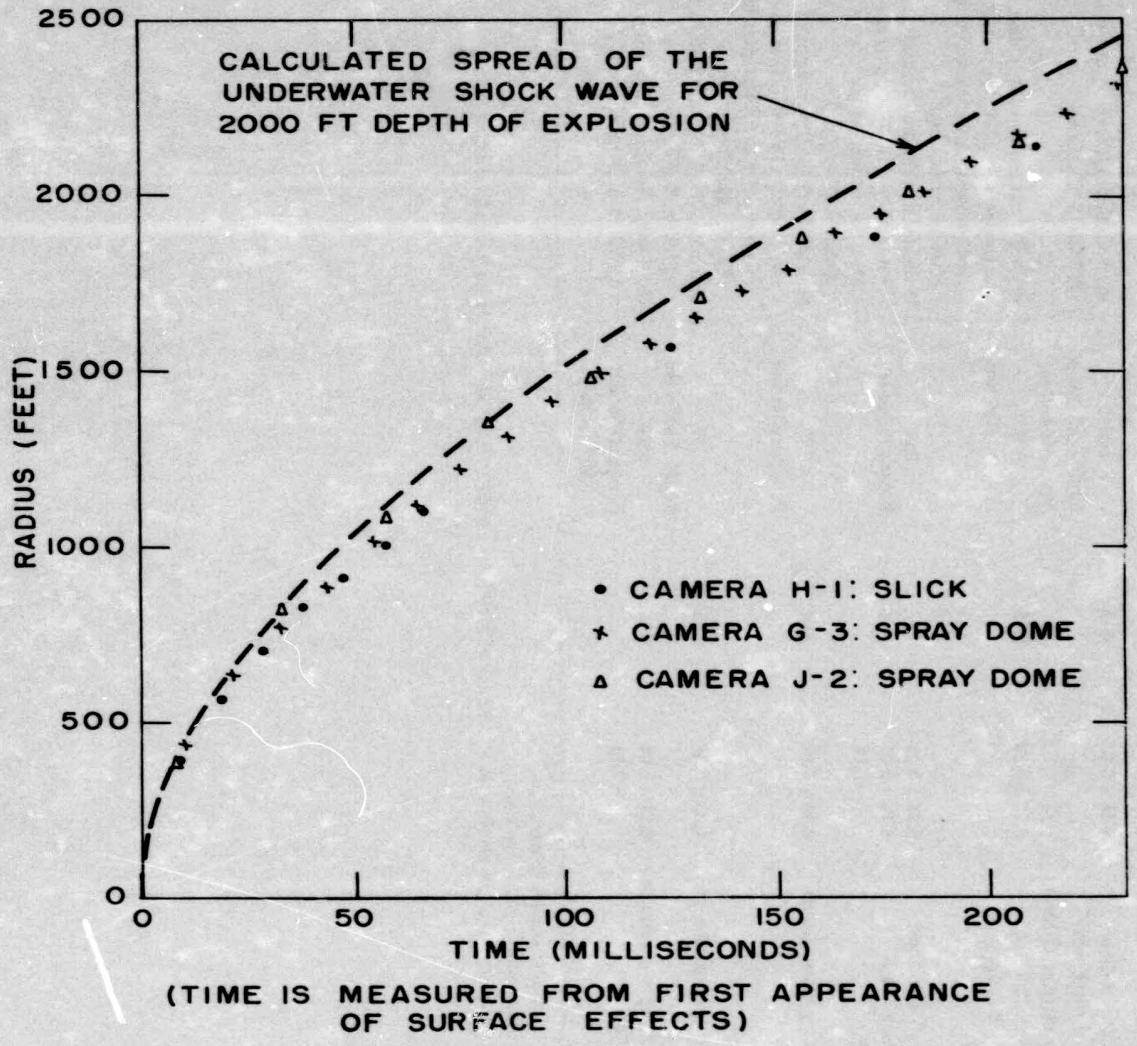


Fig. 3.4 — Spread of first visible surface effects viewed from aircraft.

CONFIDENTIAL

Had the depth of the Wigwam detonation been unknown, it might have been required to estimate the depth of explosion by measurements of the rate of spread of the first visible surface effects, such as are presented in Fig. 3.4. Provided the linear scale of the photographs is known, i.e., from the distance between two surface craft, one method of estimating the depth of explosion is to compare the observed rate of spread of the first visible surface effects with a family of curves for the spread of the underwater shock wave along the surface calculated for several depths of detonation.[3] This method, applied to the data presented in Fig. 3.4, would yield an estimated depth of explosion of 1600 to 1800 ft, depending on which of the three measurements was used. However, it should be emphasized that, in this case, the lack of agreement between these estimated depths and the "known" depth of 2000 ft must be due entirely to lack of precision in the method, which assumes that there is no time lag between the arrival of the shock wave and the occurrence of visible effects, since the linear scales of these measurements were of necessity adjusted so as to ensure agreement between the observed time of arrival of the underwater shock wave at the surface and the curve calculated for the 2000-ft depth of explosion. The preceding range of estimated depths of detonation is not inconsistent with an estimated mean deviation of the order of 10 to 15 per cent for depth determinations by such methods for a series of high-explosive tests.[3] It should be noted that the methods used[3] do not take shock-wave refraction into account.[4]

If the air shock wave from a deep underwater explosion is visible, as was the case on Wigwam, the explosion depth could also be estimated in the same manner from measurements of the spread of the intersection of the air shock front with the water surface. One disadvantage inherent in this method is the difficulty in obtaining photographs of the air shock wave. No photographic records that would have been suitable for this measurement were obtained on Operation Wigwam.

3.1.3 Shock-wave Reflections and Bubble Pulses

Following the effects of the direct underwater shock wave, slicks and spray patches which were caused by shock-wave reflections from the bottom of the ocean and by the first bubble pulse were observed in the region beyond the first spray dome. Slicks from later bubble pulses and even from bubble-pulse reflections also may have occurred since several as yet unidentified slicks were visible, particularly on the aerial color movies.

The radius-time histories of several of these slicks (those which have been identified) are roughly indicated in Fig. 3.5, along with the direct-shock-wave effects discussed in Sec. 3.1.1. In Fig. 3.5, the time scales for the growth of the slick, crack, and first spray dome have been shifted so that these may be shown as distinct phenomena; also the maximum radial extents shown for most of these phenomena are rough approximations.

At 4.10 ± 0.13 sec after SZT, an extremely faint slick was observed approaching the stern of the YFNB-13 (camera record B-3). Comparison with underwater pressure-time data shows that this slick corresponded to the peak of the first bubble pulse (Table 3.1). It is interesting to note that, although the first bubble pulse caused the formation of a large spiky secondary spray dome (Sec. 3.6), it produced only a barely detectable slick.

At about 5.6 sec after SZT, still another slick appeared at the edge of the spray dome. This slick expanded more rapidly than the first slick and was visible out to a much greater radius, at least 34,000 ft. The radius-time history of this slick shows definitely that it was due to the reflection of the initial shock wave from the bottom of the ocean (Fig. 3.6). This slick was readily visible from all surface camera stations, with the possible exception of the Curtiss, as well as from the air. (As far as the authors know there were no visual or photographic observations from the Curtiss of any slick. The motion-picture cameras were all aimed too high to show water surface near the ship.) Scientist observers, A. H. Keil and E. Swift, Jr., on the Mt. McKinley told of seeing a slick speed up to the ship. Their observation is confirmed by photographic records F-2 and F-4.

The aerial photographs show that the leading edge of the bottom-reflection slick was neither sharply defined nor continuous. The slick advanced in an irregular and random manner, undoubtedly reflecting the hilly bottom topography. Following the initial passage of the

CONFIDENTIAL

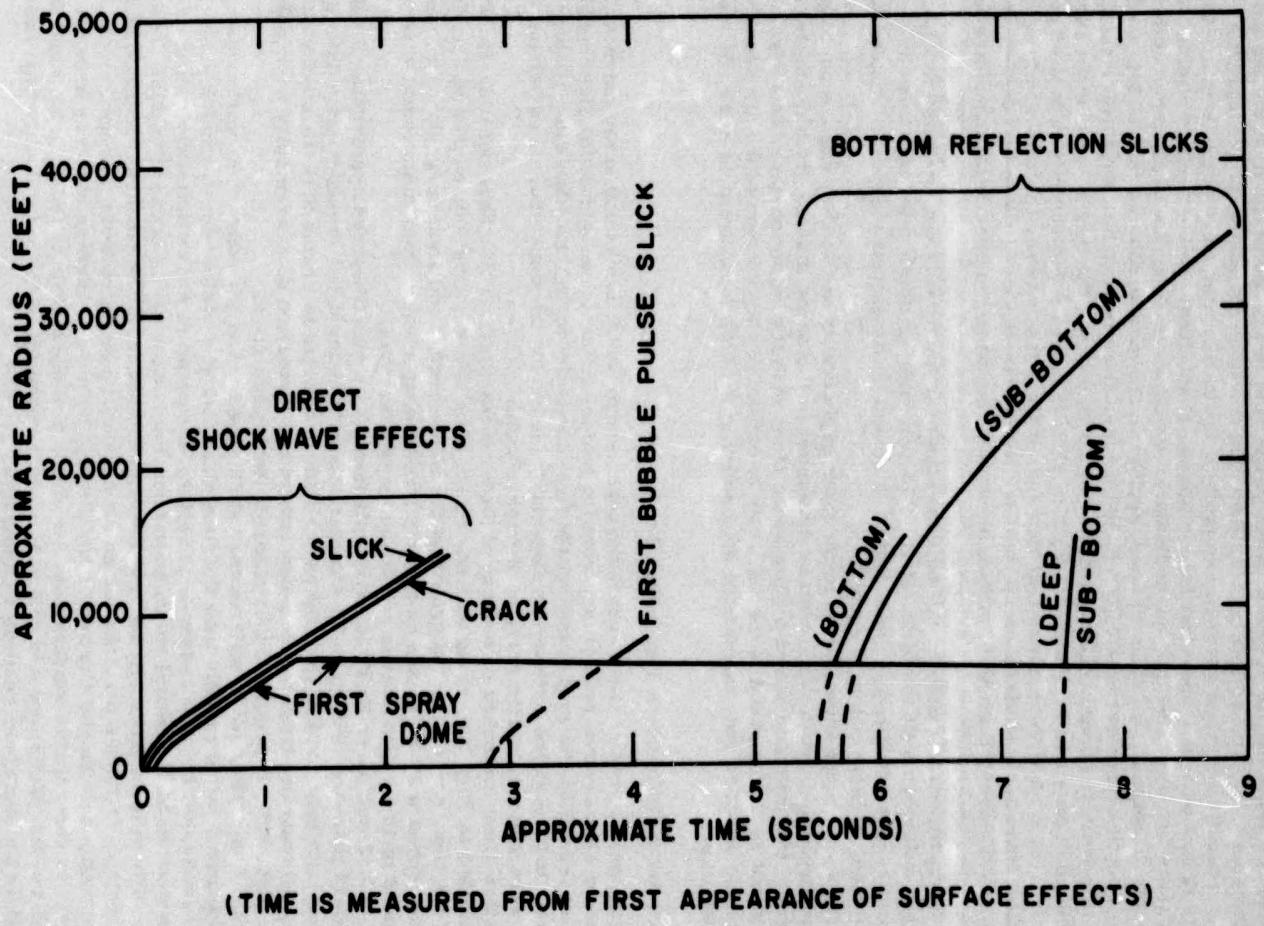


Fig. 3.5—Observed slicks and first spray dome, sequence of events.

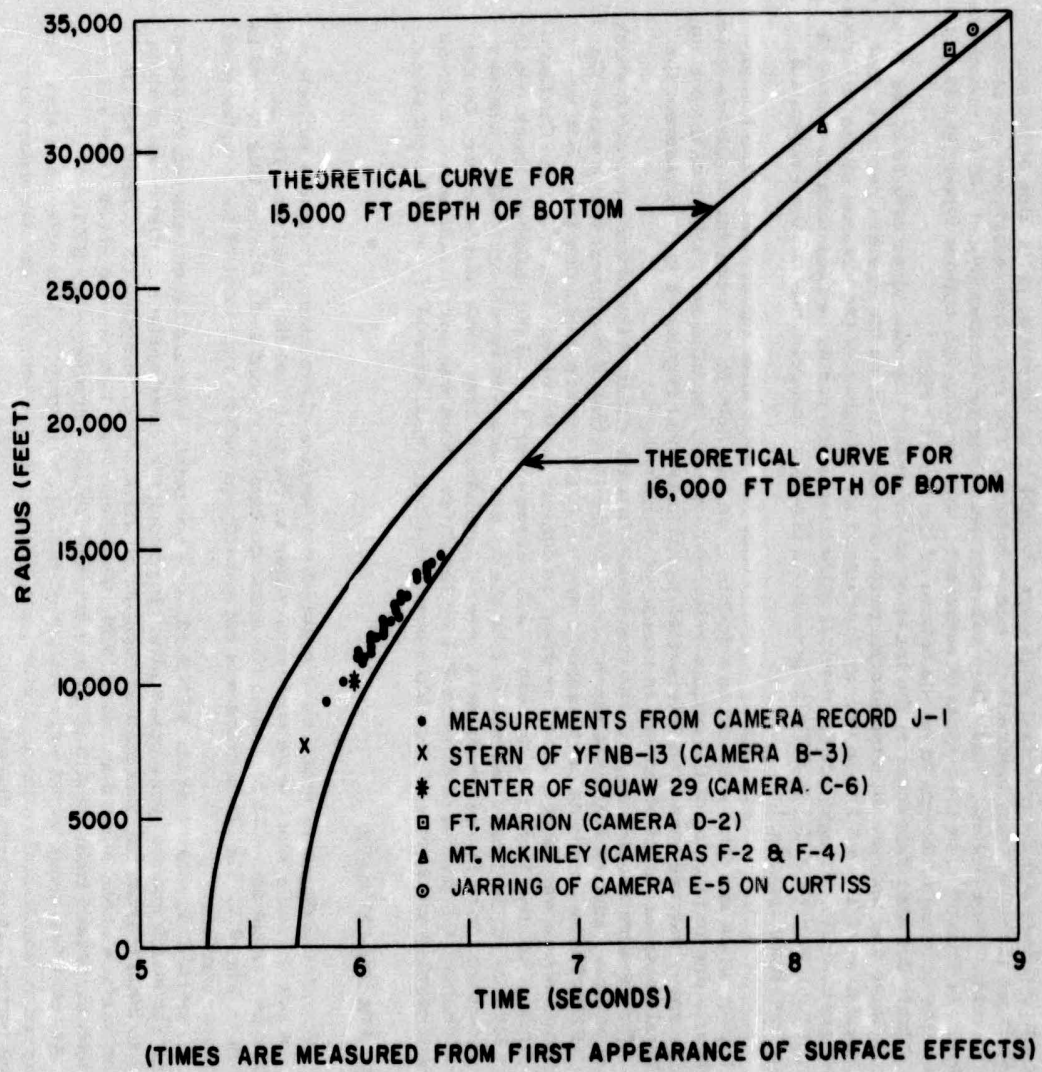


Fig. 3.6—Spread of bottom-reflected shock wave.

bottom-reflection slick, the water surface seemed to reverberate for a few seconds owing to the passage of a number of slicks, mostly quite indistinct, which probably indicated additional reflections of the shock wave from the various layers of soil and rock beneath the ocean floor and perhaps additional bubble pulses and bubble-pulse reflections.

Three of the bottom-reflection slicks were sufficiently distinct to permit correlation with particular pressure pulses recorded by Project 1.2 pressure-time gauges (Table 3.1). These pressure pulses and the resultant slicks are thought to be caused by reflection of the shock wave from three separate layers in the ocean bottom.[2] The reflection interfaces are denoted as "bottom," "sub-bottom," and "deep sub-bottom."[2] The sub-bottom (about 600 ft beneath the bottom) is thought to be the bottom of sediments, and the deep sub-bottom (about 20,000 ft beneath the bottom) is thought to be the bottom of the basaltic rock.[2]

Table 3.1 also lists some of the times of occurrence of various other effects of the direct shock wave and bottom-reflected shocks which are detectable on the camera records. The comparisons of Table 3.1 have greatly facilitated identification of the various slicks observed photographically. To date, all the distinct slicks for which radius vs time data have been obtained have corresponded to definite pressures observed independently on the Project 1.2 pressure-time records.

Isolated white patches of spray formed about 100 msec after the arrival of the bottom-reflection slick and were seen out to a radius of about 17,000 ft. The scattered patches were evidently due to focusing of the bottom-reflected shock by the hills and valleys of the bottom. These spray patches have been interpreted to indicate local regions of high pressures, the vertical components[2] of which are in excess of about 160 psi.

The camera records support the conclusion that the effect of the bottom-reflected shock wave on many surface craft was much more intense than that of the direct shock wave. On the YFNB-29 the amplitude of the angular motion of the camera house due to the bottom-reflected shock was about 5 times as great as that due to the direct shock. On the Curtiss the first noticeable jarring of camera E-5 occurred on arrival of the reflected shock. On the Fort Marion the jarring of camera D-2 by the direct shock was barely noticeable, whereas the reflected shock jarred the camera severely, causing failure of the ship's power. On the Mt. McKinley the jarring of camera F-2 by the direct shock was barely noticeable, whereas severe jarring and failure of the ship's power occurred upon arrival of the reflected shock.

3.2 AIR SHOCK WAVE

When the underwater shock wave reached the surface of the water, complete reflection did not occur, and a shock wave was transmitted to the air above the interface. The air shock front was visible above SZ for about 100 msec on camera record E-5. Part of this record is shown in Fig. 3.7. The shock front was not smooth, probably as a result of the roughness of the water surface.

Camera B-1, located on the YFNB-13, was not pointing toward SZ but showed the edges of the air shock and the spray dome advancing along the water surface at distances of about 1000 to 2000 ft from SZ. The leading edge of the air shock wave appeared to intersect the water surface ahead of the dome (Fig. 3.2). The mean angle between the shock front and the horizon increased from about 6 to 12 deg between 80 and 170 msec after SZT.

At least two shock waves were visible on the B-1 photographs. This effect has also been observed in small-scale high-explosive tests.[5] However, the source of the secondary air shock waves has not been determined.

The initial vertical velocity of the air shock and its time of emergence from the water surface were measured as a function of horizontal distance from SZ on camera record E-5. Height vs time measurements were made along vertical lines spaced at 25-ft intervals in the plane of measurement, which was at an angle of about 33 deg with true north (Table 2.4). These height vs time measurements were made up to the limit of visibility of the air shock, which ranged from 51 to 68 ft above the undisturbed water surface. Since the data were essentially linear over this short vertical extent, a straight line was fitted to each set of height vs

CONFIDENTIAL

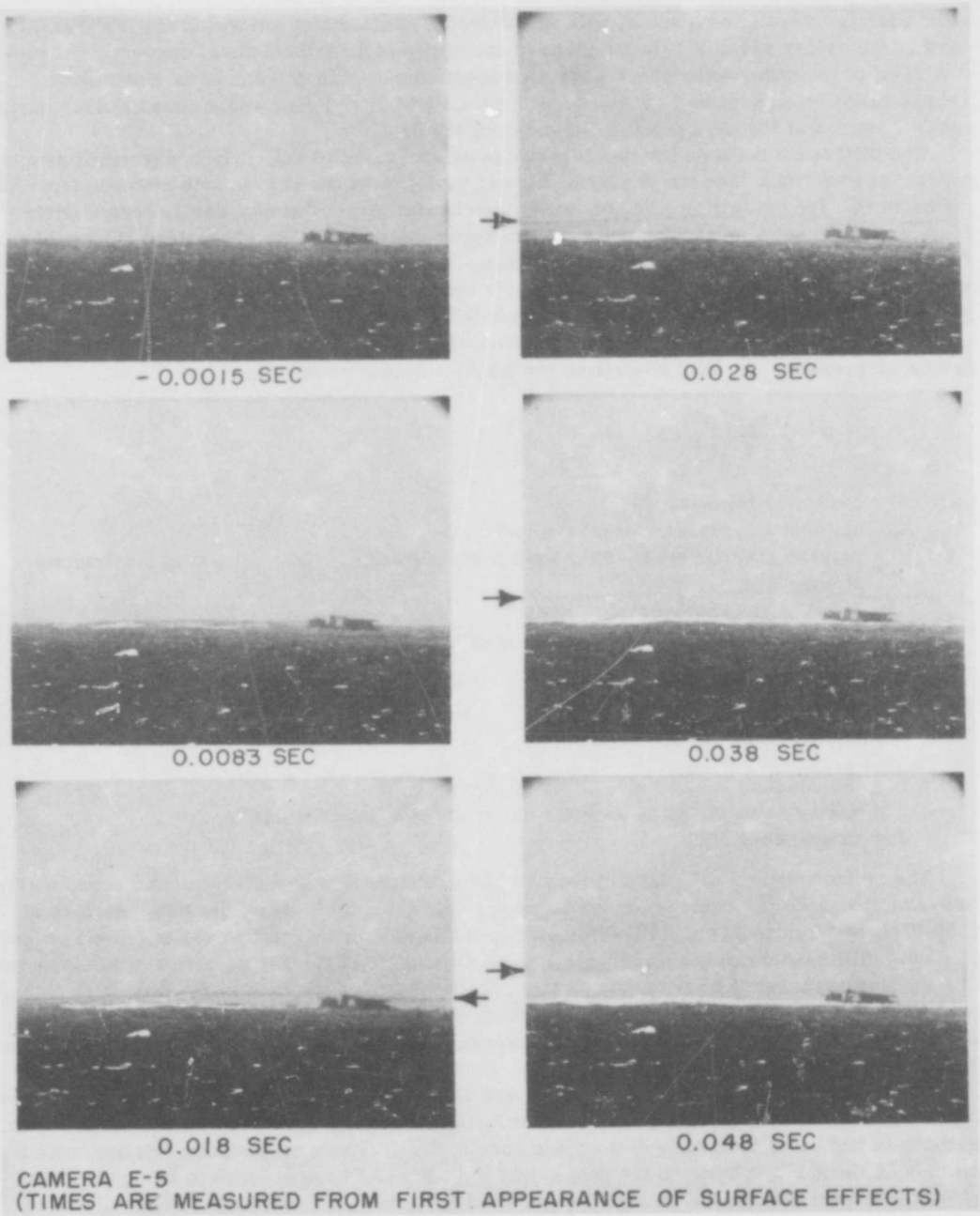


Fig. 3.7— Air shock wave.

time measurements by the method of least squares.

The times of origin of the air shock were obtained by extrapolating the least-squares lines back to the position of the undisturbed water surface. These times are given in Fig. 3.8 and show a fairly smooth distribution, with an estimated minimum at a position about 100 ft forward of the center of the YC (in the plane of measurement). A theoretical curve for the time of arrival of the underwater shock wave as a function of distance from SZ is also indicated. This is based on an assumed constant shock velocity of 5000 ft/sec and a smooth water surface and is centered at the zero position indicated by the data.

The difference between the two curves can be attributed to the surface waves and swells present at shot time. The roughly symmetrical deviation of the curves with distance from SZ indicates that the detonation probably took place beneath the crest of a swell. Such a surface condition would not displace the point of first appearance of surface phenomena but would distort the curve for the measured initial times. Where the curves are widely separated, the air shock wave probably originated in a trough and consequently required a longer time to reach the altitudes at which the measurements were made.

Air-shock velocities were determined from the slopes of the least-squares lines. In each case peak pressure was computed from the Rankine-Hugoniot relation[6]

$$P = \frac{P_0 2\gamma}{\gamma + 1}\left(\frac{U^2}{C^2} - 1\right) \tag{3.1}$$

where P = peak overpressure, psi
P_0 = ambient atmospheric pressure, psi
γ = ratio of specific heats at constant pressure and constant volume in the ambient atmosphere
U = speed of the shock wave, ft/sec
C = speed of sound in the ambient atmosphere, ft/sec

The speed of sound in air, C, was computed to be 1120 ft/sec by means of the formula,[7]

$$C = 0.03281\,[\gamma R(1 + 0.61w)T]^{1/2} \tag{3.2}$$

where R = gas constant for dry air, 2.870×10^6 ergs/g °K
w = mixing ratio, or mass of water vapor per unit mass of dry air
T = temperature, °K

The meteorological data used in the calculations were a temperature of 15.6°C and a relative humidity of 59 per cent, recorded on the Curtiss about 50 ft above the water surface at 1300 PDT, and a pressure of 1025.6 millibars, obtained by extrapolating the sea-level pressure of 1026.6 millibars observed at 1300 PDT to an altitude of 30 ft. The decrease of pressure with altitude was assumed to be the same as that reported in the 1348 PDT radiosonde data obtained on the Curtiss, or 34.5 millibars/1000 ft. These values were converted to a temperature of 288.8°K, a mixing ratio of 6.45 g/kg, and a pressure of 14.87 psi. For these atmospheric conditions, $\gamma = 1.399$.

The calculated values of peak pressure are shown in Fig. 3.9. The point of origin obtained from the times of arrival at the surface is indicated. There is obviously considerable scatter in the data and some indication of a wave nature to the pressure vs distance relation, with a spacing of about 175 ft between the peaks near the center. There appears to be no physical reason to expect this. If the data on both sides of the point of origin, to a distance of 250 ft, are combined and are fitted to a straight line, the following formula is obtained:

$$P = 4.43 - 0.00291x \tag{3.3}$$

where x = horizontal distance from SZ, ft.

Equation 3.3 indicates a peak overpressure of 4.43 psi at SZ. This value is high in relation to the peak pressure[8] of 1.36 psi recorded at the YC by Project 4.5 and the value of 2.0

CONFIDENTIAL

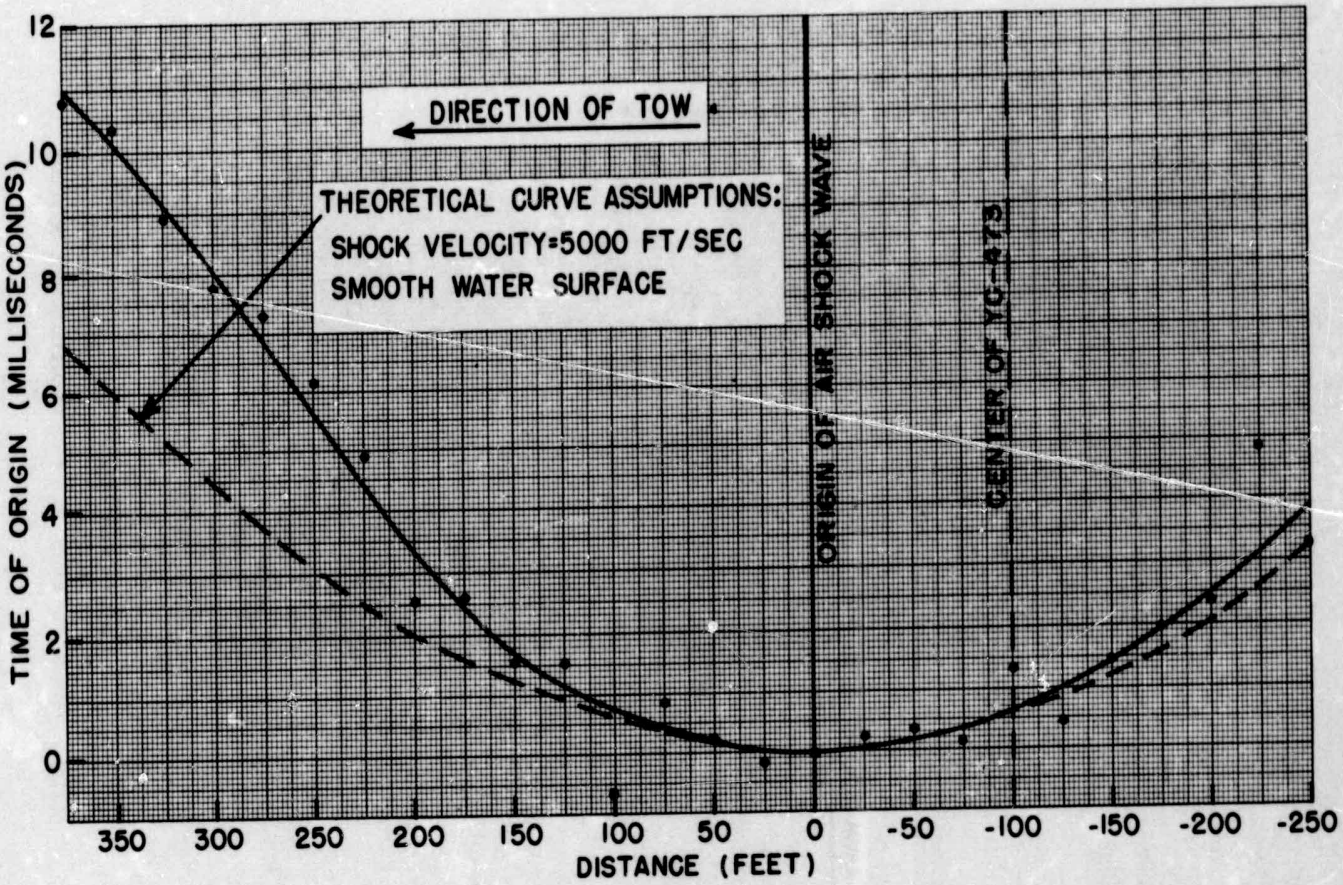


Fig. 3.8—Times of origin of air shock wave.

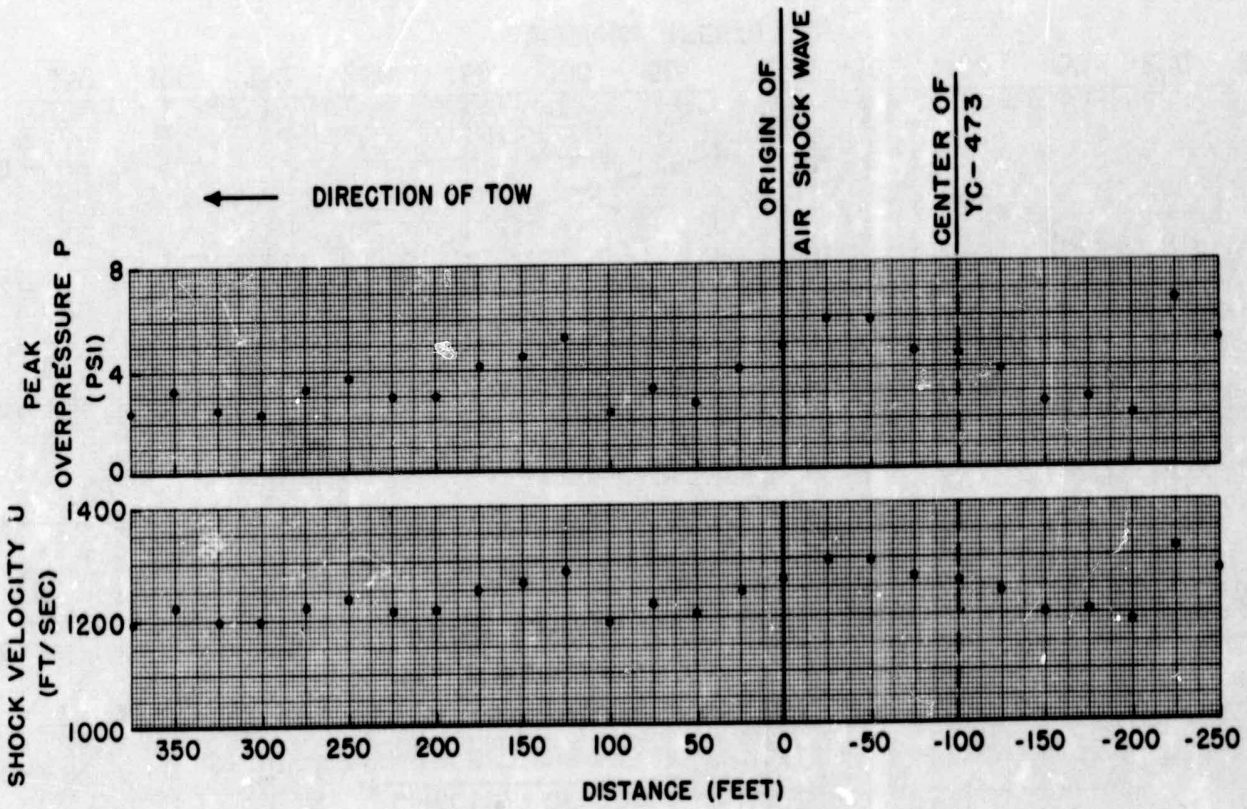


Fig. 3.9—Air-shock-wave velocity and peak overpressure.

psi indicated by scaling the Wigwam test with 32-lb TNT charges.[9]

Since a knowledge of the intensity of the air shock wave above an underwater explosion is important for the establishment of safe weapon-delivery tactics, the method used here will be examined in detail. The possible sources of error in the determination of shock-wave peak pressure will be discussed in terms of the quantities used in Eq. 3.1.

An error in ambient atmospheric pressure would produce the same percentage error in peak overpressure. However, this quantity is measured accurately with marine barometers, and it is doubtful that the error[10] in P_0 would exceed ±0.04 psi or ±0.27 per cent.

The Rankine-Hugoniot relation is based on the assumption that γ is the same on both sides of the shock front. This results in computed pressures being somewhat low, but the magnitude of the error is small for weak shocks and should not exceed −0.50 per cent for peak pressures in the range considered here. An error of ±10 per cent in the relative humidity reported at Wigwam would change the values of γ and P by ±0.01 per cent.

The accuracy of the computed speed of sound depends mainly on the accuracy of the measurement of temperature. Since the measurement[10] could possibly be in error by ±1°C, this introduces a possible error in the speed of sound at Wigwam of about ±0.18 per cent. A ±10 per cent error in relative humidity would result in an error of ±0.04 per cent in the calculated speed of sound. In addition, atmospheric turbulence causes random variations in the speed of sound which result in changes up to 0.2 per cent per second.[6] At Wigwam this factor could have introduced changes in the speed of sound of the order of 0.01 per cent during the period of measurement.

Thus the maximum possible error in the calculated speed of sound is about 0.23 per cent. An error of this magnitude would result in errors in calculated peak pressure of ±5.2 per cent at a peak pressure of 2 psi, ±2.8 per cent at a peak pressure of 4 psi, and ±2.0 per cent at a peak pressure of 6 psi.

The most likely source of fairly large errors in the values of shock velocity is in the process of scaling and measuring the records, which was accomplished by tracing an enlarged projection of each frame and measuring the tracing. Possible causes of erroneous measurement, with an estimate of their magnitudes, are error in focal length of lens, ±0.2 per cent; error in distance from Curtiss to YC, ±1 per cent; error or variation in enlargement factor, ±2 per cent; error in timing, ±0.2 per cent; and measurement errors, ±5 per cent. The assumption that the shock was traveling vertically at all positions would introduce an error of −0.04 per cent at a distance of 250 ft from SZ, where the shock would be expected to rise at an angle of 1.6 deg with the vertical.[8]

These items indicate a total of about ±8.4 per cent for the possible measurement error of a single point on a tracing. However, the values of shock velocity were each based on from four to six data points, and peak pressures were calculated at 21 positions to obtain an estimate of the pressure at SZ. These averaging processes tended to reduce the effect of random measurement errors.

A possible source of more serious error was a correction of 45 ft/sec, which was added to each measurement of air-shock velocity to compensate for the angular motion of the E-5 camera. This was based on an extrapolation of the camera motion before SZT and is subject to considerable doubt. It is conceivable that the value of 45 ft/sec is ±100 per cent or more in error.

Unfortunately, a relatively small error in the measurement of shock velocity at low pressure levels introduces a relatively large error in the peak pressure computed with Eq. 3.1. For example, at the 4-psi pressure level, a 10 per cent error in shock velocity would result in about a 100 per cent error in the peak-pressure calculation. If the 45 ft/sec correction had not been used, the measured shock velocity at SZ would have been 1210 ft/sec, which would indicate a peak pressure of about 2.9 psi.

Thus it appears that the calculated peak-pressure value of 4.43 psi cannot be used with a high degree of confidence. However, it constitutes evidence that the peak air-shock pressures of a deep underwater nuclear explosion may be higher than the peak pressures indicated by the extrapolation of small-scale high-explosive data.

This possibility is supported by the fact that the air-shock pressures observed in Baker

shot (a shallow underwater nuclear burst) in Operation Crossroads ranged from about 40 to 120 per cent higher than those indicated by scaled tests with 32-lb TNT charges. A 45-ton TNT test was more successful in scaling the Baker air shock than was any smaller high-explosive test.[11] Although the Test Baker geometry was radically different from that of Operation Wigwam and the shock wave had different characteristics, this example serves to illustrate the problems involved in extrapolating the results of small-charge tests to the nuclear scale.

3.3 CONDENSATION CLOUDS

About 2.85 sec after the first visible effect on the surface, a condensation cloud appeared directly above the burst as a result of the passage of the air shock wave (Figs. 3.1 and 3.10). The cloud was conical in shape; the vertex, pointing down, was initially about 700 ft above the surface. The top merged with the cloud layer that existed between 2800 and 3500 ft above the level of the sea. No condensation occurred in the relatively dry air above 3500 ft.

Since the edges were not sharply defined, measurements of the size and shape of the cloud are not precise. The initial angle at the vertex was about 90 deg. This angle increased and the vertex became more rounded as the bottom of the cloud evaporated. At the same time the top increased in diameter so that the cloud became flattened in shape. The apparent rate of rise of the bottom was 1300 ft/sec, and the cloud remained visible for about 1.4 sec.

A shock wave in air consists of two phases: a positive, or compression, phase and a negative, or suction, phase. The negative phase does not develop until the shock has traveled some distance from its point of origin, and it tends to be of weaker intensity and longer duration than the positive phase. The temperature of the air in the positive phase of the shock rises above the ambient level because of the adiabatic compression. The temperature then drops as the pressure decreases and reaches a value below the ambient level in the suction phase as a result of adiabatic expansion. However, the temperature changes lag behind the pressure changes.[12]

The condensation clouds that are observed in nuclear and high-explosive tests result from the cooling of the air during the passage of the negative phase of the air shock. When the air is cooled, the water vapor present in the air condenses on atmospheric nuclei, and, if conditions are suitable, a visible cloud of water droplets is formed. The shape of the cloud depends on meteorological conditions and the characteristics of the shock wave.

The meteorological factors that affect the condensation-cloud phenomena are the vertical gradients of temperature and relative humidity and the number and chemical composition of the particles in the air which can serve as condensation nuclei. The relative humidity of the air is defined as the ratio of the quantity of water vapor present to the maximum quantity possible at the given temperature and pressure. However, for practical purposes the maximum amount of water vapor that can be held in clean air depends only on the temperature. When the air is cooled, the maximum water-vapor capacity decreases and relative humidity increases.

In reality, the atmosphere is never clean but contains large numbers of particles, some of which may act as condensation nuclei. Because of the presence of sea salt and other hygroscopic substances in the air, condensation is a continuous process, beginning at low relative humidities, where small quantities of vapor condense on nuclei to form invisible, highly concentrated droplets. With a continued increase in relative humidity, the droplets increase in size until a haze and finally a fog or cloud forms.[13]

For example, a sea-salt nucleus will start to grow if the relative humidity rises above 78 per cent.[14] Therefore a cloud or fog can form at a relative humidity as low as 79 per cent if sufficient sea-salt nuclei are present. Relative humidities ranging between about 80 and 100 per cent have been observed in natural clouds and in fog, although clouds of this type generally have a relatively small droplet size and liquid-water content. However, they can be sufficiently dense to reduce visibility to low levels.

The rate of growth of a droplet depends on its diameter and the vapor-pressure gradient between the droplet and the surrounding air. At a constant temperature the rate of growth

CONFIDENTIAL



3.7 SEC

CAMERA D-3
(TIME IS MEASURED FROM FIRST APPEARANCE OF SURFACE EFFECTS)

Fig. 3.10—First condensation cloud.

CONFIDENTIAL

depends on droplet size and relative humidity.

To examine the formation of the first condensation cloud at Operation Wigwam, the radiosonde data obtained on the Curtiss at 1348 PDT were used. According to this record the surface meteorological data were pressure, 1025 millibars; temperature, 15.6°C; and relative humidity, 66 per cent. At a height of 3480 ft the pressure was 904 millibars, the temperature was 4.8°C, and the relative humidity was 83 per cent. For computation purposes it was assumed that pressure and temperature decreased linearly with height and that relative humidity increased linearly with height between these levels. Above 3480 ft, temperature increased and relative humidity decreased to values of 8.6°C and 21 per cent, respectively, at an altitude of 3800 ft. A deck of strato-cumulus clouds extended from a height of 2800 ft to the base of the temperature inversion at about 3500 ft.

It appears likely that the air below the cloud level contained an ample number of sea-salt nuclei of a wide range of sizes. These are common in oceanic regions, and their presence was demonstrated by the haziness of the air, which reduced horizontal visibility to 10 miles or less. Since the relative humidity below the clouds was less than 80 per cent, these were essentially dry particles.

The radiosonde data were used to calculate the drop in atmospheric pressure, ΔP_c, which was required to reduce the air temperature and thereby increase the relative humidity to values of 80, 85, 90, 95, and 100 per cent. This was done for altitudes ranging from the surface to the base of the temperature inversion at 3480 ft. The curves are shown in Fig. 3.11.

If the relative humidity required for the formation of a cloud is known, it is possible to estimate the necessary pressure drop from Fig. 3.11. Where the pressure decrease below the ambient level due to the passage of the suction phase of the shock wave, ΔP_s, is equal to, or in excess of, ΔP_c, condensation should occur in sufficient amount to produce a visible cloud, provided also that the pressure is reduced for a sufficient time. In Operation Wigwam the negative pressure in the air shock was not determined. The condensation cloud provided an indirect method of estimating its magnitude.

The times of arrival of the shock front at the altitudes in which the cloud formed can be estimated by using an average shock velocity of 1200 ft/sec between the surface and 3000 ft. If it is assumed that the duration of the positive phase of the shock wave was equal to the inferred time constant of 0.430 sec at the YC,[8] it then becomes possible to estimate the times of arrival of the suction phase. The air-shock data obtained with underwater high-explosive tests scaled to the Wigwam geometry[9] indicated that the positive duration remained constant up to a scaled height of 3080 ft directly above SZ. It will be assumed here that this result may be applied to the nuclear test.

It was noted that the condensation cloud first became visible at an altitude of 700 ft and above at 2.85 sec after SZT. The entire cloud had developed by 3 sec after SZT.

Figure 3.12 shows the times of arrival of the shock front and suction phase and indicates the times of formation and dissipation of the cloud. The actual time required for the cloud to form depends on the rate of decrease of pressure with the passage of the suction phase and the lag between pressure and temperature changes, both of which are unknown, as well as on meteorological conditions. Figure 3.12 permits a rough estimate of the time required for cloud formation, however, and indicates times of the order of 1 sec at the base of the cloud and 0.1 sec at the top. The cloud persisted longer at the top than at the bottom, which may be partially accounted for by the increase in relative humidity with height.

Because of the lack of condensation-nuclei data at Wigwam, it is not possible to compute from theory the time required for cloud formation as a function of relative humidity. However, condensation is relatively slow at low humidities, and it appears that only the attainment of a relative humidity of 100 per cent or higher could account for the rapid formation of the cloud.[14] It might therefore be assumed that ΔP_s was approximately equal to ΔP_c for 100 per cent relative humidity at an altitude of 700 ft and that ΔP_s exceeded ΔP_c at greater heights, which led to supersaturation of the air. Quantitatively, Fig. 3.11 indicates that the pressure drop in the suction phase equaled or exceeded 1.13 psi at a height of 700 ft. At higher levels ΔP_s would be expected to exceed the values of ΔP_c shown in the figure.

Unfortunately, few of the shock-wave records of the scaled 32-lb TNT shots were long

CONFIDENTIAL

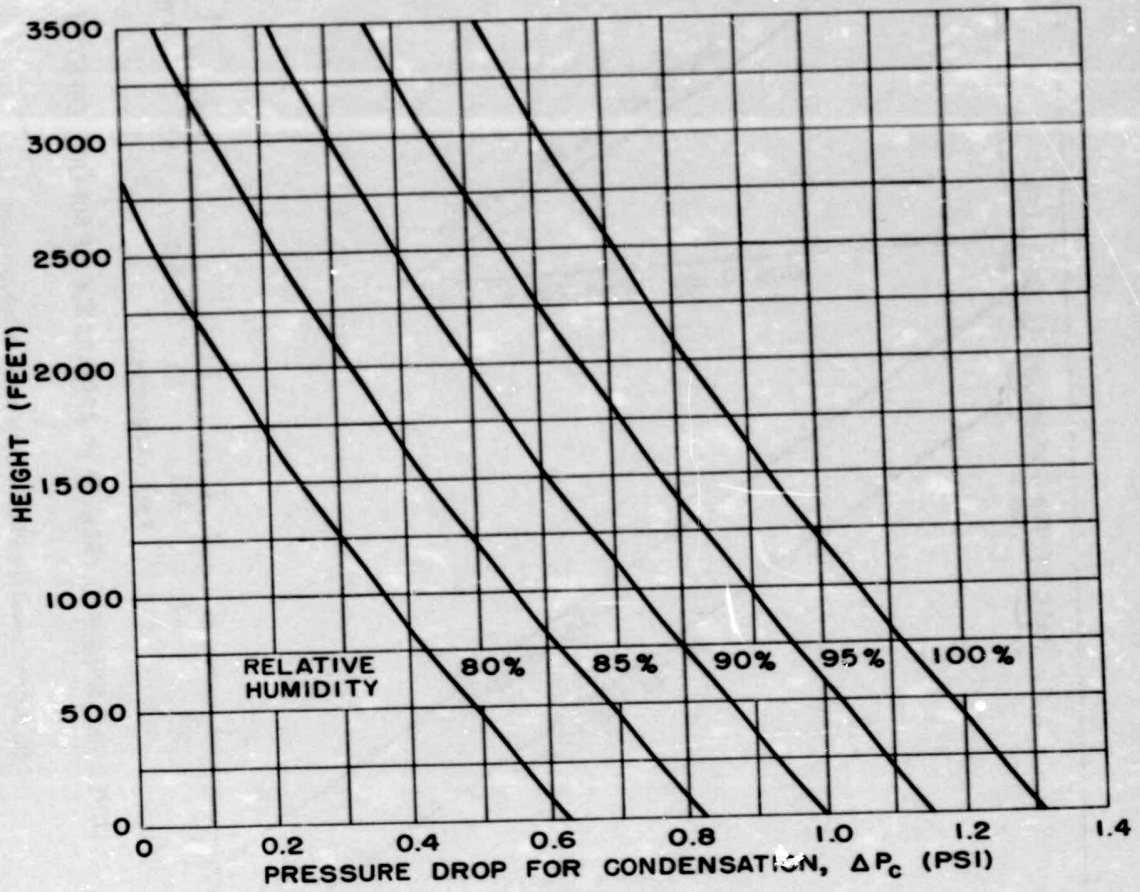


Fig. 3.11—Pressure drops required for condensation.

CONFIDENTIAL

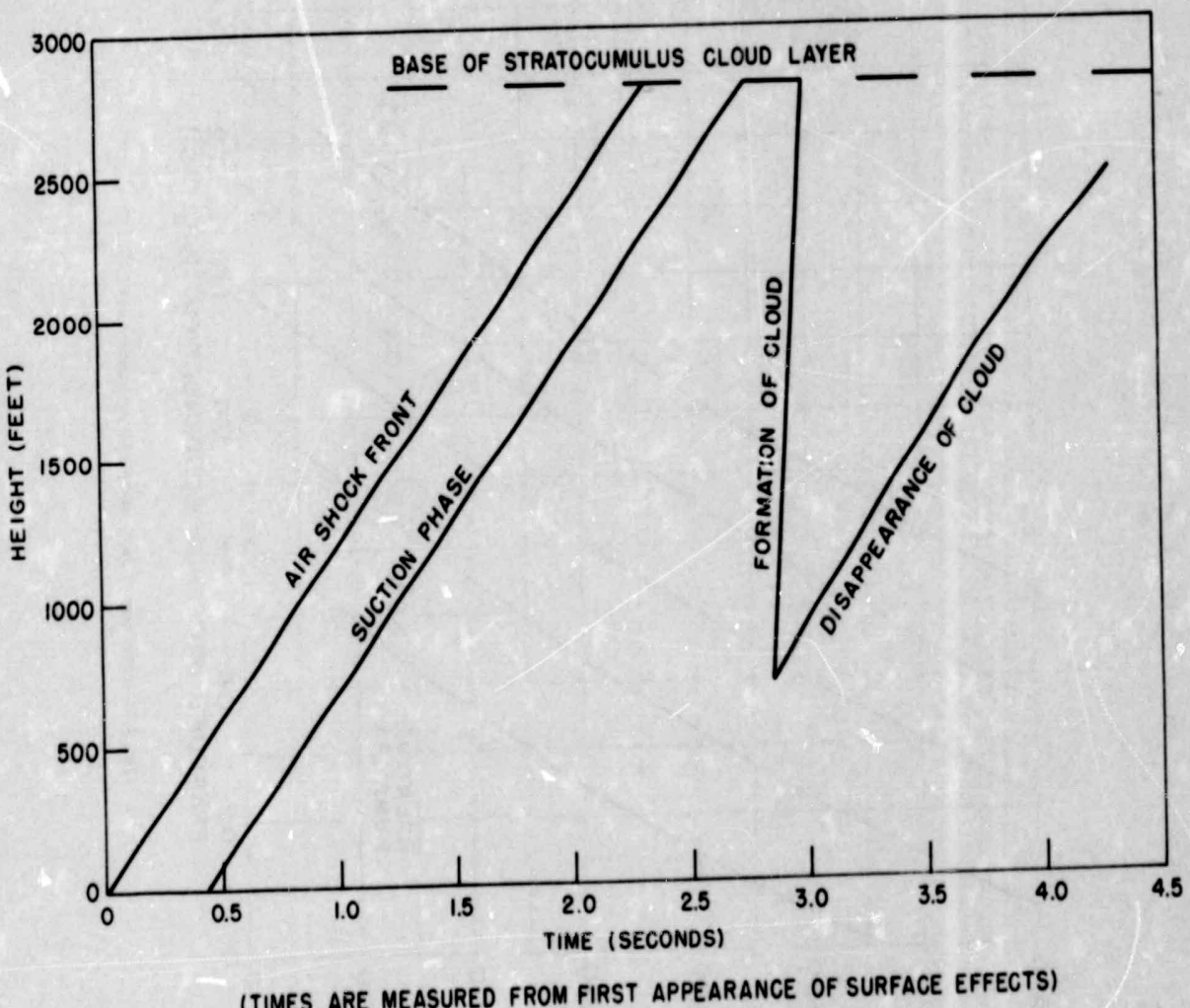


Fig. 3.12—Times of formation and dissipation of condensation cloud.

enough to show the maximum pressure drop in the negative phase.[9] These have been read at NOL, and the values of peak pressure and ΔP_s are shown in Table 3.2. Gauge positions have been scaled to the Wigwam geometry.

The data indicate a positive to negative pressure ratio of 2.1 at 492 ft above SZ and show an increase in the ratio with height above a point 2990 ft from SZ. As an approximation it will be assumed here that the peak overpressure at a point 700 ft above the YC at Wigwam was also

Table 3.2 — AIR-SHOCK DATA FROM SCALED TNT TESTS

Gauge position scaled to Wigwam				
Vertical distance, ft	Horizontal distance, ft	Peak overpressure (P), psi	Peak negative pressure (ΔP_s), psi	Pressure ratio positive/negative
492	0	1.8	0.84	2.1
62	2990	0.4	0.33	1.2
492	2990	0.5	0.24	2.1
492	2990	0.4	0.12	3.3
1230	2990	0.5	0.13	3.8

2.1 times as intense as the negative pressure. Since ΔP_s was assumed to be 1.13 psi, this implies a peak positive pressure of 2.4 psi at that level.

If the scaled peak-pressure measurements[9] are plotted as a function of height above SZ, an approximately linear relation is indicated to a full-scale height of about 2000 ft. Peak pressures of 2.0 psi and 1.65 psi are shown at the surface and at an altitude of 700 ft, respectively. By use of the ratio between these values, the 2.4-psi Wigwam pressure at 700 ft can be extrapolated to 2.9 psi at the surface. This is intermediate between the values of 2.0 psi indicated in scaled high-explosive tests and 4.43 psi calculated from the Wigwam air-shock velocity. Because of the many assumptions in the method, the value of 2.9 psi is, of course, subject to considerable uncertainty.

The shape of the condensation cloud can be accounted for by drawing the contours of constant ΔP_s in cross section. These are shown in Fig. 3.13. The assumption has been made that the contours have approximately the same shape as the peak-pressure contours obtained with high-explosive scaling of the Wigwam shot, but the values assigned to the contours are speculative. The lines of constant atmospheric ΔP_c for a relative humidity of 100 per cent are also shown. The shaded area indicates the region where $\Delta P_s \geq \Delta P_c$. The shape of the shaded area is approximately that of the Wigwam condensation cloud.

A second, less clearly defined condensation cloud appeared about 8.5 sec after SZT. The base was initially about 2400 ft above the surface of the water, and the lower edge of the cloud appeared to rise at a rate of 1000 ft/sec. The entire cloud had disappeared in about 0.7 sec.

The time of appearance of the cloud indicates an origin of the shock front at the surface between 5 and 6 sec after the appearance of the first shock. This indicates that the air shock wave that formed the second cloud was produced by the arrival of the bottom reflection of the primary underwater shock wave at the surface of the water.

Assuming, as before, that $\Delta P_s = \Delta P_c$ at the base of the cloud, a value of 0.73 psi is obtained for the pressure drop in the suction phase of the second shock at a height of 2400 ft.

3.4 WEAPON POSITION

Projections of photographs of the radial spread of visible surface effects at early times were measured in order to determine the center of the surface disturbance and thereby estimate the horizontal excursion of the weapon from its intended location directly beneath the well of the YC-473. Aerial photographs of the expanding slick taken from the three photo-

CONFIDENTIAL

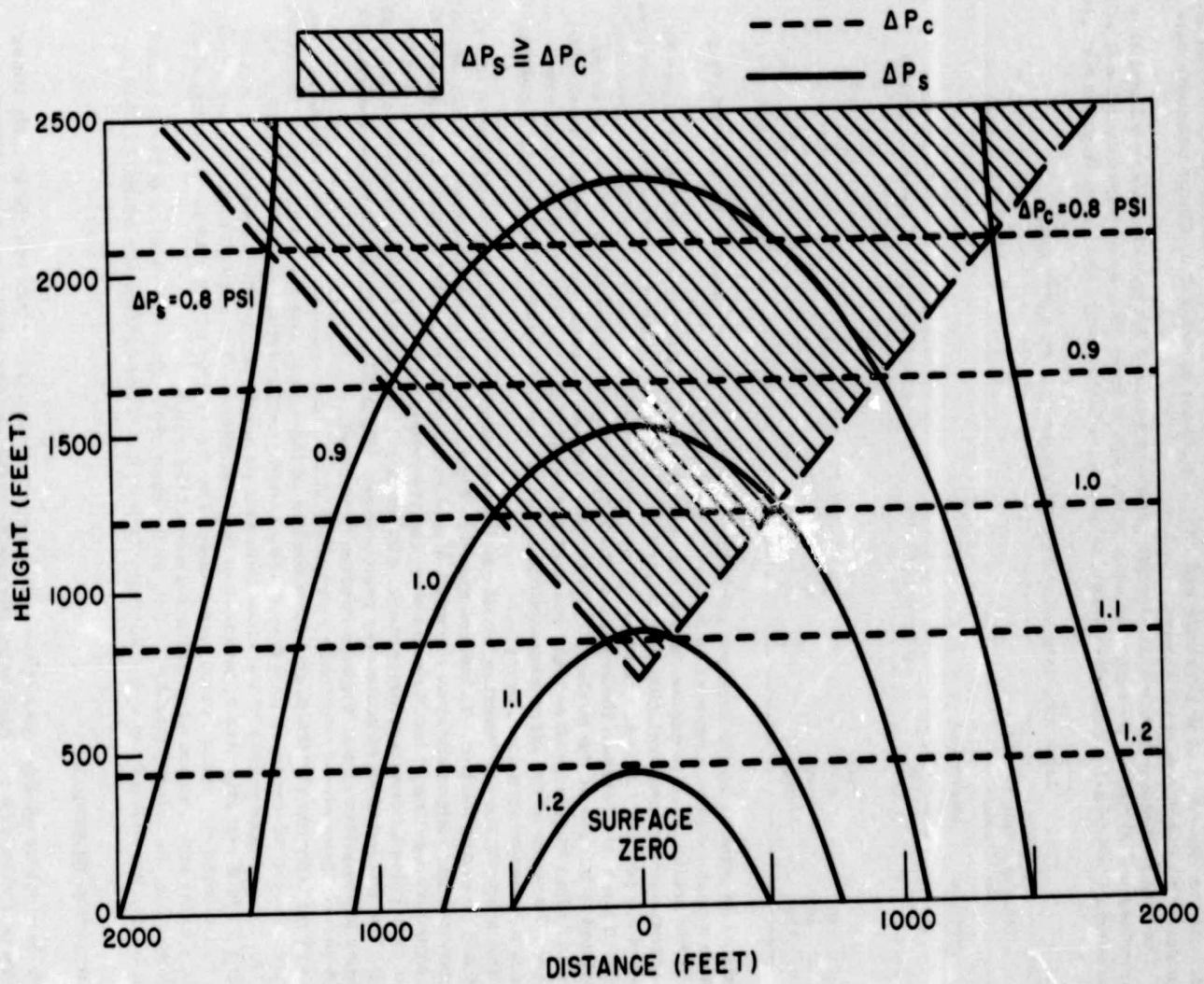


Fig. 3.13—Contours of ΔP_c and ΔP_s.

graphic aircraft, together with a photographic record of the air shock wave taken from the Curtiss, were used for this measurement. It was felt that surface photography of the initial spray would be less reliable for this purpose because of the lack of symmetry caused by surface roughness. Neither was the edge of the slick clearly defined for the same reason.

The weapon-positioning data were obtained from the aircraft photographs by measuring the position of the YC relative to the edges of the slick on several frames from each record. The weapon position relative to the YC as seen from the Curtiss was obtained by noting the minimum of the distribution of measured data points for the time of emergence of the air shock vs horizontal distance from the YC (Fig. 3.8).

The weapon-position data are summarized in Table 3.3 and in Fig. 3.14, which is a projection plot locating the weapon relative to the well of the YC by means of the data from the four camera stations.

Table 3.3 — APPARENT HORIZONTAL EXCURSION OF WEAPON AS VIEWED FROM DIFFERENT CAMERA STATIONS

Camera	True bearing of camera from YC-473, deg	Apparent excursion of weapon from intended position
E-5	303	80 ft forward
G-1, G-2, G-3	218	70 ft aft
H-1, H-2	87	6 ft forward
J-2	279	24 ft forward

On the basis of the data plotted in Fig. 3.14, it is estimated that the detonation took place within 40 ft of a position 105 ft to starboard and 10 ft forward of the intended position directly below the well of the YC. (In the Preliminary Report ITR-1059 of Project 1.5, it was estimated that the detonation took place within 50 ft of its intended position. In this early determination only forward and aft excursion was considered; it was assumed erroneously that lateral excursion was negligible.) This area is indicated in Fig. 3.14 by a circle. In determining this probable location of the weapon, the aerial photographs were considered more important than the E-5 record.

The preceding measurement of the excursion of the weapon is in good agreement with the horizontal excursion due to drag on the weapon cable calculated by Project 2.8 on the basis of the motion of the array and the ocean currents in the area.[15] Assuming an effective drag area proportional to the number of individual cables, Project 2.8 calculated an excursion of the weapon of 99 ft to starboard and 13 ft forward of its intended position. Such close agreement between the calculated and measured excursion is probably fortuitous.

3.5 MOTION OF YC-473

The YC-473 was visible on the E-5 record for about 0.5 sec after the first disturbance of the water surface (Fig. 3.7). It was then obscured by the rising spray. The aerial photographs showed the YC for about the same length of time since the lines of sight from the photographic aircraft were almost horizontal. The YC was pitching before the burst occurred and was at an angle of about 2 deg with the horizon, with the bow elevated, when the underwater shock wave reached the surface.

The vertical motion of the YC was determined from the E-5 record. Measurements were made at the bow and at distances of 18, 40, 65, 87, and 109 ft aft of the bow. These locations were chosen for relative ease of measurement since the details of the structures on the barge were difficult to see on the photographs. The measurements of the rise of the helicopter platform are believed to be more reliable than measurements of the motion of the forward half of the barge because this was more clearly defined than the other structures.

CONFIDENTIAL

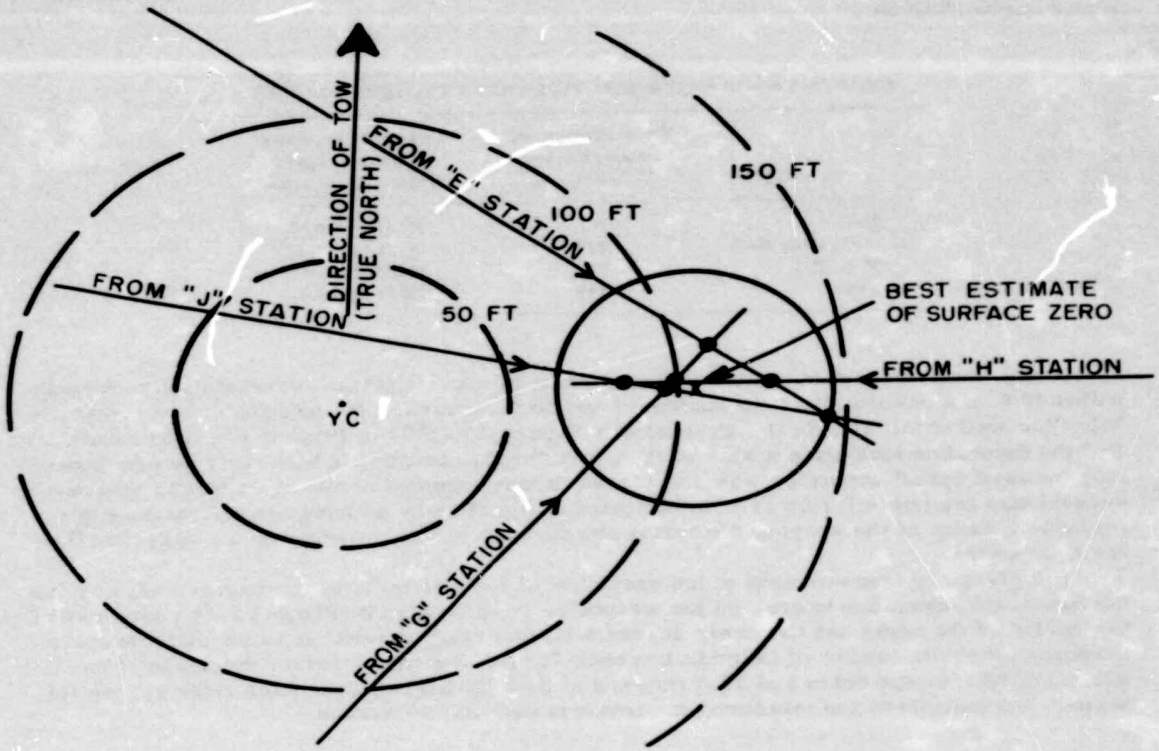


Fig. 3.14—Position of weapon in relation to well of YC-473.

The measured data points are shown in Fig. 3.15. There is considerable scatter, and the initial time of rise is not certain since the motion was not measurable until about 0.04 sec had elapsed. However, the initial velocity of rise could be estimated for each position by determining the slope of the height vs time curve from about 0.04 to 0.10 sec. At later times some of the measurements indicated a rapid deceleration.

The measured velocities are given in Fig. 3.15. The average of the six readings is 75.8 ft/sec. As a check the velocity was measured on record C-6, although the frame rate was slower than that on the E-5 record and the resolution was somewhat poorer. In addition, the YC was viewed bow-on; thus only one position could be measured. However, the measured rate of rise on the C-6 record was 73.2 ft/sec, which is in good agreement with the average observed on E-5.

The maximum measured speed of rise occurred 40 ft behind the bow at the position of the U frame that straddled the well through which the bomb was lowered.[16] The vertical velocities were lowest at the bow and stern, indicating that the barge was starting to buckle aft of the U frame. It appears likely that the YC eventually split into two parts, possibly at the aft end of the well. At a later time a portion of the YC became visible in the rising plumes.

According to a theoretical treatment[17] the barge was expected to rise with a velocity approaching the initial velocity of the spray dome. This prediction was based on the assumption that the thickness of the top layers of water rising at a velocity indicated by Eq. 1.4, or close to that velocity, would be at least as great as the draft of the vessel. Another approach, which leads to the same result, would be to assume that the YC would be displaced by the shock wave in the same manner as the surface water.

It was determined by Project 1.2.1 that the peak underwater shock pressure[1] at the position of the barge was 3010 psi. If this value is inserted in Eq. 1.4, an initial velocity of 86.7 ft/sec is obtained.

Since the proper value of T is uncertain and is probably small for large charges and for rough water,[18,19] Eq. 1.5 was not used. In the calculations the shock front propagation velocity, U, at the surface[2] was taken to be 5030 ft/sec, and the value of water density, ρ, was 1.99 slugs/ft^3.

The average measured velocity of 75.8 ft/sec was about 13 per cent less than that indicated by Eq. 1.4. The agreement between the maximum measured vertical velocity of the YC (86.7 ft/sec) and the velocity indicated by Eq. 1.4 is probably not significant since the individual measurements are not precise and may have errors as great as ±10 per cent.

3.6 SPRAY DOMES

3.6.1 Description

Aerial photographs showed that the first spray dome was not sharply outlined and that the spray formed ridges and valleys which probably coincided with the existing crests and troughs of the rough sea surface. This effect was also observed from the YFNB-13, which was close to the edge of the spray dome. Camera G-2 in Fig. 3.16 shows the striations and the edge of the dome as viewed from the air. Irregularities were observed in the upper surface, and buoys from the tow cable (Fig. 3.16) were seen to rise above the dome, followed by trails of spray. The primary spray dome spread radially along the water surface at an extremely rapid rate and reached a maximum diameter of about 14,000 ft. The radial growth as seen from surface camera stations is shown in Fig. 3.3. Views of the spray dome as seen from three observation points are shown in Fig. 3.16.

Tracings of the expanding dome profile as a function of time are shown in Fig. 3.17. It should be noted that the contours were fairly smooth at early times. As the height increased, the irregularities became more pronounced, and jets or spikes rose above the main dome.

The initial velocity of rise of the spray dome was measured in the vicinity of SZ on several records to provide data for estimating the peak pressure of the underwater shock wave (Sec. 3.6.2). It would have been desirable to measure the velocity at the position indicated in Fig. 3.14 as the point directly above the weapon. However, on some records the spray

CONFIDENTIAL

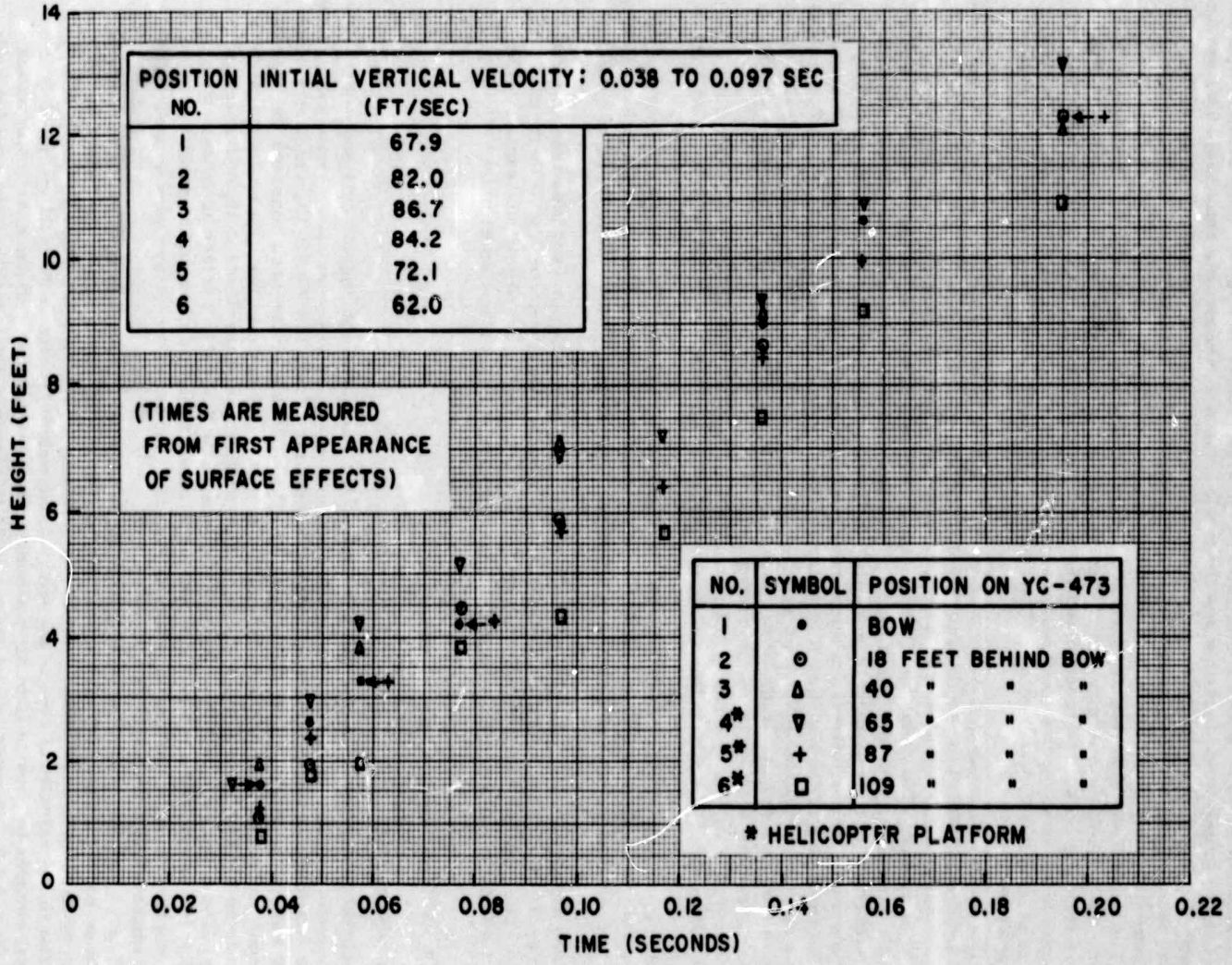


Fig. 3.18—Vertical motion of YC-473.

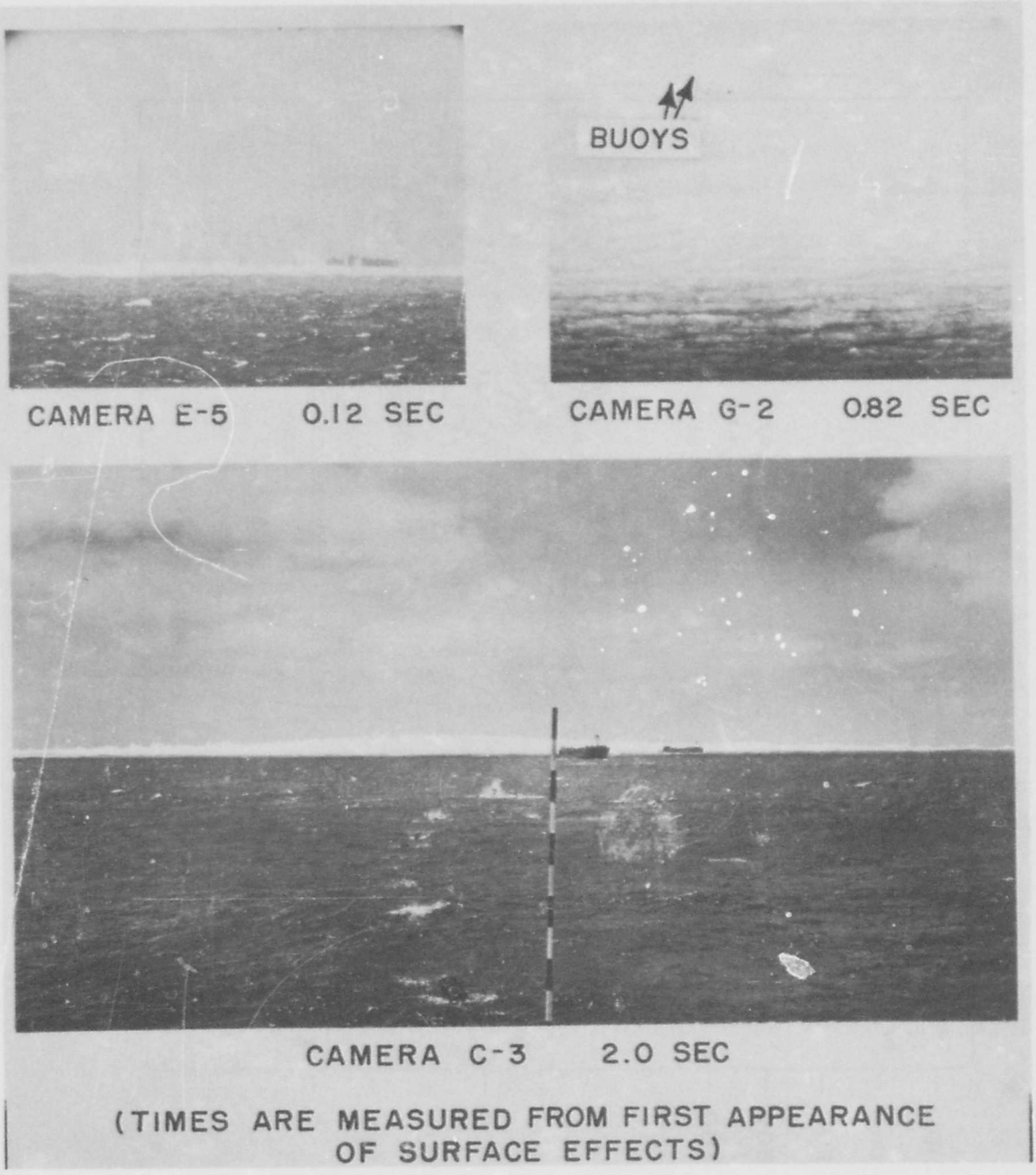


Fig. 3.16—First spray dome.

CONFIDENTIAL

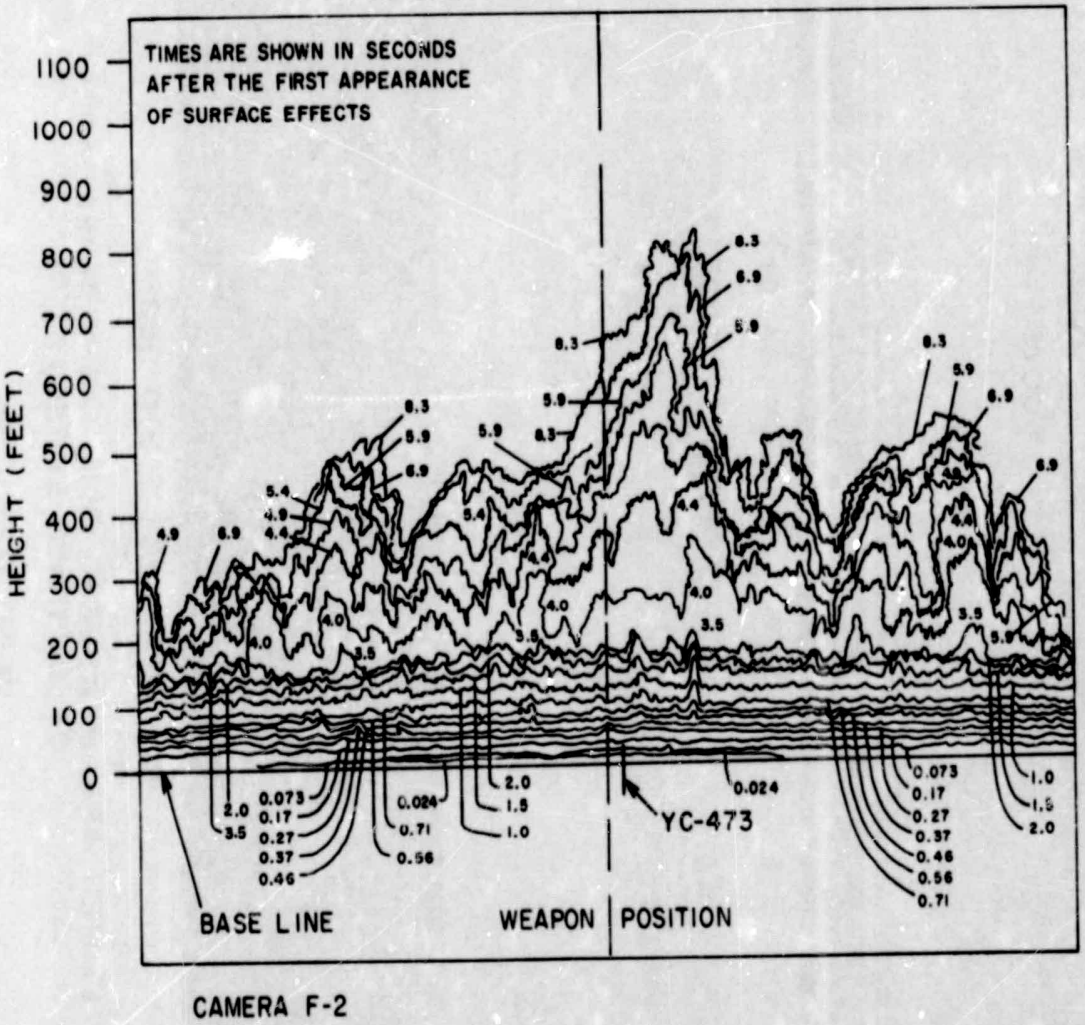


Fig. 3.17—Tracing of dome profiles.

appeared to be influenced by the presence of the YC, and on others the spray dome was not clearly defined or was irregular at SZ. When it was felt that errors would be introduced by measuring the dome velocity at SZ, measurements were made at positions in the vicinity where the dome was smoother and more clearly defined. Since theory indicates that the initial spray velocity should be reduced by only about 0.3 per cent at a distance of 100 ft from SZ, the measurements were confined to this region. In each case the velocity was obtained by fitting a least-squares line to the data points before pronounced deceleration occurred. The values are given in Table 3.4.

The average vertical growth of the center of the spray dome is presented in Fig. 3.18, which shows a composite of several measurements. The height of the bulk of the spray, as well as the greatest height of the spikes, is shown.

Table 3.4—INITIAL VELOCITY OF SPRAY IN VICINITY OF SZ

Camera	Distance from SZ, ft	Initial velocity, ft/sec	Time interval used, seconds after SZT
C-6	0	124	0.12–0.63
E-5	55	119	0.03–0.32
D-2	15	106	0.09–0.59
F-1	0	106	0.11–0.46
F-1	48	120	0.11–0.46
F-2	4	113	0.12–0.76

The primary dome had reached a height of about 160 ft when a second dome, formed by the first bubble pulse, rose above it. At this time, which was about 2.5 sec after the initial dome appeared, the first spray dome had almost attained its maximum height. An extrapolation of the height vs time curve indicates a maximum height of about 170 ft if no secondary dome effects had occurred. However, as shown in Fig. 3.18, the highest spikes reached a height of about 250 ft. The profile of the dome at the time it had almost reached its maximum height is shown by the contour labeled 2.0 sec in Fig. 3.17. The higher lines show the second dome.

The probable time of appearance of the second dome at the water surface was 2.3 ± 0.1 sec after the appearance of the first dome. When corrected for the estimated bubble migration[2] of 400 ft, this provides an estimate of the period of the first bubble oscillation of about 2.4 sec. This value is less than the average period[2] recorded by Project 1.2, which was 2.88 sec. The difference may possibly be attributed to the gradual rise in pressure preceding the arrival of the sharply defined pressure peak measured on the gauge records. However, since the gauges were at positions on one side of the burst at depths of 500 and 1000 ft, an alternative explanation is that the bubble pulse was possibly not symmetrical about the origin and may have had a different shape at positions directly above the burst. Differences of this nature have been observed in small-scale experimental work and can be attributed to the fact that the collapsed bubble may have a mushroom shape instead of a spherical shape.

The second dome was extremely spiky in appearance (Fig. 3.19) because of the disturbed condition of the surface following the formation of the primary dome. The vertical growth of the highest spike of the second dome is shown graphically in Fig. 3.18, which indicates a maximum height of about 900 ft. The initial velocity of the second dome was greater than the initial velocity of the first dome. However, this does not imply that the peak pressure in the bubble pulse was greater than the peak pressure in the primary underwater shock wave since Eq. 1.4 is not applicable to secondary spray domes. The main body of the second dome had a diameter of about 5000 ft, although scattered tufts of spray extended to greater distances.

There was evidence on the photographic records of the formation of spray at later times, but it was not possible to determine the nature of this effect with certainty since it did not extend beyond the first and second domes.

CONFIDENTIAL

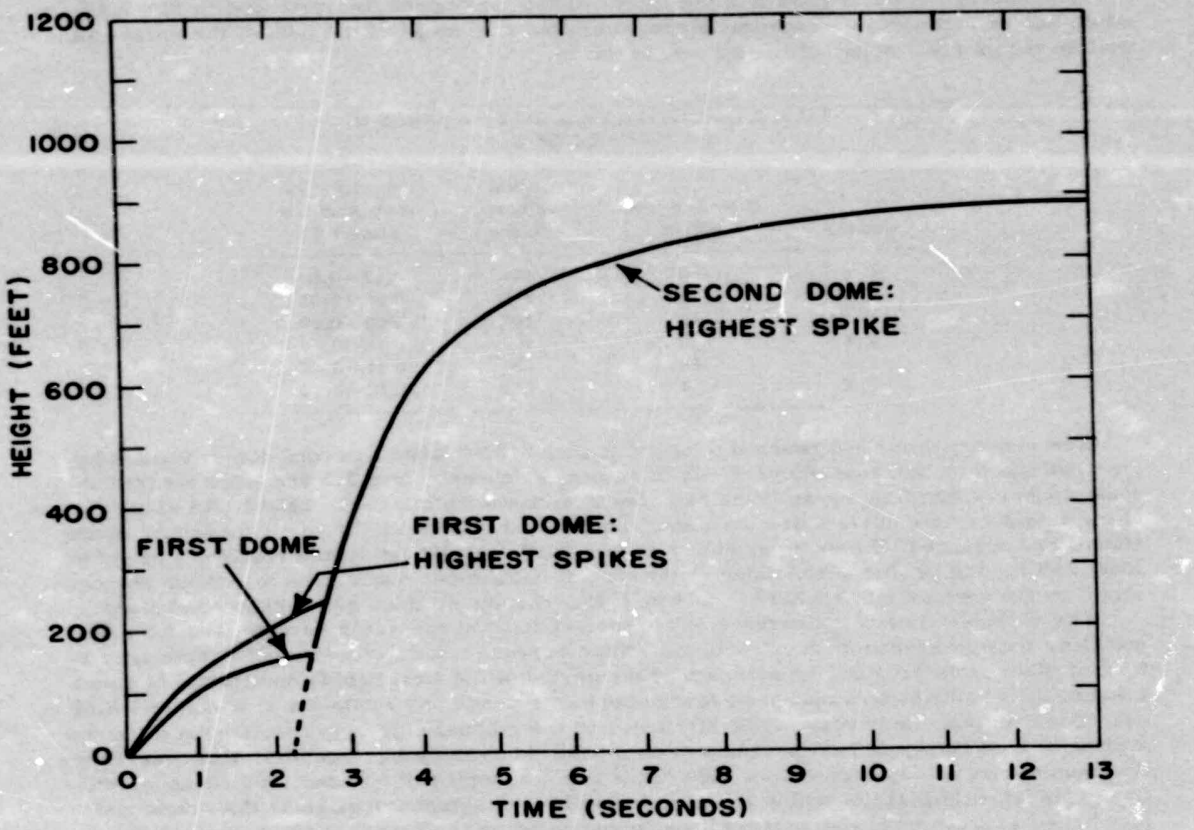
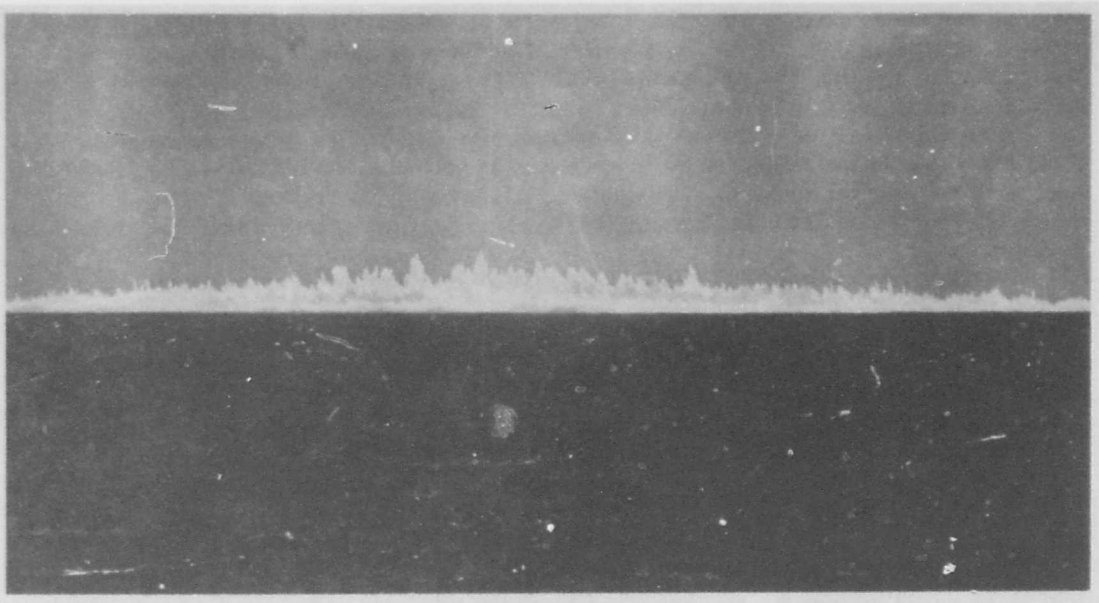


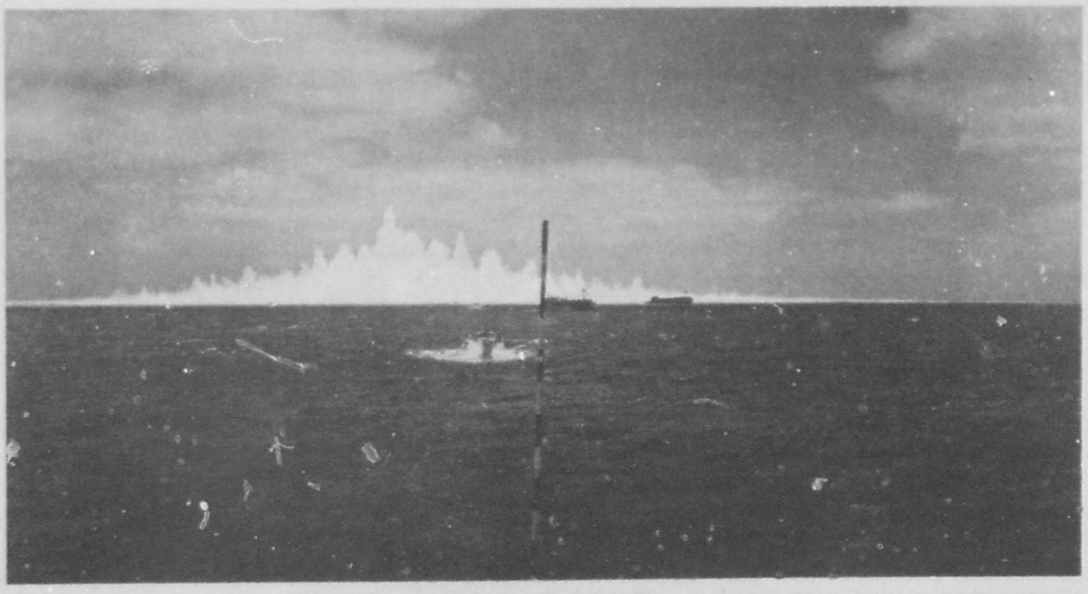
Fig. 3.18—Height of spray domes vs time.

CONFIDENTIAL



3.0 SEC

CAMERA E-3 A



6.0 SEC

CAMERA C-3

(TIMES ARE MEASURED FROM FIRST APPEARANCE OF SURFACE EFFECTS)

Fig. 3.19—Second spray dome.

CONFIDENTIAL

3.6.2 Calculations of Underwater-shock-wave Peak Pressures

The arithmetic mean of the initial spray-dome velocities presented in Table 3.4 is 115 ft/sec. Substituting this value in Eq. 1.4 and solving for peak pressure yields a value of 3990 psi. In the calculations, ρU was taken to be 10,000 lb sec/ft^3 (Sec. 3.5). The value of 3990 psi is 33 per cent higher than the peak pressure of 3010 psi obtained by extending the Project 1.2.1 data to the water surface by the use of the published formula.[1] This difference cannot be accounted for in terms of measurement error since the errors should not exceed about ±10 per cent for the average value given. The value of ρU is probably correct to ±0.5 per cent. If a value for T were inserted in the calculation, the computed peak pressure would be greater than 3990 psi.

Measurements of the initial velocity of the dome were also made at distances extending to 1600 ft from SZ to see whether underwater peak pressures calculated at these positions would show better agreement with the observed values. In Fig. 3.20, the computed peak pressures are compared with a smooth curve[1] that was fitted to the observed pressures. The calculated values range generally from 15 to 60 per cent higher and exhibit the same discrepancy with the measured pressures as was shown at SZ.

The disagreement between the peak underwater pressures indicated by instrumentation and those calculated from Eq. 1.4 is not fully understood. Although the formula has been used with some degree of success in high-explosive work, there are anomalous results in the literature which have not been fully explained. Some of the reported results are summarized here.

In a study of the surface phenomena of sixteen 1-, 2-, and 8-oz charges,[20] it was observed that spray formation was a discontinuous process and that a small amount of barely visible spray was projected ahead of the main body. However, the initial velocities of both the fine faster spray and the main body of spray were less than those indicated by Eq. 1.4.

Experimentation with 69 charges weighing from 0.05 lb to about 4 lb indicated that the percentage standard deviation of peak pressures computed with Eq. 1.4 averaged about 6 per cent and that the computed peak pressures were in good agreement with theory.[18] Two tests with charges weighing about 5 lb yielded a difference of only about 1 per cent between calculated pressures and pressures recorded with gauges.[21]

When the depths of explosion of 39 charges weighing from 100 to 1000 lb were determined by measuring the initial velocity of rise of the centers of the spray domes, an average error of about 6 per cent was obtained, and the measured spray velocities were within about 7 per cent of the acoustic particle velocity at the surface.[22] However, it was necessary to ignore the high dome velocity shown in each photographic record for the first few frames (about 0.1 sec).

The explosion depths calculated from the initial dome velocities of a series of five 245-lb charges exploded at a known depth showed an average deviation[23] of about 5 per cent. This series also showed evidence of high initial velocities for a brief period.

When a series of twenty-three 240-lb charges was fired statically to test the dome-velocity method, the calculated peak pressures agreed to within 6 per cent with values recorded by gauges.[24] High initial velocities were reported in this study also but were not used in the calculations.

The data from 42 charges ranging in weight from 44 to 4450 lb were analyzed from the point of view of theory, and measured dome velocities were compared with those calculated by means of Eq. 1.4 and a knowledge of the explosion pressure-time curve.[25] In this case the measured velocities were less than indicated by Eq. 1.4.

It should be noted here that spikes of spray which rose above the main dome were frequently observed in the small-scale tests. However, these were not measured, and only the smoothed dome was used for the determination of velocities. This method was also followed on Wigwam.

The high initial velocities were reported only when the method of reference 22 was applied.[22–24] In this technique a plot of h/t against t was made, where h is the spray dome height and t is the time. The plots exhibited considerable scatter at early times, but the data points usually fell on a fairly straight line after about 0.3 sec. This straight line was ex-

CONFIDENTIAL

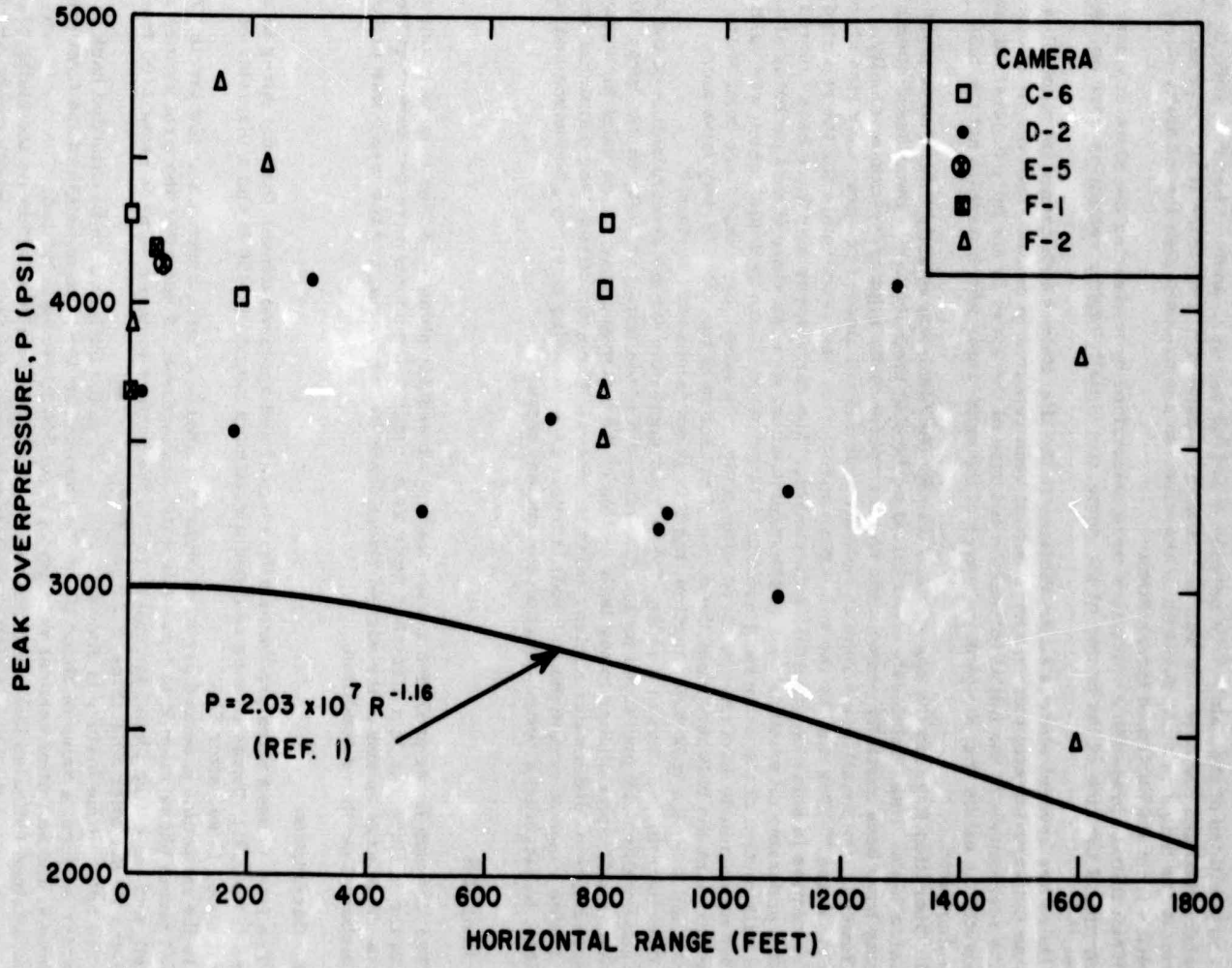


Fig. 3.20—Calculated peak overpressure at the surface vs distance.

trapolated back, and the value of h/t at t = 0 was assumed to represent initial velocity. These initial velocities were in good agreement with theory.

The positions of the data points between 0 and 0.3 sec were doubtful because zero time was not established and the base line was sometimes ill-defined.[22] Therefore it is not possible to determine the magnitude and duration of the reported anomalously high initial spray-dome velocities from the published information.

When initial spray-dome velocities were determined by measuring the slope of a streak photograph of the rise of the center of the dome, the initially higher velocities were not observed.[18,21]

There are several obvious contradictions in the literature which cannot be reconciled because the experimental methods have not all been reported in detail. However, it is clear that the mechanism of the initial formation and rise of the spray is not fully understood, and the possibility exists that the peak pressure of the underwater shock wave is not the only governing factor.

In Operation Wigwam the sea surface was rougher than that usually tolerated in high-explosive tests. This doubtlessly contributed to the observed scatter in the measurements and may have been partially responsible for the unexpectedly high spray-dome velocity.

However, the small-scale results indicate that a small amount of spray may rise above the main dome.[20] This may be the same phenomenon that was responsible for the reported high velocities in some larger scale experiments. The early spray may have been ignored in some programs or smoothed out in the measurement process since it was probably absorbed in the bulk motion of the dome very quickly.[26] In the Wigwam spray dome, which was vastly greater in magnitude than any observed previously, this early spray may have been dense enough to mask the bulk motion of the dome. The motion of the YC-473 may have more closely indicated the bulk water motion, but this is not known with certainty.

The observations showed that Eq. 1.4 was not applicable for the determination of the Wigwam underwater peak pressures by the measurement of the initial velocity of the spray. It is felt that this formula applies to the bulk motion of the water and may not be valid for spray measurements on underwater nuclear tests in general. The subject requires additional study over a wide range of conditions to obtain a better understanding of spray phenomena and, if possible, to establish a better equation for nuclear tests.

3.7 PLUMES

The Wigwam burst produced a mass of large irregular plumes. At the time of plume formation the surface was in a disturbed state as a result of the shock-wave and bubble-pulse effects. The large spikes of the second spray dome were present, and the water was probably in a turbulent cavitated condition.

3.7.1 Description

The first plumes were predominantly vertical and appeared denser than the spray in the domes (Fig. 3.21). These plumes reached a maximum height of 1450 ft and a diameter of 2000 ft about 19 sec after SZT.

In the meantime a second group of plumes, radial in nature, appeared at low levels. This second plume phase seemed to leave the water surface about 6 sec after the first plumes appeared, and the entire plume formation fell to the surface to cover an area about 3100 ft in diameter 25 sec after SZT (Figs. 3.21 and 3.22).

The height-time history is shown in Fig. 3.23. If the initial curve is extended back to the water surface, a value of about 10 sec is obtained for the time of origin of the first group of plumes, and an initial vertical velocity of about 300 ft/sec is indicated. The maximum height attained indicates that atmospheric drag had little retarding effect on the rising plumes. The data show that the plumes settled back more slowly than they rose, which can be attributed to the breakup of the plumes into droplets. Part of this mist remained air-borne while most of the plume material dropped back toward the surface. The radial expansion of the first and

CONFIDENTIAL

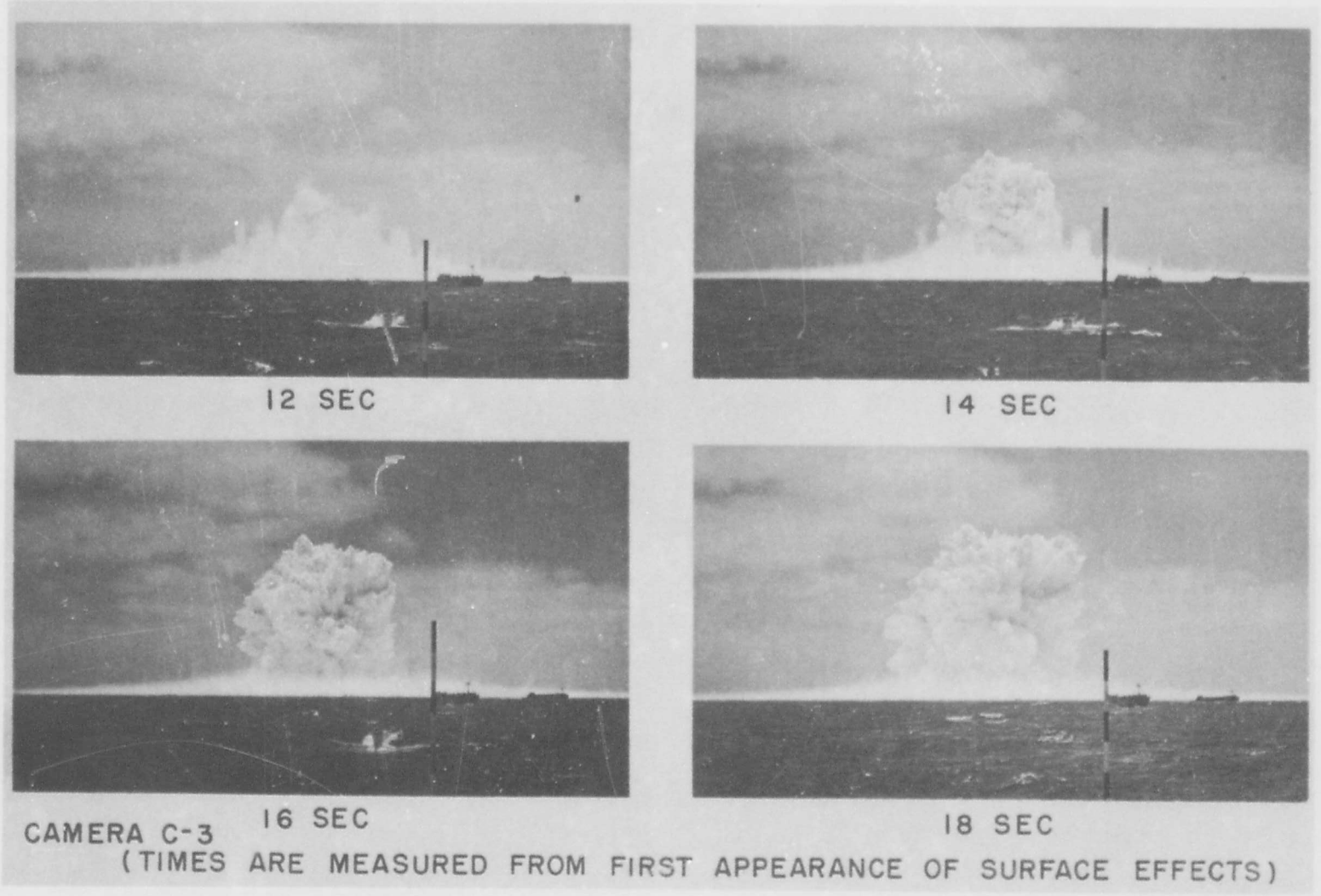


Fig. 3.21—Plume formation.

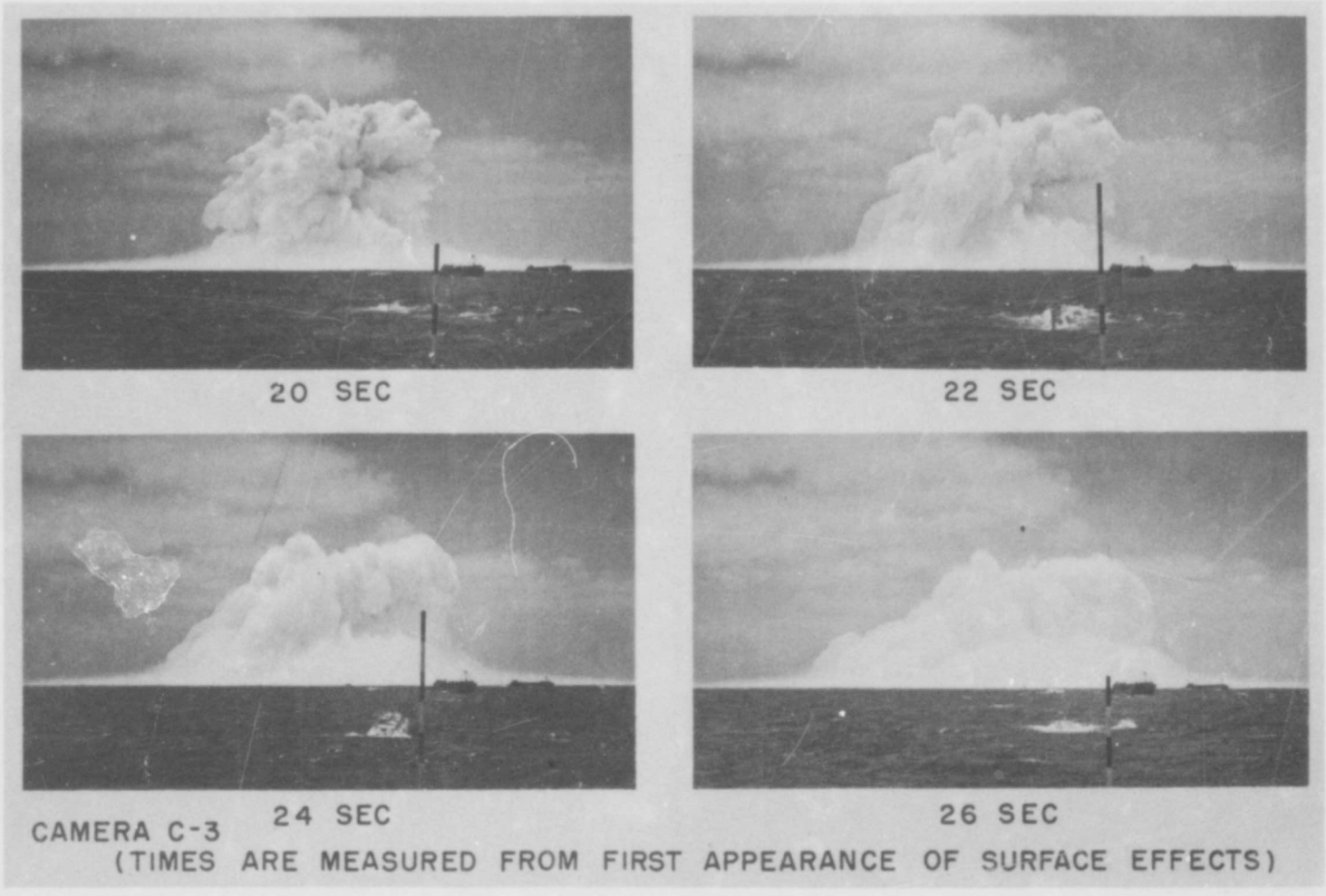
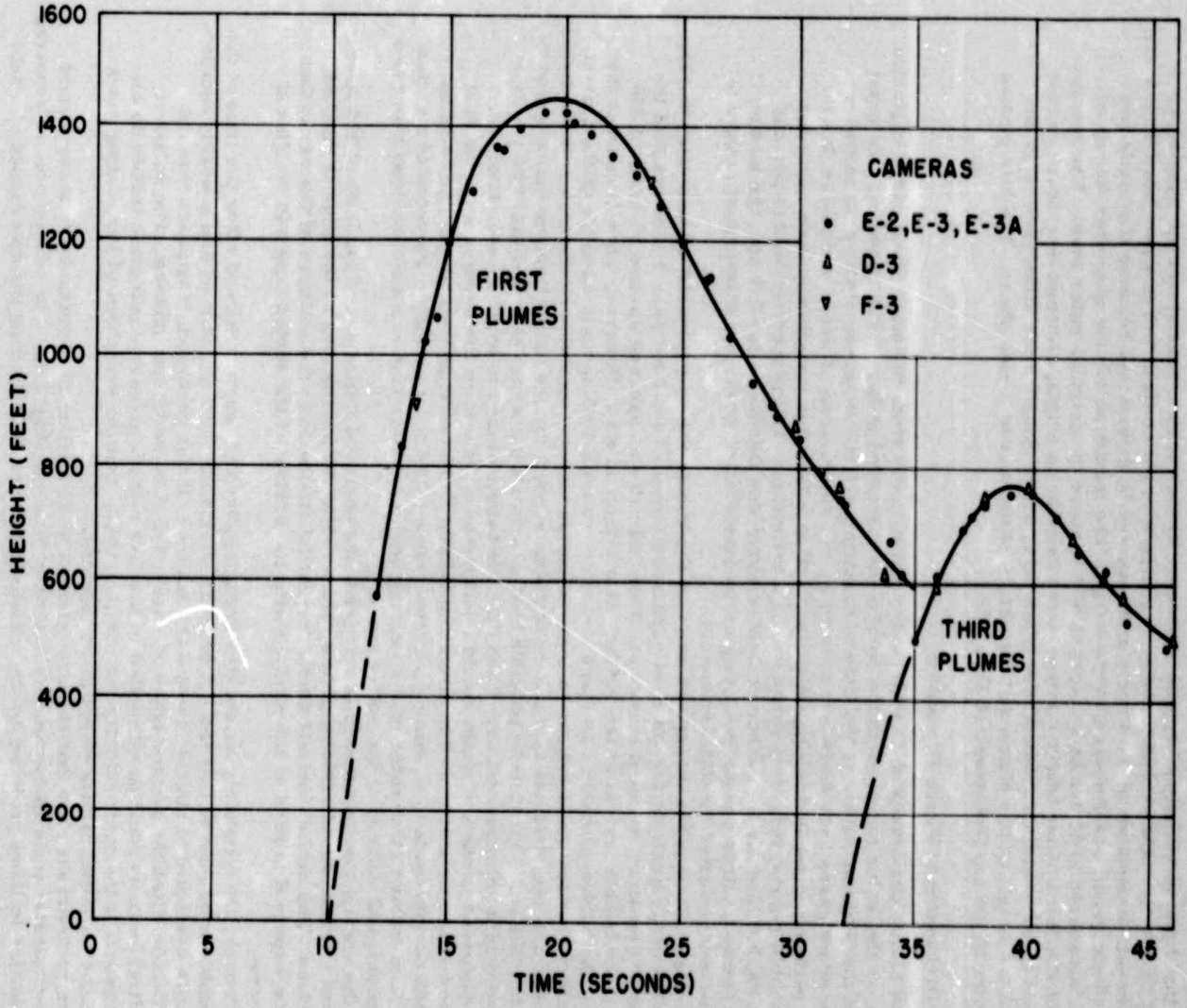


Fig. 3.22—Plume collapse.



(TIMES ARE MEASURED FROM FIRST APPEARANCE OF SURFACE EFFECTS)

Fig. 3.23—Plume height vs time.

second plume phase is shown in Fig. 3.24. Measurements were made to the extremities of the plumes.

A third plume formation became visible at 35 sec, when it rose above the base surge formed by the first and second plumes, reaching a height of about 770 ft 4 sec later (Fig. 3.23). The over-all dimensions of the third plumes cannot be determined because the lower two-thirds of the group was obscured by the surge. The maximum visible diameter was about 1000 ft, measured at 42 sec at a height of 400 ft above the original water level. The extrapolation of the third plume height vs time curve back to its origin, although necessarily crude, indicates an arrival time about 32 sec after SZT, which gives a time difference of 16 sec between the origin of this plume and the origin of the second plume phase. The late plumes are shown in the top photograph of Fig. 3.25.

3.7.2 Discussion of Plume Formation

The plume phenomena of an underwater burst result from the emergence of the explosion bubble, or the water surrounding the bubble, as discussed in Sec. 1.4.2. However, the exact state of the Wigwam bubble at the time of breakthrough is not known. During its initial expansion some gases were doubtless formed by the dissociation of water molecules, but the bubble probably consisted mostly of steam.[27] The underwater pressure gauges recorded three bubble pulses, indicating three bubble oscillations. The respective bubble periods[2] were 2.88, 2.6, and 1.9 sec. Since no bubble pulse was detected after 7.4 sec, the bubble, if it still existed, either was not pulsating or was oscillating weakly as it migrated upward toward the surface after the third minimum.

An upper limit to the average velocity of the bubble can be estimated by assuming that the bubble did not migrate during its first expansion (one-half the first period) and reached the surface 10 sec after the burst occurred. This indicates an average upward velocity of 230 ft/sec if the bubble arrived at the surface at a minimum size. However, when it reached the surface, the bubble probably was large enough to cause a welling up in advance of the arrival of the center, which would indicate a lower average velocity, possibly of the order of 200 ft/sec.

There are two alternate hypotheses that can account for the plume phenomena observed in Operation Wigwam. First, it is possible that nearly all the steam had condensed by the time the third bubble minimum occurred and that the bubble ceased to exist in its original form. If this happened, a mass of water would continue to move toward the surface as a result of the momentum acquired from the migrating bubble.[27] The first plumes to emerge could be explained on this basis by assuming that the rising mass of water was in the form of a vortex ring.[27] The water in the center of such a ring would probably rise at a velocity less than twice the translational velocity of the entire mass.

If the vortex-ring hypothesis is accepted, the observed initial plume velocity of 300 ft/sec indicates a translational velocity greater than 150 ft/sec for the ring at the time it reached the surface. The second (radial) plumes might be attributed to the collapse of the cavity that would be expected to form at the surface with the arrival of the vortex ring and ejection of the plumes.

However, the possibility exists that enough gases and vapor remained after the time of the third bubble minimum so that the bubble characteristics were maintained and a weakly oscillating bubble continued to migrate toward the surface. If this occurred, it appears that the rising bubble lifted the surface layer of water, which broke up into plumes. The relatively high initial velocity could be attributed to the fact that all parts of a pulsating bubble do not move upward at the same velocity and the possibility that the expansion of the venting gases would have an initial driving effect on the plumes.

The photographs show that the first plumes were similar in appearance to those formed in high-explosive tests approximately scaled to Wigwam (Fig. 1.2). The second plumes appeared to be similar to those produced by the collapse of the cavity following the emergence of a high-explosive gas bubble.

When individual plume trajectories in the first plume formation were traced back, almost all showed the same point of origin beneath the surface. The same observation has been made

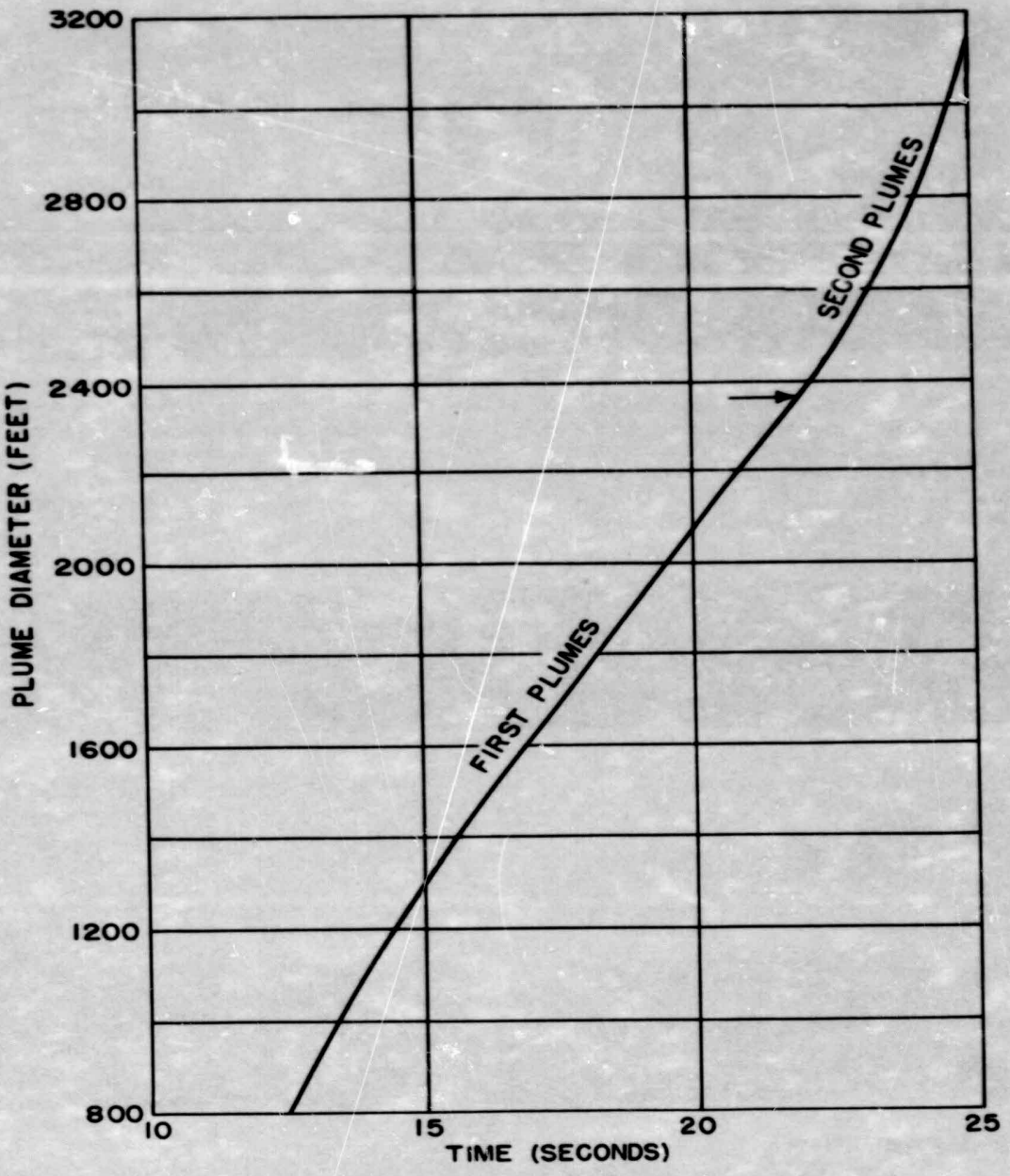


Fig. 3.24—Diameter of plumes vs time.

CONFIDENTIAL

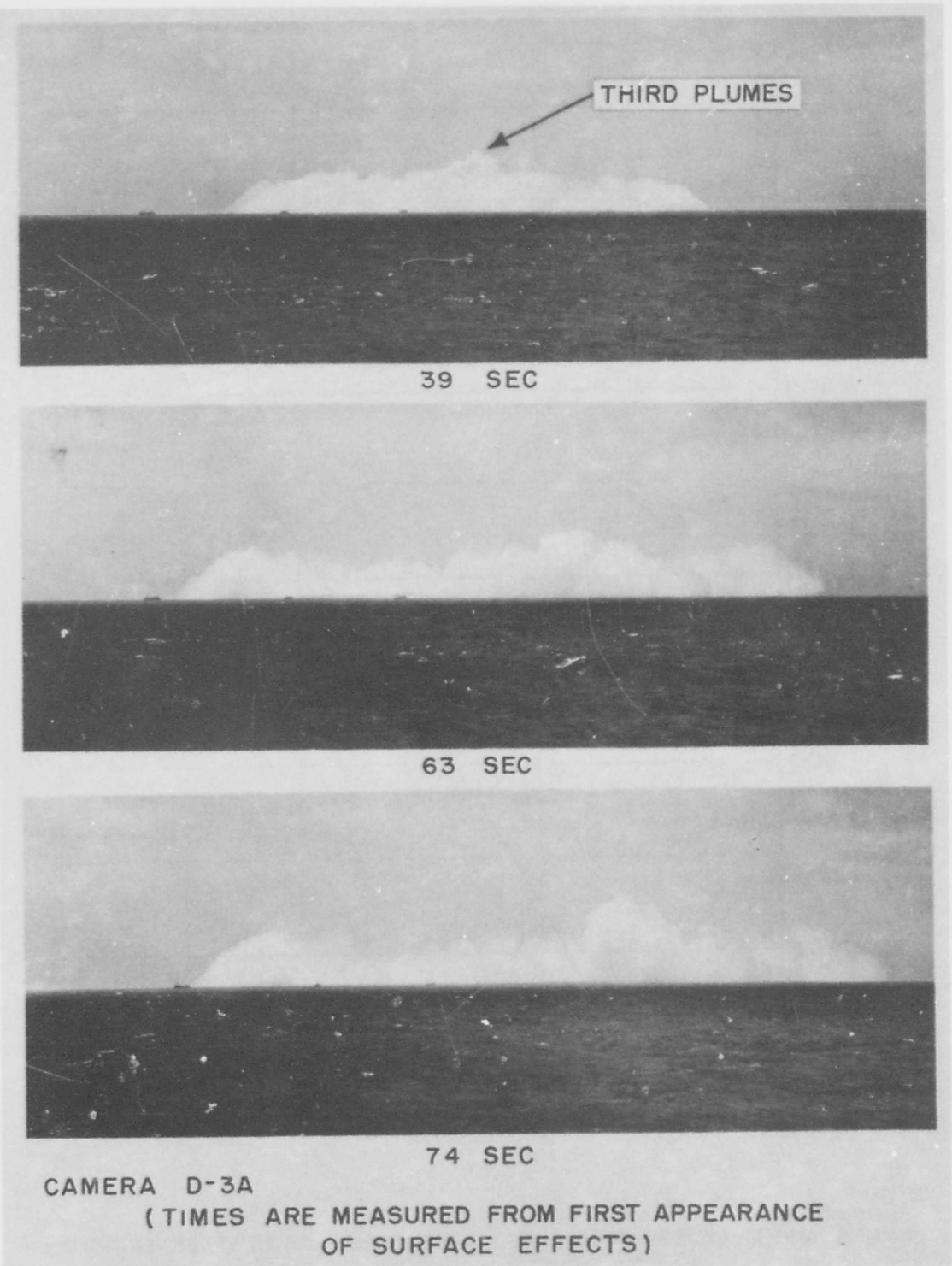


Fig. 3.25—Base surge at early times.

CONFIDENTIAL

in relatively shallow high-explosive tests when the gas bubbles broke the surface. It indicates the existence of a single symmetrical bubble in high-explosive tests, but it is also consistent with the vortex-ring concept.

This problem has important implications in regard to the disposition of the radioactive contaminants from the burst since a venting bubble would probably eject a relatively larger proportion of contaminants to the atmosphere than a liquid vortex ring.

The time interval between the appearance of the second and third plume phases is in agreement with the central wave period of about 16 sec at early times (Sec. 3.9). Since the train of surface waves was generated by the rise and fall of the water level at SZ, the similarity of the interval between plume appearances and the wave periods is evidence that the late plumes were produced by the oscillation of the water surface and not by a delayed venting of explosion products.

3.8 BASE SURGE

The plumes that formed in the Wigwam test broke up into a fine spray which settled back and spread out radially to form a base surge. The second plumes, which appeared at low levels at 16 sec, moved out rapidly to form its leading part. The first plumes, which had reached a greater height, collapsed and spread behind the initial surge. This process is illustrated in Fig. 3.22. The development of the base surge from the plumes was continuous, but the surge could be clearly identified about 26 sec after SZT. The action was turbulent, and thorough mixing of the plumes probably occurred. It seems likely that the third plume phase also contributed material to the surge cloud.

The base surge was roughly circular in shape but was not smooth in outline and contained several lobes. Its appearance at early times is shown in Fig. 3.25. Measurements of the radial growth of the base surge were made from camera stations D, E, and F until 90 sec after SZT. The mean radius-time curve, measured from the center of the surge, is shown in Fig. 3.26 and indicates an average initial radial velocity of 59 knots from 26 to 40 sec, followed by an average velocity of 24 knots from 40 to 65 sec and an average velocity of 15 knots from 65 to 90 sec.

Figure 3.27 shows the smoothed outermost contours of the base surge from 30 to 90 sec after SZT. These were approximately circular in outline and indicated a drift to the southwest which was consistent with the northeast surface wind direction observed on the Curtiss.

The upwind and downwind extent of the surge, as measured from SZ in Fig. 3.27, is presented in Fig. 3.28. The upwind curve levels off at about 60 sec at an upwind extent of about 2900 ft, and the downwind curve indicates an average velocity of about 33 knots between 60 and 90 sec. These values indicate that it is reasonable to assume that the surge cloud was carried downwind at the surface wind speed of 17 knots observed on the Curtiss. Exact agreement cannot be expected because of the irregularities in the shape of the base surge, measurement difficulties, and small variations in the ambient wind speed and direction. However, it appears that the upwind-surge velocity was equal to, or less than, the wind velocity after 60 sec and that the wind velocity was added to the downwind radial growth.

After 90 sec from SZT (about 64 sec after the appearance of the base surge), the surge became increasingly difficult to measure, particularly in the upwind direction. However, it was possible to obtain an approximate radial growth curve for the period from 100 to 200 sec from the H-3 record, as shown in Fig. 3.28. The data show considerable scatter because of the tenuous nature of the surge cloud at these late times.

The motion of the surge upwind of SZ was estimated from the D-3 and E-2 records for the period from 100 to 160 sec. Between 130 and 160 sec the upwind edge of the main surge cloud moved downwind at a steady speed of 5 knots. At the same time the crosswind growth was about 5 knots. It seems clear that, although the forward edge moved at approximately the speed of the wind, plus the radial expansion due to its own kinetic energy, the upwind or trailing edge of the base surge was retarded in its downwind motion by frictional effects. Consequently the surge cloud was gradually elongated along the wind axis.

It should be noted here that a shallow tenuous mist was observed upwind of the main surge

CONFIDENTIAL

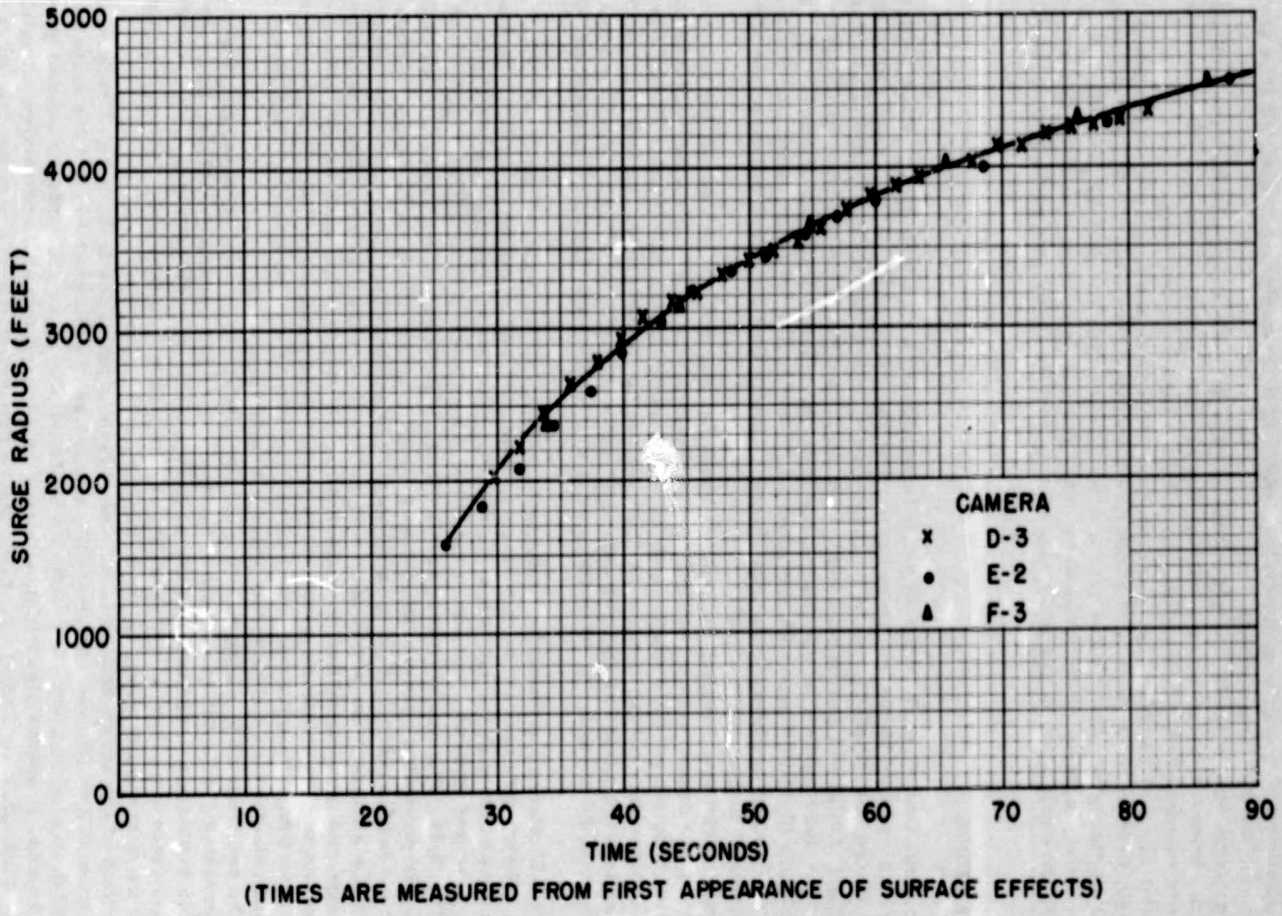


Fig. 3.26—Early base-surge radial growth.

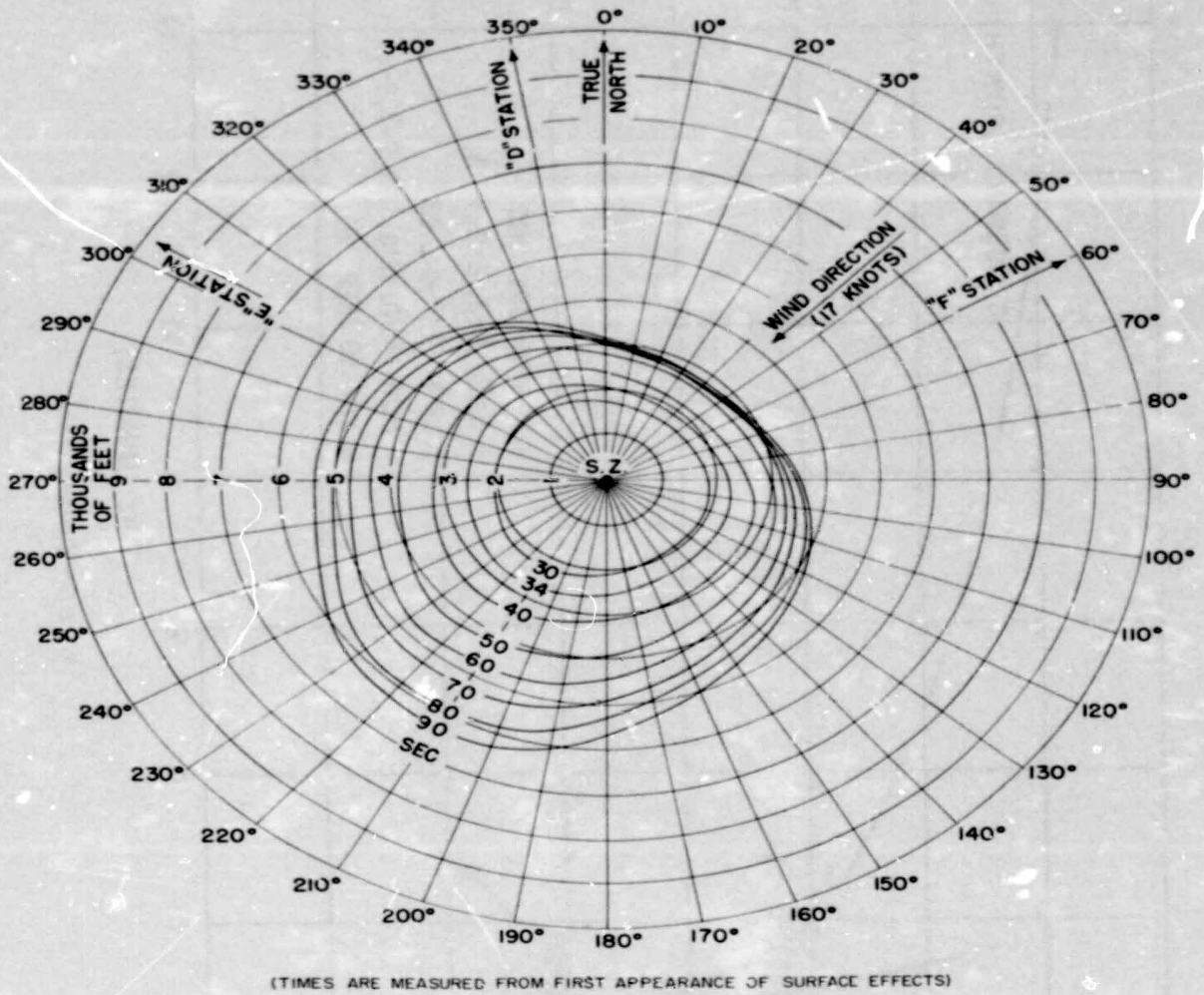


Fig. 3.27—Base-surge contours.

CONFIDENTIAL

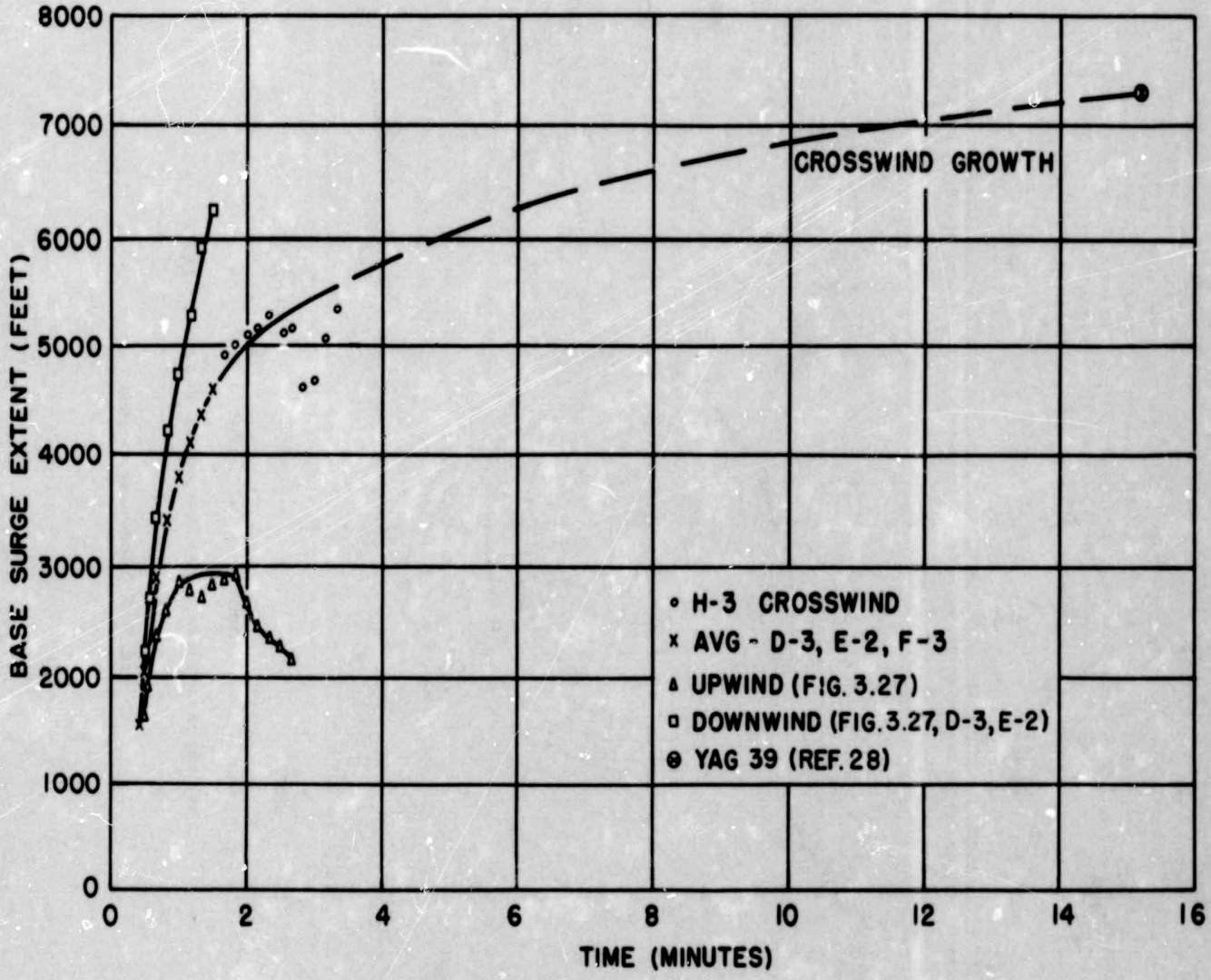


Fig. 3.28—Base-surge extent.

cloud between 2 and 3 min after the shot. This shallow cloud was approximately stationary and did not follow the downwind motion of the base surge. It appeared to be left behind, at least temporarily, when the surge was transported out of the area by the wind.

The density of the surge cloud was gradually reduced by expansion, by mixing with the ambient air, and by deposition of droplets. The lobes of the surge began to separate, and some remained larger and more clearly defined than others. The surge mist became invisible from surface positions about 4 min after the test but could be observed from the air until about 23 min had elapsed.

It was reported by Project 2.4 that the YAG-39 was located at a range of 11,100 yd and a true bearing of 190 deg from SZ at shot time.[28] Its course was 010°T and its speed was 5 knots. At H+2 min the course was changed to 300°T and speed was increased to 10 knots. Project 2.7 reported that air-borne activity was intercepted at H+15.2 min at a distance approximately 5 nautical miles downwind.[29] This indicates that the base surge continued to move toward the southwest at a speed of 17 knots and had possibly attained a radius of 7300 ft when it reached the YAG-39.

On this basis an interpolated curve of surge radial growth for the first 15 min after surge formation occurred is included in Fig. 3.28. The smoothed curve is fairly straight between 7 and 15 min and indicates an average radial velocity of about 100 ft/min during this period. Since it seems reasonable to assume that radial growth was controlled mainly by atmospheric turbulent diffusion at these late times, the value of 100 ft/min provides an estimate of the magnitude of this effect. The surge cloud probably continued to expand laterally as it moved downwind.

The base surge increased steadily in height as well as in radius. Measurements obtained at the highest part of the surge are reproduced in Fig. 3.29. These show considerable scatter as a result of the irregular, turbulent nature of the vertical growth of the surge and the difficulty in positioning the highest parts exactly. New condensation appeared to occur in the top of the dominant lobe of the base surge at about 3 min after SZT. This effect is shown in the bottom picture of Fig. 3.30, which illustrates the late stages of surge behavior.

The measurements in Fig. 3.29 indicate a maximum visible base-surge height of about 1900 ft at 4 min. The surge probably continued to increase in height, although its vertical extent was limited to the thickness of the atmospheric layer beneath the base of the temperature inversion at 3480 ft. The stable air in the inversion layer would act as a lid and would resist the penetration of air from the turbulent region below.

It was reported that the wind decreased in speed and backed to the north-northeast between the surface and an altitude of 2000 ft. Therefore the cloud was gradually distorted by the effect of the wind shear, and droplets or particles that were in the upper levels of the surge cloud followed a trajectory different from those remaining near the water surface.

3.9 SURFACE WAVES

Although the photographic coverage was not planned to include the measurement of the explosion surface waves, considerable wave data were obtained from the YFNB and aircraft records. Views of the explosion surface waves are shown in Figs. 3.30, 3.31, and 3.35. (The first two waves observed, Nos. 0 and 1, appeared to be breaking as they emerged from the base surge. This effect is believed to be due to the superposition of wind waves traveling in the opposite direction.) The train of waves was also indicated by the vertical motion, or heave, and by the pitch of the barges. (No noticeable roll of the barges occurred because of the passage of the train of explosion surface waves since the YFNB's were heading in the direction of travel of these waves and their wave length, about 1300 ft between the highest waves, was much greater than the length of the barges.) In addition, from about 7 to 30 min after SZT, the pattern of concentric waves was quite visible on the McKean surface-search radar (Figs. 10 and 11, reference 30). The gain on this radar had been set high, and therefore a strong sea return cluttered the scope face. The explosion surface waves modulated the sea return, making them clearly visible.[31]

On both the aerial and the surface camera records, four separate wave crests were ob-

CONFIDENTIAL

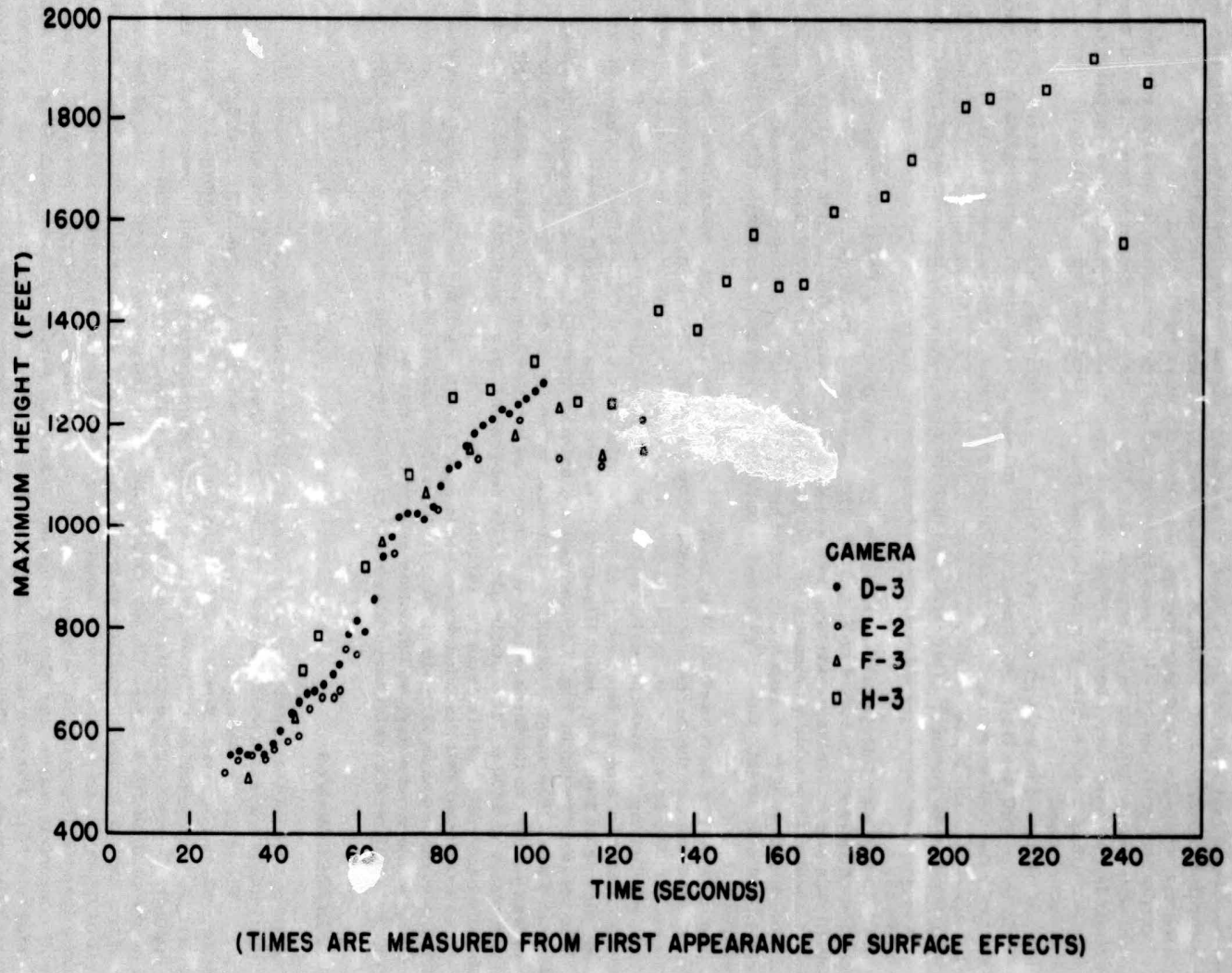
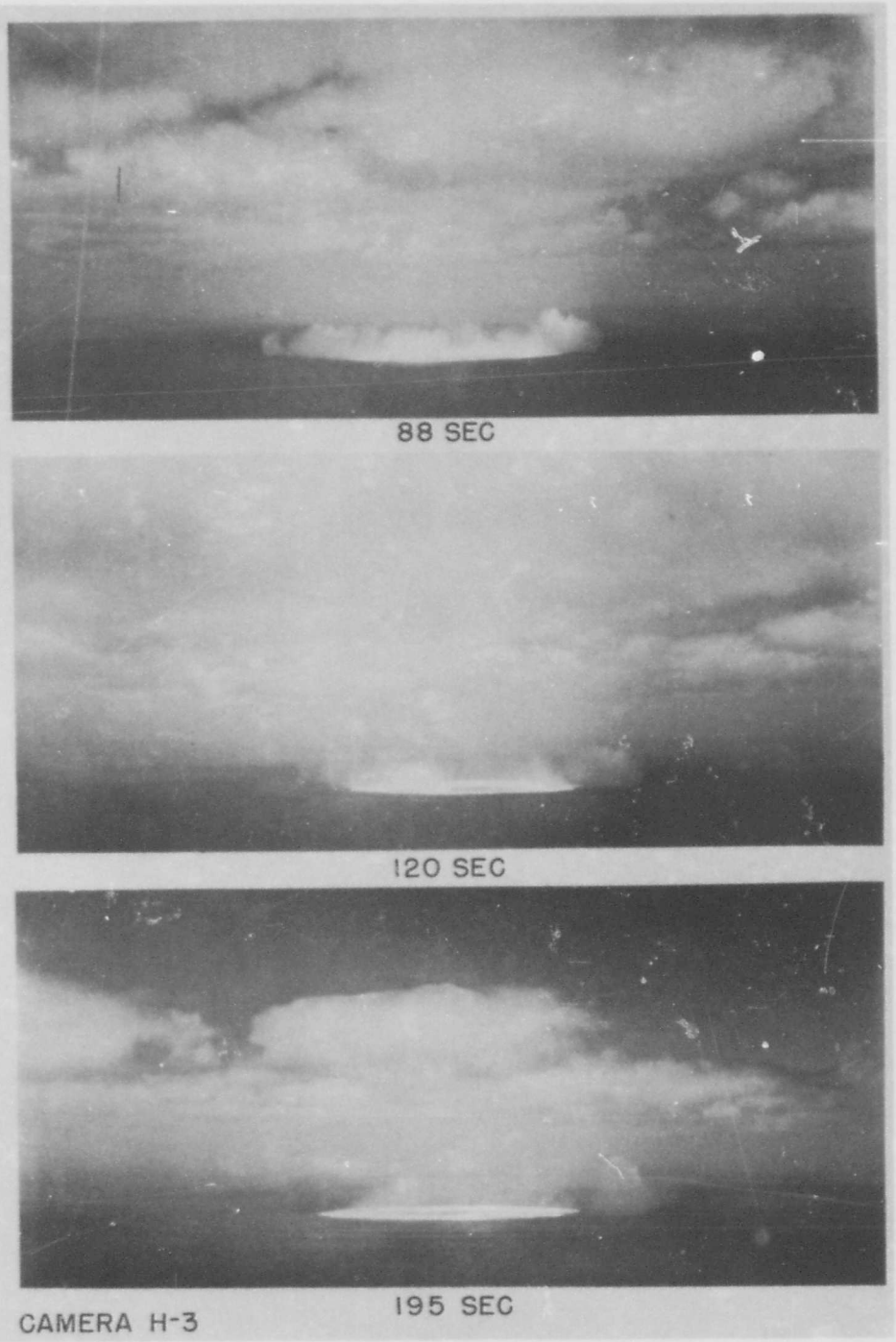


Fig. 3.29—Base-surge height vs time.



(TIMES ARE MEASURED FROM FIRST APPEARANCE OF SURFACE EFFECTS)

Fig. 3.30—Base surge at late times.

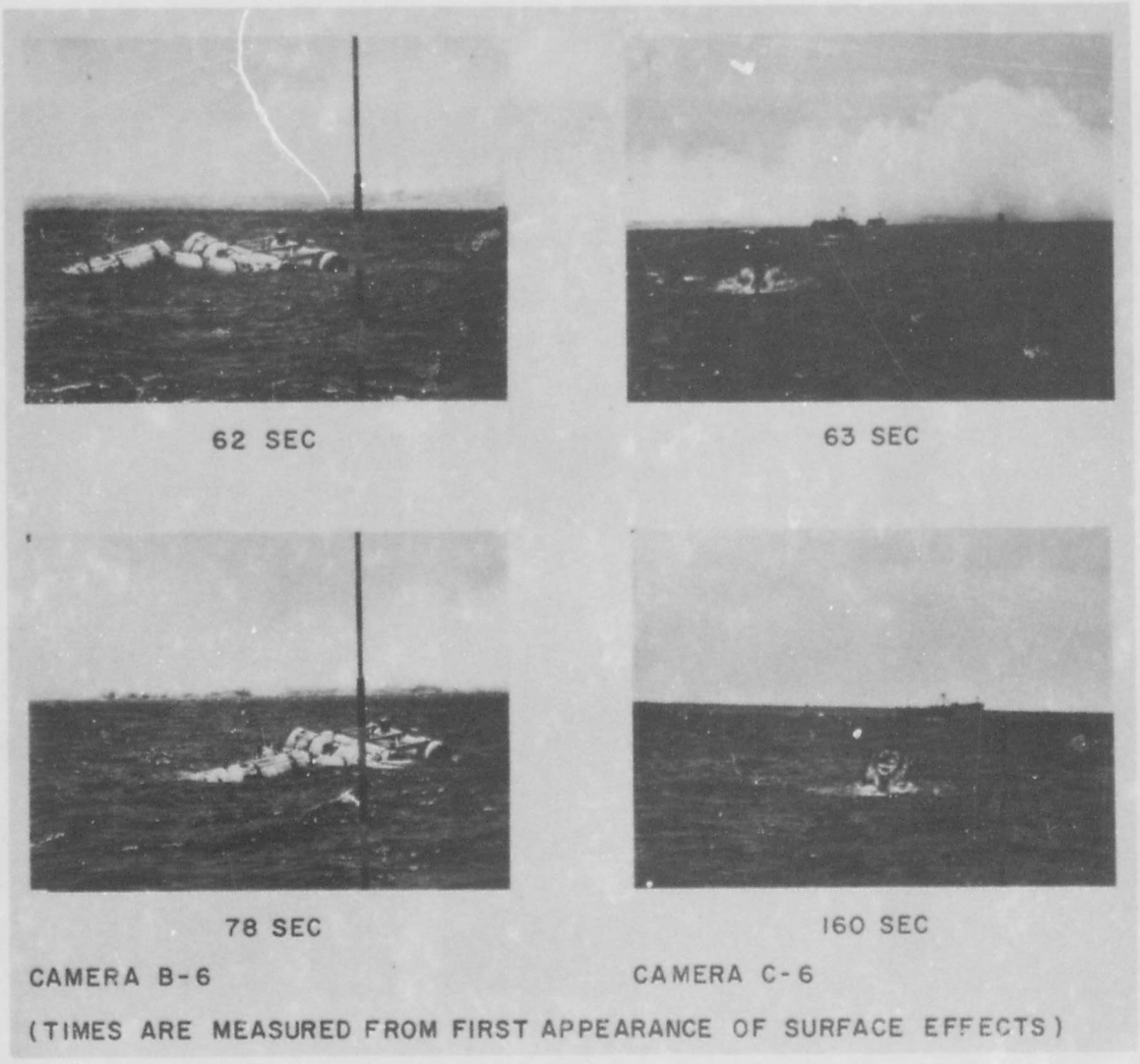


Fig. 3.31—Surface waves.

served passing the YFNB-12. The first wave crest observed at the YFNB-12 has been arbitrarily called wave No. 1; later waves have been numbered consecutively. A single earlier wave, not observable at the YFNB-12, was visible just outside the base surge in the region of the O-2 and A-2 M-boats (about 3500 ft from SZ); this wave has been labeled wave No. 0.

To obtain wave-height vs time measurements at the three YFNB positions, two methods were used: (1) direct measurement of the rise and fall of the YFNB and (2) integration of the product of the pitch and the wave velocity with respect to time.

The vertical motion of the YFNB-12, indicated by measurements of the average displacement of a point near the bow and a point near the stern of the barge relative to the crests of the oncoming explosion waves as viewed by cameras C-3 and C-3A on the YFNB-29, is shown by the lower curve in Fig. 3.32. Wave crests were used as reference lines because of the obscuration of the true horizon; the discontinuity and the subsequent upward drift of the data points are due to the shifting of these reference lines. Since the wave crests happened to be at nearly the same distance from the YFNB-29 as the YFNB-12, little apparent motion due to vertical motion of the cameras was introduced into this measurement.

The measured trough-to-crest heights* of the individual waves (Nos. 1 to 4) which passed the YFNB-12 were 30, 37, 35, and 26 ft, respectively (from data shown in Fig. 3.32). These wave heights were measured from the wave-train envelope at the time of the corresponding wave crest. The maximum trough-to-crest height* of the envelope was 37 ft and occurred between the second and third waves. That this envelope does not precisely fit all the measured data, particularly for wave No. 4, is attributed to the superposition of existing swells and wind waves on the explosion surface waves. It is estimated from these measurements that the existing sea conditions were causing a rise and fall of the barges of about 10 to 15 ft.

Measurements of the rise and fall of the YFNB-13 with the passage of the explosion waves were also made, using camera records from the YFNB-29. These measurements are considered less reliable, however, than those of the vertical motion of the YFNB-12 for the following reasons: (1) the explosion waves were smaller, and thus the relative effect of the background noise from the prevailing sea conditions was greater, and (2) since the reference line for most of these measurements was the true horizon (not the crests of approaching waves), the apparent motion of the YFNB-13 was approximately equal to the difference between the vertical motions of the YFNB-13 and the cameras on the YFNB-29.

Nevertheless, a measurement (not shown in Fig. 3.32) of the vertical motion of the mast of the YFNB-13 relative to the horizon gave a quite reasonable value of 26 ft for the maximum trough-to-crest height of the wave train passing the YFNB-13, provided that an unusually high measured trough-to-crest height of about 35 ft for wave No. 5 is discounted. It appears likely that the unusually high measured amplitude for wave No. 5 was due to wave No. 3 passing the YFNB-29 about 180 deg out of phase with wave No. 5.

Pitch vs time measurements were obtained from one camera on each barge. Since the product of the tangent of the pitch angle of the barge and the wave velocity of the explosion waves equals the rate of rise of the water surface, this product was graphically integrated with respect to time in order to obtain the height vs time history of the explosion waves at each barge position.

The integrals of pitch X wave velocity were calculated using a constant wave velocity of 84 ft/sec. This value is equal to twice the measured group velocity of 42 ft/sec for radial distances from SZ less than 12,000 ft (discussed below). Actually the wave velocity is equal to twice the group velocity only for the highest crest in the train;[32] earlier waves may be moving considerably faster and later waves considerably slower. Use of a constant wave velocity for this measurement probably introduced considerable distortion into the wave height vs time curves but should not change the maximum trough-to-crest height of the wave train appreciably.

Integrals of the measured pitch X wave velocity for the YFNB-13 and the YFNB-29 are shown as the upper two curves in Fig. 3.32. The maximum trough-to-crest heights for the

---

* This includes a correction of +1 or +2 ft for settling of the YFNB into the wave crests and cradling in the troughs.

CONFIDENTIAL

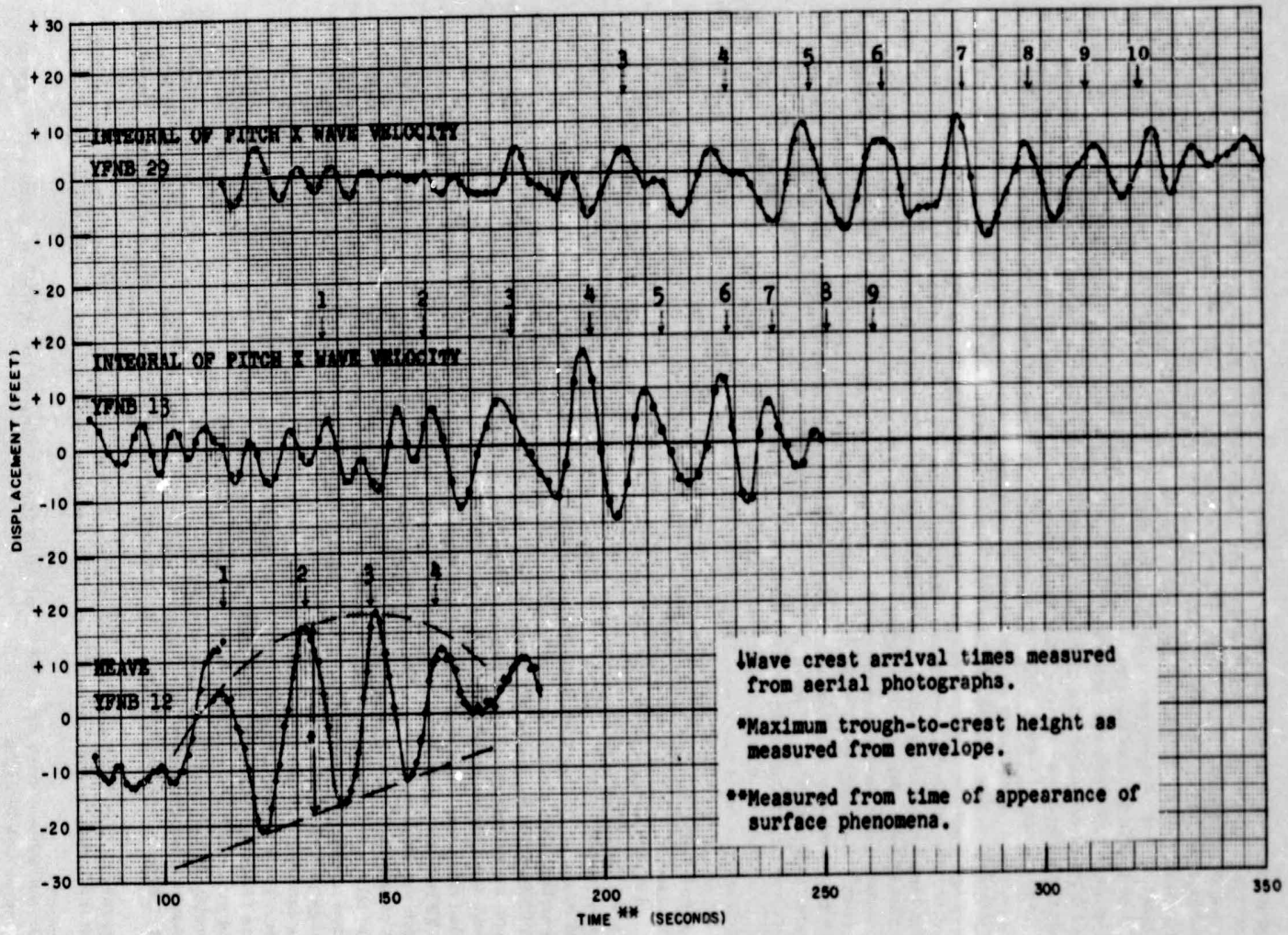


Fig. 3.32—Vertical motion of barges with passage of surface waves.

wave train as measured from the envelopes of these curves, as well as a similar measurement of the wave train passing the YFNB-12, are given in Table 3.5.

Figure 3.33 is a plot of the maximum trough-to-crest height of the wave train vs radial distance from the YC. The straight line, or theoretical decay curve of HR = constant, was plotted through the point (5520 ft, 37 ft) obtained from the measurement of the heave of the YFNB-12, where H = maximum trough-to-crest height and R = radial distance. This gives a value of 204,000 ft^2 for the constant as compared with the highest predicted value[31] of 80,000 ft^2, an increase by a factor of about 2.5. It can be seen from Table 3.5 and Fig. 3.33 that the maximum heights obtained by the two methods agreed in all cases to within 1 or 2 ft. Although the method of integrating the product of the wave velocity and tangent of the pitch angle with

Table 3.5 — MAXIMUM WAVE HEIGHTS

Source of measurement and camera No.	Radial distance from YC-473, ft	Max. height (trough-to-crest), ft
Heave of YFNB-12 (C-3, C-3A)	5,520	37
Pitch of YFNB-12 (A-6)	5,520	38
Pitch of YFNB-13 (B-6)	7,950	24
Vertical motion of YFNB-13 mast minus YFNB-29 camera motion (C-3A)	8,040	26
Pitch of YFNB-29 (C-3A)	10,950	19

respect to time might appear to be of questionable reliability, it was advantageous to use it since it reduced the effects of the wind waves relative to those of the explosion waves and did not introduce the motion of a second barge into the measurement. The close fit of this maximum-wave-height data from both methods of measurement to the theoretical decay curve is encouraging, particularly in view of the indirect methods used to arrive at these values.

Considerable radius-time data for some 24 wave crests were obtained from the aircraft camera records and photographs of the McKean surface-search radarscope. These data are given in Fig. 3.34 and in Table 3.6. Times of arrival of many of the wave crests at the three YFNB's were measured from camera record H-3. In addition, radii of eight of the waves were measurable on a single frame from aerial camera record J-3, on which the YFNB-13 and the YFNB-29 were visible and served as reference markers to establish radial distances from the YC. The remaining data (set off by the broken lines in the upper right corner of Fig. 3.34) were obtained from photographs of the McKean surface-search radarscope. Figure 3.34 presents all these radius-time measurements, including a region of interpolated data from about 5 to 9 min after SZT.

Where possible, the highest crest in the wave train was estimated from the aerial photographs. These data points were used in Fig. 3.34, along with an estimated time of origin for the wave train of 20 sec after SZT, to determine the straight line approximating the locus of the highest wave for wave radii of less than about 12,000 ft. The slope of this line gives a value of 42 ft/sec for the group velocity of the wave train in this region.

If the line is extended into the region of data obtained from the radar, it no longer appears to indicate the position of the highest wave since the extended line falls well below the center of the measured data points and its slope is somewhat less than the theoretical one-half of the slope of the intersecting wave loci. Therefore the locus of the highest wave has been estimated for radial distances greater than 12,000 ft by a connecting line drawn to intersect the wave-crest loci with, on the average, one-half the slope of the wave-crest loci. This line gives a value of 49 ft/sec for the group velocity of the wave train at radial distances greater than about 12,000 ft from the YC.

At early times (from about 100 to 300 sec after SZT and at radial distances from about 3000 to 12,000 ft), the wave system was characterized by a central wave length of about 1300 ft and a central wave period of about 16 sec, which are consistent with the measured group

CONFIDENTIAL

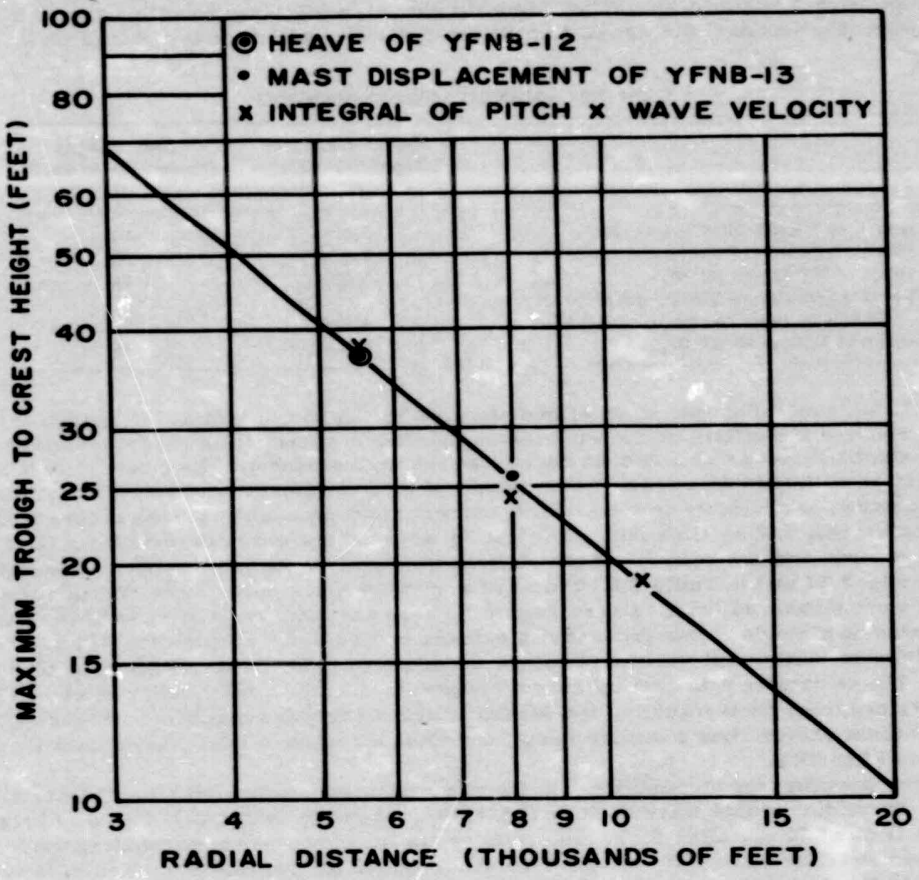


Fig. 3.33—Maximum wave height vs radial distance.

Fig. 3.34—See page 34.

Table 3.6—WAVE RADII VS TIME DATA

Wave No.	Location and radial distance of wave crest at various times
0	A-2 boat (3400 ft, 78 sec)
1	A-2 boat (3400 ft, 95 sec); YFNB-12 (5520 ft, 114 sec); YFNB-13 (7950 ft, 137 sec)
2	O-2 boat (3650 ft, 112 sec); YFNB-12 (5520 ft, 132 sec); YFNB-13 (7950 ft, 160 sec)
3	A-2 boat (3400 ft, 126 sec); YFNB-12 (5520 ft, 147 sec); YFNB-13 (7950 ft, 179 sec); YFNB-29 (10,950 ft, 205 sec)
4	YFNB-12 (5520 ft, 162 sec); YFNB-13 (7950 ft, 197 sec); YFNB-29 (10,950 ft, 228 sec)
5	YFNB-13 (7950 ft, 214 sec); YFNB-29 (10,950 ft, 247 sec)
6	YFNB-13 (7950 ft, 228 sec); YFNB-29 (10,950 ft, 264 sec)
7	YFNB-13 (7950 ft, 239 sec); (13,680 ft, 312 sec)
8	YFNB-13 (7950 ft, 251 sec); (12,210 ft, 312 sec)
9	YFNB-13 (7950 ft, 262 sec); bow of YFNB-29 (11,080 ft, 312 sec)
10	(10,180 ft, 312 sec)
11	(9450 ft, 312 sec)
12	(8890 ft, 312 sec); (30,000 ft, 537 sec); (37,000 ft, 594 sec); (44,000 ft, 650 sec)
13	(8430 ft, 312 sec); (30,000 ft, 557 sec); (37,000 ft, 617 sec); (44,000 ft, 676 sec)
14	Center of YFNB-13 (7950 ft, 312 sec); (23,000 ft, 511 sec); (30,000 ft, 577 sec); (37,000 ft, 641 sec); (44,000 ft, 703 sec)
15	(23,000 ft, 529 sec); (30,000 ft, 597 sec); (37,000 ft, 663 sec); (44,000 ft, 727 sec)
16	(23,000 ft, 547 sec); (30,000 ft, 618 sec); (37,000 ft, 685 sec); (44,000 ft, 751 sec)
17	(23,000 ft, 565 sec); (30,000 ft, 637 sec); (37,000 ft, 706 sec)
18	(23,000 ft, 582 sec); (30,000 ft, 656 sec); (37,000 ft, 728 sec)
19	(23,000 ft, 598 sec); (30,000 ft, 674 sec); (37,000 ft, 747 sec)
20	(23,000 ft, 614 sec); (30,000 ft, 692 sec); (37,000 ft, 765 sec)
21	(23,000 ft, 630 sec); (30,000 ft, 708 sec); (37,000 ft, 781 sec)
22	(23,000 ft, 644 sec); (30,000 ft, 723 sec)
23	(23,000 ft, 658 sec); (30,000 ft, 737 sec)

velocity of 42 ft/sec for this region. At a later time (from about 500 to 700 sec after SZT and at radial distances from about 20,000 to 30,000 ft), after the wave system apparently had stabilized so that it was similar to that predicted by theory for waves of infinitesimal amplitude,[32] the wave system was characterized by a central wave length of about 1700 ft and a central wave period of about 18 sec, which are again consistent with the measured group velocity of 49 ft/sec for this region.

The maximum trough-to-crest height of the wave train was characterized by the relation $HR = 204{,}000\ ft^2$. This relation for the maximum trough-to-crest height of the wave train was shown to hold for radial distances from 5500 to 11,000 ft and probably holds for radial distances considerably beyond this range. The disagreement with predictions can perhaps be attributed to the lack of wave data from tests deep enough to reproduce the Wigwam bubble behavior. It was therefore necessary to extrapolate data from shallower high-explosive tests.

3.10 FOAM RING

After the plumes formed by the emerging bubble had subsided, a clearly defined white circular patch of foam was observed at the location of SZ. This is shown in Fig. 3.30, and its later appearance is illustrated in Fig. 3.35. The water within the ring was relatively smooth. Evidently an upward flow of water occurred in the vicinity of SZ. This water spread outward radially and sank, thus resulting in the accumulation of foam and floating debris at the ring.[33] The phenomenon appeared to be similar in nature to the carbon slicks observed after underwater high-explosive tests. However, no quantitative data from small-scale tests are available for comparison with the Wigwam result.

CONFIDENTIAL

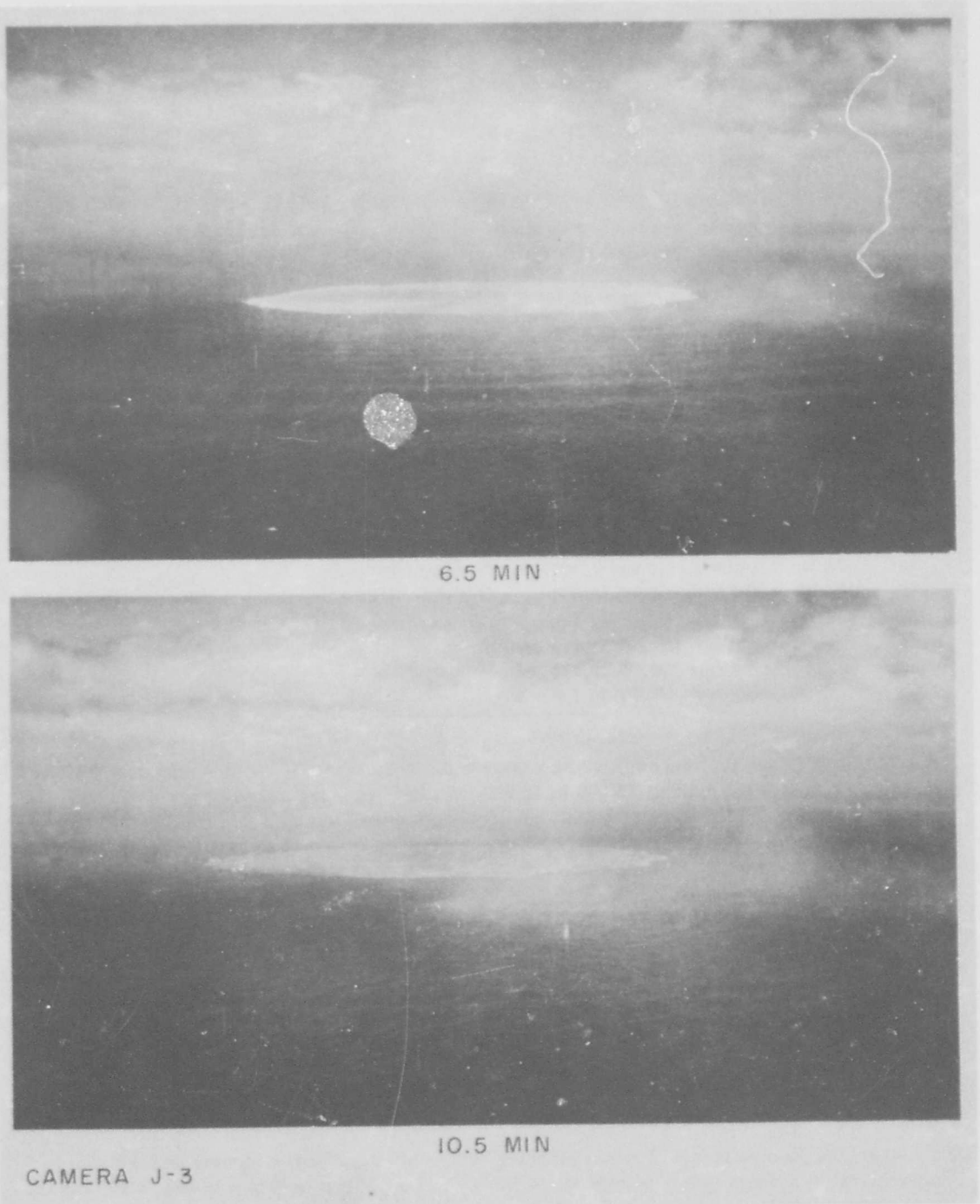


Fig. 3.35—Foam ring.

CONFIDENTIAL

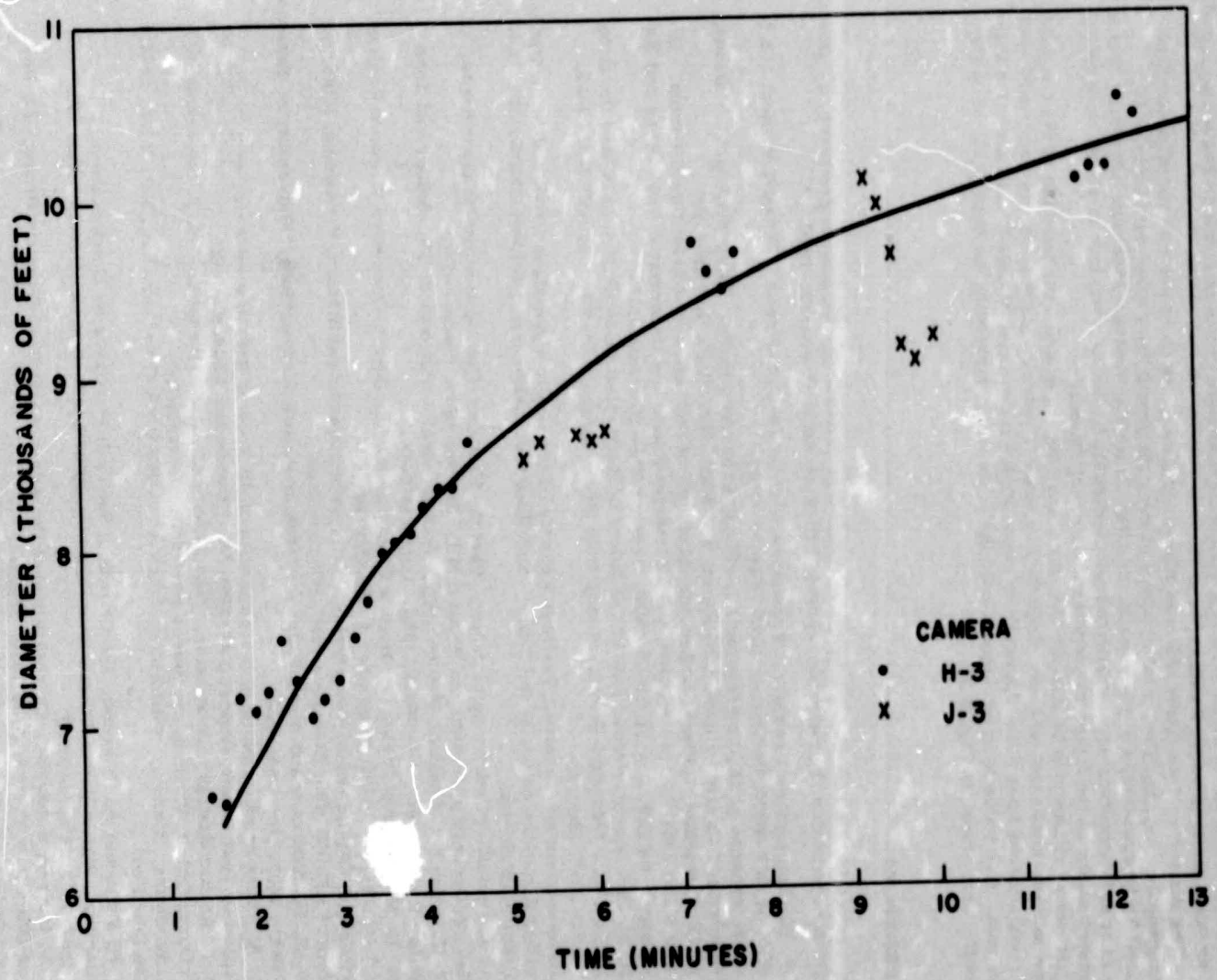


Fig. 3.36—Foam-ring diameter vs time.

The area within the foam ring was visible as a smooth circular patch on the photographs of the McKean surface-search radarscope.

The diameter of the foam ring was measured as a function of time on the H-3 and J-3 photographic records. The erratic nature of the data points, as presented in Fig. 3.36, is caused by irregularities in the edge of the ring. Since the photographic aircraft were circling the ring and diameters were measured perpendicular to the camera line of sight, each measurement shown in the figure represents a different diameter.

It seems reasonable to assume that the foam ring coincided with the edge of the contaminated surface water that was examined by Project 2.4 survey aircraft. It was reported[28] that the contaminated area had a diameter of about 11,400 ft between 20 and 33 min after the Wigwam test. This value is in agreement with the diameter indicated by an extrapolation of the smooth curve shown in Fig. 3.36.

REFERENCES

[References 18, 26, and 32 have been reproduced in Underwater Explosion Research, a compendium of British and American reports, Office of Naval Research, 1950.]

1. C. B. Cunningham, Free-field Pressures, Station Zero, Operation Wigwam Project 1.2.1 Report, WT-1006, December 1955. (Secret–RD)
2. C. J. Aronson et al., Underwater Free-field Pressures to Just Beyond Target Locations, Operation Wigwam Project 1.2 Report, WT-1005, May 1956. (Secret–RD)
3. R. R. Halverson, Methods of Ranging the Depth of Explosion of Aerial Depth Bombs. III. The Shock-wave Spread Method, Div. 2 Interim Report on Underwater Explosives and Explosions, UE-26, Report OSRD-4259, October 1944. (Confidential)
4. R. R. Brockhurst, Predictions of the Effect of Refraction on Peak Pressure and Duration of Explosion Pressure Waves, Woods Hole Oceanographic Institution, Ref. No. 55-14, March 1955. (Secret)
5. Measurement of the Initial Vertical Velocity of the Water Formation Produced by an Underwater Explosion on the Model Scale, Road Research Laboratory, Report UNDEX-38, June 1943. (Confidential)
6. A. J. Frolich, Blast Measurements. Part II. Free-air Peak-pressure Measurements, Sec. 2, Operation Greenhouse Report, WT-20, June 1951. (Secret–RD)
7. J. C. Johnson, "Physical Meteorology," Massachusetts Institute of Technology and John Wiley & Sons, Inc., New York. 1954. (Unclassified)
8. M. L. Merritt, Air Pressures from a Deep Underwater Burst, Operation Wigwam Project 4.5 Report, WT-1035, December 1955. (Secret–RD)
9. Effects of Explosions in Deep Water, Waterways Experiment Station, Vicksburg, Miss., Report AFSWP-960, February 1956. (Confidential)
10. W. E. K. Middleton and A. F. Spilhaus, "Meteorological Instruments," University of Toronto Press, 1953. (Unclassified)
11. G. A. Young et al., Effects of the Explosion of 45 Tons of TNT Under Water at a Depth Scaled to Test Baker, Report NAVORD-3624, December 1954. (Secret)
12. U. S. Atomic Energy Commission, "The Effects of Atomic Weapons," U. S. Government Printing Office, Washington, September 1950. (Unclassified)
13. H. R. Byers, "General Meteorology," McGraw-Hill Book Company, Inc., New York, 1944. (Unclassified)
14. C. H. Keith and A. B. Arons, The Growth of Sea-salt Particles by Condensation of Atmospheric Water Vapor, Woods Hole Oceanographic Institution Contribution No. 665, August 1953. (Unclassified)
15. P. L. Horrer, Subsurface Configuration of the Array, Operation Wigwam Project 2.8 Report (Part I), WT-1018, June 1956. (Secret)
16. A. K. Billmeyer, Weapons Placement at Operation Wigwam, Operation Wigwam Project 4.1 Report, WT-1033, May 1955. (Secret–RD)

17. R. S. Price, The Structure of the Spray Dome from an Underwater Explosion and Its Effect on Floating Objects, Operation Wigwam Project 1.2, Monthly Status Report No. 4, App. B, November 1954. (Secret–RD)
18. D. A. Wilson, B. A. Cotter, and R. S. Price, The Determination of Peak Pressure of an Underwater Explosion from a Study of the Initial Dome Velocity, Report NAVORD-13-47, May 1947. (Unclassified)
19. H. Kolsky, J. P. Lewis, M. T. Sampson, and C. I. Snow, Splashes from Underwater Explosions. Part II. Domes from Deep Charges, Imperial Chemical Industries Limited, Report UNDEX-163, October 1945. (Confidential)
20. The Surface Phenomena Due to the Underwater Explosion of Small Charges, Road Research Laboratory, Report UNDEX-60, August 1943. (Confidential)
21. A. B. Arons and A. M. Shanes, Measurement of Shock Wave Peak Pressure by the Dome Velocity Method, Div. 2 Interim Report on Underwater Explosives and Explosions, UE-27, Report OSRD-4406, November 1944. (Confidential)
22. C. L. Pekeris, Determination of Depth of Explosion of Statically Fired Depth Bombs from Photographs of the Dome of Spray, Columbia University, OSRD Div. 6, Sec. 6.1, June 1944. (Confidential)
23. R. R. Halverson, Methods of Ranging the Depth of Explosion of Aerial Depth Bombs. II. The Dome Velocity Method, Div. 2 Interim Report on Underwater Explosives and Explosions, UE-25, Report OSRD-4149, September 1944. (Confidential)
24. R. R. Halverson and R. S. Price, Dome-velocity Method of Determining Depth of Explosion as Applied to a Series of Mk 54 Depth Charges Statically Planted over a Wide Range of Depths, Div. 2 Interim Report on Underwater Explosives and Explosions, UE-30, Report OSRD-4810, February 1945. (Confidential)
25. H. M. Schauer, The Plumes Caused by Underwater Explosions, Underwater Explosions Research Unit, Norfolk Naval Shipyard, Report UERD-5-48, 1948. (Unclassified)
26. E. N. Fox, "A Review of Underwater Explosion Phenomena," Cambridge University Press, New York, 1947. (Unclassified)
27. H. G. Snay, J. F. Butler, and A. N. Gleyzal, Predictions of Underwater Explosion Phenomena, Operation Wigwam Project 1.1 Report, WT-1004, January 1956. (Secret–RD)
28. M. B. Hawkins, Determination of Radiological Hazard to Personnel, Operation Wigwam Project 2.4 Report, ITR-1062, May 1955. (Confidential–RD)
29. F. A. French, Fall-out and Airborne Activity in Operation Wigwam, with Notes on Surface Effects, Operation Wigwam Project 2.7 Report, WT-1017, May 1955. (Confidential–RD)
30. E. H. Boldrick and V. G. Heger, Photographic Recording of Ship-borne Radar Information, Operation Wigwam Project 0.31 Report, WT-1038, May 1955. (Secret–RD)
31. A. B. Focke, Interim Summary Report of the Scientific Director of Operation Wigwam, Report ITR-1053, May 1955. (Secret–RD)
32. W. G. Penney, Gravity Waves Produced by Surface and Underwater Explosions, Report UNDEX-119, March 1945. (Unclassified)
33. W. G. Van Dorn, Collection of Early Water Samples for Radiochemical Analysis of Yield, Operation Wigwam Project 2.1 Report, ITR-1089, May 1955. (Confidential–RD)

CHAPTER 4

EVALUATION OF RESULTS

4.1 SUMMARY

The intersection of the underwater shock wave with the surface of the water was visible as a rapidly expanding ring of darkened water, or slick, which reached a radius of about 14,000 ft. A spray dome also spread rapidly along the surface, lagging behind the slick by a few milliseconds at early times. The dome reached a maximum radius of about 7000 ft.

The first spray dome rose with an initial vertical velocity of about 115 ft/sec at the center. According to a theory that had been applied successfully to high-explosive results, the spray velocity indicated a peak overpressure of 3990 psi in the underwater shock wave at SZ. This value was about 33 per cent greater than that indicated by pressure gauges. The difference can be partially attributed to the roughness of the sea surface but also probably indicates the failure of the formula used in high-explosive tests to apply to the Wigwam spray dome because of differences in the mechanism of spray formation.

The maximum height attained by the first dome was estimated to be 170 ft. Just before the maximum height was reached, a spiky second dome rose rapidly above the first to a height of about 900 ft. This dome originated about 2.3 sec after SZT and resulted from the arrival at the surface of the pressure wave produced by the first collapse of the explosion bubble. The first bubble pulse also formed an extremely faint second slick.

At about 5.6 sec after SZT a clearly visible slick appeared, resulting from the passage of the shock wave that was reflected from the bottom of the ocean. Multiple slicks were then observed, due to the reflection from successive layers in the bottom. The maximum radius of these bottom-reflection slicks was at least 34,000 ft. Scattered patches of spray appeared after the arrival of the slicks to a radius of 17,000 ft. These may be important in regard to ship damage and are relatively unpredictable since they are caused by shock reflection from irregularities in the ocean floor.

The shock wave transmitted to the air upon the arrival of the primary shock at the water surface remained visible for about 100 msec, which permitted the measurement of its vertical speed at several points and hence the computation of its peak pressures by use of the Rankine-Hugoniot relation. These calculations indicated a peak overpressure of 4.43 psi at SZ. This value is high in relation to the peak overpressure of 1.36 psi recorded by Project 4.5 and the value of 2.0 psi indicated by small-charge TNT tests scaled to Wigwam, but it is subject to considerable uncertainty because of measurement difficulties.

A cone-shaped condensation cloud was formed above SZ with the passage of the negative phase of the air shock wave. This cloud extended from 700 ft to about 2800 ft in altitude and persisted from about 2.85 to 4.25 sec after SZT. An indirect calculation, based on the cloud height, meteorological conditions, and high-explosive data, indicated a value of 2.9 psi for the peak positive overpressure in the air shock wave at the water surface. This result is not precise because of the many assumptions in the method.

The spread of the initial surface effects along the water indicated that the position of the weapon at detonation was approximately 105 ft to starboard and 10 ft forward of its intended location beneath the well of the YC-473.

Photographic measurements of the rise of the YC with the arrival of the shock wave indicated an average initial velocity of about 76 ft/sec. The barge appeared to buckle at the aft end of the well.

The state of the explosion bubble when it arrived at the surface about 10 sec after SZT is not known. However, the resultant plumes rose to a height of about 1450 ft. A second group of plumes originated about 6 sec later and spread radially along the surface, reaching a diameter of about 3100 ft at 25 sec after SZT. The combined plumes continued to spread laterally and formed a well-defined base surge.

A third group of plumes appeared above the base surge at 35 sec after SZT and reached a height of 770 ft. These probably resulted from the oscillation of the water surface.

The entire base surge was clearly visible only to 90 sec after SZT, but parts of the cloud could be seen from surface camera stations for about 4 min and from the air for about 23 min. Although the evidence is limited, the base surge appeared to grow to a radius of about 6500 ft within 7 min as a result of its own kinetic energy. The maximum observed height was 1900 ft at 4 min. A slow lateral and vertical expansion continued, with turbulent diffusion as the controlling factor. The surge cloud was transported toward the southwest at the speed of the wind.

Photographic data on the train of surface waves generated by the explosion indicated maximum wave heights of about 37 ft at the YFNB-12 (5520 ft radius), 26 ft at the YFNB-13 (7950 ft radius), and 19 ft at the YFNB-29 (10,950 ft radius). At least 24 waves were measurable, and radius-time data were obtained to a distance of about 45,000 ft from SZ. The wave-group velocity was about 42 ft/sec to a radius of 12,000 ft and about 49 ft/sec at greater distances. The wave system had a central wave length of about 1300 ft and a central wave period of about 16 sec to a radius of 12,000 ft; at distances from 20,000 to 30,000 ft, it had a central wave length of about 1700 ft and a central wave period of about 18 sec.

About 90 sec after the detonation, when the base surge was starting to become tenuous, a smooth circular patch of water became visible at SZ, the edge of which was marked by an expanding ring of foam and debris. The aerial photographs indicated an increase in diameter from about 6500 to 10,400 ft between 100 sec and 13 min after SZT. It is believed that the foam ring marked the extent of the contaminated surface water remaining after the test.

The over-all accuracy of the data presented here is probably about ±10 per cent. The measurements of the late stages of base-surge behavior and the growth of the foam ring are subject to greater uncertainty but are probably reliable to within ±20 per cent. The air-shock-wave peak pressures are the least reliable since small errors in the measurements of the rise of the visible shock wave introduce large errors in the calculated peak pressures at the low pressure levels observed. The indirect calculation, based on the condensation cloud, contained several assumptions of unknown validity. The reliability of these pressure values is unknown, but the error is conceivably of the order of 50 to 75 per cent.

4.2 COMPARISON WITH CROSSROADS BAKER

Baker shot in Operation Crossroads is the only other underwater nuclear burst on record. This was a shallow burst that vented rapidly during the first expansion of the bubble; consequently the shock-wave and plume phenomena were radically different from the effects at Wigwam. However, Baker shot produced a base surge about 17,000 ft in diameter, which was similar in some respects to the Wigwam surge.

In general, it was believed that the base surges formed by deep explosions would be relatively small, but the occurrence of a large base surge (13,000 ft in diameter) following the 2000-ft Wigwam detonation indicated that this problem must be re-examined because of the importance of the surge as a medium for the spread of radioactive contaminants.

The question is complicated because the mechanisms of base-surge formation differed in the two tests. The Crossroads surge was formed mainly by the vertical subsidence of a hollow

CONFIDENTIAL

cylindrical column. In such shallow-water tests the droplets and entrained gases in the column walls settle and spread outward along the surface. The Wigwam surge was formed from plumes with high radial components of velocity, and three stages of plumes contributed to its growth.

In shallow underwater tests the radial growth of the base surge can be scaled in terms of the maximum diameter of the vertical column formed by the expanding explosion gases.[1] It will be necessary to develop new scaling laws for deeper bursts, based on other parameters.

4.3 CONCLUSIONS

The following conclusions can be drawn from the results presented in this report.

1. As stated in Sec. 1.1, it is possible to obtain considerable information about an underwater explosion and the accompanying shock-wave and bubble phenomena by the analysis of photographs of the surface effects. To accomplish this purpose, an extensive array of accurately positioned cameras and a smooth water surface are needed.

Since the surface of the water was rough at the time of Operation Wigwam, the phenomena resulting from the arrival of the shock waves at the surface were distorted and were difficult to measure. Because of the cloud cover, photographic aircraft remained at low altitudes and could not fly directly over the burst. In addition, aircraft distances were not established with precision by means of radar. Consequently it was not possible to obtain precise information concerning the nature of the underwater shock waves and bubble pulses from the photographic measurements. However, the photographic data were generally consistent with the gauge results except for the disagreement between the observed peak underwater pressures and the values calculated with Eq. 1.4 on the basis of initial spray-dome velocities. The rise of the weapon barge probably set a lower limit to the bulk motion of the water within the dome, and the velocity of the barge was approximately as indicated by Eq. 1.4.

The plume and base-surge effects were expected to be irregular in shape because of the depth of the burst. Since these phenomena are less reproducible than the shock-wave effects, less precision is required in their measurement, and the photographic data obtained on Wigwam were considered to be satisfactory.

The photographic measurements of the growth of the foam ring provided a useful record of the early spread of the contaminated surface water at a time when close approach by radiological survey aircraft would have been hazardous.

2. The Wigwam test showed that current knowledge of the mechanism of spray-dome formation is inadequate for explaining the initial rise of the dome. Consequently it is not possible at present to calculate underwater peak pressures from measured dome velocities in a nuclear test.

However, if experimental conditions, including weapon yield, charge depth, water depth, and the nature of the bottom are known, it is possible to make reasonably good predictions of the radial growth of the slicks resulting from the direct and bottom-reflected shock waves.

At present the size of secondary spray domes cannot be predicted. Little attention has been devoted to this subject in high-explosive work, but the second dome at Wigwam was definitely higher than would be expected on the basis of small-scale tests.

3. Although the values calculated for the peak air-shock pressure at SZ are of doubtful numerical accuracy, they indicate the possibility that the air-shock pressures at Wigwam were higher than those shown by the direct extrapolation of 32-lb high-explosive test results.

4. Operation Wigwam indicated that the plumes from a deep underwater nuclear burst can be large enough to be hazardous to aircraft and that both the plumes and base surge can constitute serious radiological hazards to personnel in contact with these phenomena at early times.[2,3] However, the mechanism of the Wigwam plume formation is not fully understood, and it is not possible at present to extrapolate the Wigwam data to other yields and depths with confidence.

5. The surface waves at Operation Wigwam were considerably higher than predicted.

CONFIDENTIAL

4.4 RECOMMENDATIONS

The following recommendations stem from the conclusions presented in Sec. 4.3.

1. It is recommended that future underwater nuclear tests be photographed extensively from the surface and the air. Favorable weather conditions are of prime importance for surface-phenomena studies and should receive careful consideration. A large amount of the money and effort invested in a surface-phenomena project may be wasted if unsatisfactory or incomplete results are obtained because of poor experimental conditions.

Photography is the main source of data on the formation, growth, and dissipation of the plumes and base surge, which are hazardous to ships and aircraft. A knowledge of these phenomena is essential for the development of naval tactics for the employment of nuclear weapons. Photography also provides data on the early spread of contaminated water at the surface. However, the potentialities of photography as a source of shock-wave and bubble-pulse data cannot be realized until a better understanding of their surface effects is obtained. In any case gauge records will be required for a complete pressure-time history of the underwater shock wave.

Recommendations concerning photographic coverage and the use of radar for the positioning of photographic aircraft are included in Sec. 2.4.

2. Spray-dome phenomena require additional study; in particular, the relation between initial spray-velocity and underwater-shock parameters and the forces affecting the heights attained by primary and secondary domes. If the former problem can be resolved, the use of photography might permit a reduction in the number of underwater pressure gauges used in underwater nuclear tests. The heights attained by the domes have practical significance in evaluating the hazards to low-flying aircraft engaged in the delivery of antisubmarine weapons.

3. The strength of the Wigwam air shock wave can be established with certainty only by conducting additional deep underwater tests with nuclear weapons. However, scaled high-explosive tests with charges weighing several tons might provide useful information since previous experience has indicated the difficulties involved in the extrapolation of small-charge data to tests of a nuclear magnitude.

In view of the present uncertainty it is recommended that the relatively high peak-pressure values determined by photographic means be considered when it is necessary to estimate the hazard to friendly ships or aircraft engaged in the delivery of nuclear antisubmarine weapons. The peak pressures indicated in scaled high-explosive tests would be preferable as a guide for estimating the damage to enemy craft from a deep underwater nuclear explosion.

To resolve this question, experiments with large high-explosive charges and nuclear weapons should be conducted.

4. Since the bubble behavior and the subsequent plume and base-surge phenomena of deep bursts are not fully understood, it is essential that these effects be studied in detail and that workable scaling laws for high-explosive and nuclear bursts be developed. The work done at NOL for shallow bursts will be extended to deeper conditions with this purpose in view. The results of the 300-lb TNT program conducted prior to the Wigwam test will be published, and it is planned to combine these data with other available material to obtain a better understanding of the phenomena and to put current knowledge on a quantitative basis. In addition, it is possible that further study of the Wigwam records will provide a better insight into the mechanisms of bubble venting and plume formation.

A separate study of the late stages of base-surge behavior for both underwater and underground explosions is also planned. These studies are needed primarily because of the radiation menace to personnel who might be engaged in nuclear warfare. The base surge from an underwater explosion is an insidious hazard at late times since it may resemble a group of ordinary cumulus clouds, as at Crossroads Baker, or it may become an invisible radioactive aerosol, as at Wigwam.

5. Additional work is needed in the field of surface waves to provide reliable predictions for relatively deep underwater explosions. A primary requirement is for reliable data from scaled high-explosive tests, but a better understanding of the bubble behavior on nuclear tests is also needed before wave predictions can be made with a high degree of confidence.

CONFIDENTIAL

REFERENCES

1. M. L. Milligan and G. A. Young, The Scaling of Base Surge Phenomena of Shallow Underwater Explosions, Report NAVORD-2987, May 1, 1954. (Confidential)
2. M. B. Hawkins, Determination of Radiological Hazard to Personnel, Operation Wigwam Project 2.4 Report, ITR-1062, May 1955. (Confidential – RD)
3. F. A. French, Fall-out and Air-borne Activity in Operation Wigwam, with Notes on Surface Effects, Operation Wigwam Project 2.7 Report, WT-1017, May 1955. (Confidential – RD)

DISTRIBUTION

Military Distribution Categories 5-23 and 5-90

ARMY ACTIVITIES

Asst. Dep. Chief of Staff for Military Operations, D/A, Washington 25, D. C. ATTN: Asst. Executive (R&SW)	1
Chief of Research and Development, D/A, Washington 25, D. C. ATTN: Atomic Division	2
Chief of Ordnance, D/A, Washington 25, D. C. ATTN: ORDTX-AR	3
Chief Signal Officer, D/A, P&O Division, Washington 25, D. C. ATTN: SIGRD-8	4
The Surgeon General, D/A, Washington 25, D. C. ATTN: Chief, R&D Division	5
Chief Chemical Officer, D/A, Washington 25, D. C.	6–7
The Quartermaster General, D/A, Washington 25, D. C. ATTN: Research and Development	8
Chief of Engineers, D/A, Washington 25, D. C. ATTN: ENGNB	9–12
Chief of Transportation, Military Planning and Intelligence Div., Washington 25, D. C.	13
Commanding General, Headquarters, U. S. Continental Army Command, Ft. Monroe, Va.	14–16
President, Board #1, Headquarters, Continental Army Command, Ft. Sill, Okla.	17
President, Board #2, Headquarters, Continental Army Command, Ft. Knox, Ky.	18
President, Board #4, Headquarters, Continental Army Command, Ft. Bliss, Tex.	19
Commanding General, U. S. Army Caribbean, Ft. Amador, C. Z. ATTN: Cml. Off.	20
Commanding General, U. S. Army Europe, APO 403, New York, N. Y. ATTN: OPOT Div., Combat Dev. Br.	21–22
Commanding General, U. S. Army Pacific, APO 958, San Francisco, Calif. ATTN: Cml. Off.	23–24
Commandant, Command and General Staff College, Ft. Leavenworth, Kans. ATTN: ALLLS(AS)	25–26
Commandant, The Artillery and Missile School, Ft. Sill, Okla.	27
Secretary, The U. S. Army Air Defense School, Ft. Bliss, Tex. ATTN: Maj. Gregg D. Breitegan, Dept. of Tactics and Combined Arms	28
Commanding General, Army Medical Service School, Brooke Army Medical Center, Ft. Sam Houston, Tex.	29
Director, Special Weapons Development Office, Headquarters, CONARC, Ft. Bliss, Tex. ATTN: Capt. T. E. Skinner	30
Commandant, Walter Reed Army Institute of Research, Walter Reed Army Medical Center, Washington 25, D. C.	31
Superintendent, U. S. Military Academy, West Point, N. Y. ATTN: Prof. of Ordnance	32
Commandant, Chemical Corps School, Chemical Corps Training Command, Ft. McClellan, Ala.	33
Commanding General, Research and Engineering Command, Army Chemical Center, Md. ATTN: Deputy for RW and Non-toxic Material	34
Commanding General, Aberdeen Proving Ground, Md. ATTN: Director, Ballistic Research Laboratories	35–36
Commanding General, The Engineer Center, Ft. Belvoir, Va. ATTN: Asst. Commandant, Engineer School	37
Commanding Officer, Engineer Research and Development Laboratory, Ft. Belvoir, Va. ATTN: Chief, Technical Intelligence Branch	38
Commanding Officer, Picatinny Arsenal, Dover, N. J. ATTN: ORDBB-TK	39
Commanding Officer, Frankford Arsenal, Philadelphia 37, Pa. ATTN: Col. Tewes Kundel	40

Commanding Officer, Army Medical Research Laboratory, Ft. Knox, Ky. 41
Commanding Officer, Chemical Corps Chemical and Radiological Laboratory, Army Chemical Center, Md. ATTN: Tech. Library 42–43
Commanding Officer, Transportation R&D Station, Ft. Eustis, Va. 44
Director, Technical Documents Center, Evans Signal Laboratory, Belmar, N. J. 45
Director, Waterways Experiment Station, PO Box 631, Vicksburg, Miss. ATTN: Library 46
Director, Armed Forces Institute of Pathology, Walter Reed Army Medical Center, 6825 16th Street, N.W., Washington 25, D. C. 47
Director, Operations Research Office, Johns Hopkins University, 7100 Connecticut Ave., Chevy Chase, Md., Washington 25, D. C. 48
Commanding General, Quartermaster Research and Development Command, Quartermaster Research and Development Center, Natick, Mass. ATTN: CBR Liaison Officer 49–50
Commanding Officer, Diamond Ordnance Fuze Laboratories, Washington 25, D. C. 51
Technical Information Service Extension, Oak Ridge, Tenn. 52–56

NAVY ACTIVITIES

Chief of Naval Operations, D/N, Washington 25, D. C. ATTN: OP-36 57–58
Chief of Naval Operations, D/N, Washington 25, D. C. ATTN: OP-03EG 59
Director of Naval Intelligence, D/N, Washington 25, D. C. ATTN: OP-922V 60
Chief, Bureau of Medicine and Surgery, D/N, Washington 25, D. C. ATTN: Special Weapons Defense Div. 61
Chief, Bureau of Ordnance, D/N, Washington 25, D. C. 62
Chief, Bureau of Ships, D/N, Washington 25, D. C. ATTN: Code 348 63
Chief, Bureau of Yards and Docks, D/N, Washington 25, D. C. ATTN: D-440 64
Chief, Bureau of Supplies and Accounts, D/N, Washington 25, D. C. 65
Chief, Bureau of Aeronautics, D/N, Washington 25, D. C. 66–67
Chief of Naval Research, Department of the Navy, Washington 25, D. C. ATTN: Code 811 68
Commander-in-Chief, U. S. Pacific Fleet, Fleet Post Office, San Francisco, Calif. 69
Commander-in-Chief, U. S. Atlantic Fleet, U. S. Naval Base, Norfolk 11, Va. 70
Commandant, U. S. Marine Corps, Washington 25, D. C. ATTN: Code A03H 71–74
President, U. S. Naval War College, Newport, R. I. 75
Superintendent, U. S. Naval Postgraduate School, Monterey, Calif. 76
Commanding Officer, U. S. Naval Schools Command, U. S. Naval Station, Treasure Island, San Francisco, Calif. 77
Commanding Officer, U. S. Fleet Training Center, Naval Base, Norfolk 11, Va. ATTN: Special Weapons School 78
Commanding Officer, U. S. Fleet Training Center, Naval Station, San Diego 36, Calif. ATTN: (SPWP School) 79–80
Commanding Officer, U. S. Naval Damage Control Training Center, Naval Base, Philadelphia, Pa. ATTN: ABC Defense Course 81
Commanding Officer, U. S. Naval Unit, Chemical Corps School, Army Chemical Training Center, Ft. McClellan, Ala. 82
Commander, U. S. Naval Ordnance Laboratory, Silver Spring 19, Md. ATTN: EE 83
Commander, U. S. Naval Ordnance Laboratory, Silver Spring 19, Md. ATTN: EH 84
Commander, U. S. Naval Ordnance Laboratory, Silver Spring 19, Md. ATTN: R 85
Commander, U. S. Naval Ordnance Test Station, Inyokern, China Lake, Calif. 86
Officer-in-Charge, U. S. Naval Civil Engineering Res. and Evaluation Lab., U. S. Naval Construction Battalion Center, Port Hueneme, Calif. ATTN: Code 753 87
Commanding Officer, U. S. Naval Medical Research Inst., National Naval Medical Center, Bethesda 14, Md. 88
Director, Naval Air Experimental Station, Air Material Center, U. S. Naval Base, Philadelphia, Pa. 89
Director, U. S. Naval Research Laboratory, Washington 25, D. C. ATTN: Mrs. Katherine H. Cass 90
Commanding Officer and Director, U. S. Navy Electronics Laboratory, San Diego 52, Calif. 91
Commanding Officer, U. S. Naval Radiological Defense Laboratory, San Francisco, Calif. ATTN: Technical Information Division 92–93
Commanding Officer and Director, David W. Taylor Model Basin, Washington 7, D. C. ATTN: Library 94
Commander, U. S. Naval Air Development Center, Johnsville, Pa. 95

Commanding Officer and Director, U. S. Naval Engineering Experiment Station, Annapolis, Md. ATTN: Code 705 — 96
CINCPAC, Pearl Harbor, T. H. — 97
Commander, Norfolk Naval Shipyard, Portsmouth 8, Va. ATTN: Code 270 — 98
Technical Information Service Extension, Oak Ridge, Tenn. (surplus) — 99–103

AIR FORCE ACTIVITIES

Asst. for Atomic Energy Headquarters, USAF, Washington 25, D. C. ATTN: DCS/O — 104
Director of Operations, Headquarters, USAF, Washington 25, D. C. ATTN: Operations Analysis — 105
Director of Plans, Headquarters, USAF, Washington 25, D. C. ATTN: War Plans Div. — 106
Director of Research and Development, DCS/D, Headquarters, USAF, Washington 25, D. C. ATTN: Combat Components Div. — 107
Director of Intelligence, Headquarters, USAF, Washington 25, D. C. ATTN: AFOIN-IB2 — 108–109
The Surgeon General, Headquarters, USAF, Washington 25, D. C. ATTN: Bio. Def. Br., Pre. Med. Div. — 110
Asst. Chief of Staff, Intelligence, Headquarters, U. S. Air Forces Europe, APO 633, New York, N. Y. ATTN: Directorate of Air Targets — 111
Commander, 497th Reconnaissance Technical Squadron (Augmented), APO 633, New York, N. Y. — 112
Commander, Far East Air Forces, APO 925, San Francisco, Calif. ATTN: Special Asst. for Damage Control — 113
Commander-in-Chief, Strategic Air Command, Offutt Air Force Base, Omaha, Nebr. ATTN: Special Weapons Branch, Inspector Div., Inspector General — 114
Commander, Tactical Air Command, Langley AFB, Va. ATTN: Documents Security Branch — 115
Commander, Air Defense Command, Ent AFB, Colo. — 116
Research Directorate, Headquarters, Air Force Special Weapons Center, Kirtland Air Force Base, N. Mex., ATTN: Blast Effects Res. — 117–118
Commander, Air Research and Development Command, PO Box 1395, Baltimore, Md. ATTN: RDDN — 119
Commander, Air Proving Ground Command, Eglin AFB, Fla. ATTN: Adj./Tech. Report Branch — 120
Director, Air University Library, Maxwell AFB, Ala. — 121–122
Commander, Flying Training Air Force, Waco, Tex. ATTN: Director of Observer Training — 123–130
Commander, Crew Training Air Force, Randolph Field, Tex. ATTN: 2GTS, DCS/O — 131
Commandant, Air Force School of Aviation Medicine, Randolph AFB, Tex. — 132–133
Commander, Wright Air Development Center, Wright-Patterson AFB, Dayton, Ohio. ATTN: WCOSI — 134–139
Commander, Air Force Cambridge Research Center, L. G. Hanscom Field, Bedford, Mass. ATTN: CRQST-2 — 140–141
Commander, Air Force Special Weapons Center, Kirtland AFB, N. Mex. ATTN: Library — 142–144
Commander, Lowry AFB, Denver, Colo. ATTN: Department of Special Weapons Training — 145
Commander, 1009th Special Weapons Squadron, Headquarters, USAF, Washington 25, D. C. — 146
The RAND Corporation, 1700 Main Street, Santa Monica, Calif. ATTN: Nuclear Energy Division — 147–148
Commander, Second Air Force, Barksdale AFB, La. ATTN: Operations Analysis Office — 149
Commander, Eighth Air Force, Westover AFB, Mass. ATTN: Operations Analysis Office — 150
Commander, Fifteenth Air Force, March AFB, Calif. ATTN: Operations Analysis Office — 151
Commander, Western Development Div. (ARDC), PO Box 262, Inglewood, Calif. ATTN: WDSIT. Mr. R. G. Weitz — 152
Technical Information Service Extension, Oak Ridge, Tenn. (surplus) — 153–157

OTHER DEPARTMENT OF DEFENSE ACTIVITIES

Asst. Secretary of Defense, Research and Development, D/D, Washington 25, D. C. ATTN: Tech. Library — 158
U. S. Documents Officer, Office of the U. S. National Military Representative, SHAPE, APO 55, New York, N. Y. — 159
Director, Weapons Systems Evaluation Group, OSD, Rm. 2E1006, Pentagon, Washington 25, D. C. — 160
Armed Services Explosives Safety Board, D/D, Building T-7, Gravelly Point, Washington 25, D. C. — 161
Commandant, Armed Forces Staff College, Norfolk 11, Va. ATTN: Secretary — 162
Commander, Field Command, Armed Forces Special Weapons Project, PO Box 5100, Albuquerque, N. Mex. — 163–168

CONFIDENTIAL

Commander, Field Command, Armed Forces Special Weapons Project, PO Box 5100, Albuquerque, N. Mex. ATTN: Technical Training Group 169–170
Commander, Field Command, Armed Forces Special Weapons Project, P.O. Box 5100, Albuquerque, N. Mex. ATTN: Deputy Chief of Staff, Weapons Effects Test 171–175
Chief, Armed Forces Special Weapons Project, Washington 25, D. C. ATTN: Documents Library Branch 176–186
Office of the Technical Director, Directorate of Effects Tests, Field Command, AFSWP, PO Box 577, Menlo Park, Calif. ATTN: Dr. E. B. Doll 187
Commanding General, Military District of Washington, Rm. 1543, Building T-7, Gravelly Point, Va. 188
Technical Information Service Extension, Oak Ridge, Tenn. (surplus) 189–193

ATOMIC ENERGY COMMISSION ACTIVITIES

U. S. Atomic Energy Commission, Classified Technical Library, 1901 Constitution Ave., Washington 25, D. C. ATTN: Mrs. J. M. O'Leary (for DMA) 194–197
Los Alamos Scientific Laboratory, Report Library, PO Box 1663, Los Alamos, N. Mex. ATTN: Helen Redman 198–199
Sandia Corporation, Classified Document Division, Sandia Base, Albuquerque, N. Mex. ATTN: H. J. Smyth, Jr. 200–204
University of California Radiation Laboratory, PO Box 808, Livermore, Calif. ATTN: Clovis G. Craig 205–207
Weapon Data Section, Technical Information Service Extension, Oak Ridge, Tenn. 208
Technical Information Service Extension, Oak Ridge, Tenn. (surplus) 209–250